Aus dem Institut für Virologie
der Universität zu Köln
Direktor: Universitätsprofessor Dr. med. F. Klein

Somatic hypermutation introduces bystander mutations that prepare SARS-CoV-2 antibodies for emerging variants

Inaugural-Dissertation zur Erlangung der Doktorwürde
der Medizinischen Fakultät
der Universität zu Köln

vorgelegt von
Michael Korenkov
aus Bergisch Gladbach

promoviert am 15. Dezember 2025

Gedruckt mit Genehmigung der Medizinischen Fakultät der Universität zu Köln

2026

Dekan:	Universitätsprofessor Dr. med. G. R. Fink
1. Gutachter:	Universitätsprofessor Dr. med. F. Klein
2. Gutachterin:	Professorin Dr. med. C. Lehmann

Erklärung

Ich erkläre hiermit, dass ich die vorliegende Dissertationsschrift ohne unzulässige Hilfe Dritter und ohne Benutzung anderer als der angegebenen Hilfsmittel angefertigt habe; die aus fremden Quellen direkt oder indirekt übernommenen Gedanken sind als solche kenntlich gemacht

Bei der Auswahl und Auswertung des Materials sowie bei der Herstellung des Manuskriptes habe ich keine Unterstützungsleistungen erhalten.

Weitere Personen waren an der Erstellung der vorliegenden Arbeit nicht beteiligt. Insbesondere habe ich nicht die Hilfe einer Promotionsberaterin/eines Promotionsberaters in Anspruch genommen. Dritte haben von mir weder unmittelbar noch mittelbar geldwerte Leistungen für Arbeiten erhalten, die im Zusammenhang mit dem Inhalt der vorgelegten Dissertationsschrift stehen.

Die Dissertationsschrift wurde von mir bisher weder im Inland noch im Ausland in gleicher oder ähnlicher Form einer anderen Prüfungsbehörde vorgelegt.

Teile der vorliegenden Dissertationsschrift basieren auf den folgenden Publikationen:

Kreer, C.*, Zehner, M.*, Weber, T., Ercanoglu, M.S., Gieselmann, L., Rohde, C., Halwe, S., **Korenkov, M.**, Schommers, P., Vanshylla, K., Di Cristanziano, V., Janicki, H., Brinker, R., Ashurov, A., Krähling, V., Kupke, A., Cohen-Dvashi, H., Koch, M., Eckert, J.M., Lederer, S., Pfeifer, N., Wolf, T., Vehreschild, M.J.G.T., Wendtner, C., Diskin, R., Gruell, H., Becker, S., Klein, F., 2020. Longitudinal Isolation of Potent Near-Germline SARS-CoV-2-Neutralizing Antibodies from COVID-19 Patients. Cell 182, 843-854.e12. https://doi.org/10.1016/j.cell.2020.06.044 *contributed equally

Die in dieser Arbeit angegebenen Experimente zur PCR und Sequenzierung von B Zellen, Klonierung und Herstellung von monoklonalen Antikörpern sowie die Durchführung von ELISAs sind nach entsprechender Anleitung durch Dr. Christoph Kreer sowie Dr. Matthias Zehner von mir selbst durchgeführt worden. Die Planung der Experimente sowie die Analyse der Daten erfolgte durch Dr. Christoph Kreer und Dr. Matthias Zehner. Die Arbeit wurde durch Prof. Florian Klein supervidiert.

Gruell, H., Vanshylla, K., **Korenkov, M.**, Tober-Lau, P., Zehner, M., Münn, F., Janicki, H., Augustin, M., Schommers, P., Sander, L. E., Kurth, F., Kreer, C., & Klein, F. (2022). SARS-CoV-2 Omicron sublineages exhibit distinct antibody escape patterns. *Cell Host & Microbe*, *30*(9), 1231-1241.e6. https://doi.org/10.1016/j.chom.2022.07.002

Die in dieser Arbeit getesteten monoklonalen Antikörper wurden von mir kloniert und in Zellkultur hergestellt. Die Planung und Durchführung der Experimente sowie die Analyse der Daten erfolgte durch Dr. Henning Grüll und Dr. Kanika Vanshylla. Die Arbeit wurde durch Prof. Florian Klein supervidiert.

Korenkov, M.*, Zehner, M.*, Cohen-Dvashi, H., Borenstein-Katz, A., Kottege, L., Janicki, H., Vanshylla, K., Weber, T., Gruell, H., Koch, M., Diskin, R., Kreer, C.†, Klein, F.†, 2023. Somatic hypermutation introduces bystander mutations that prepare SARS-CoV-2 antibodies for emerging variants. *Immunity* S1074761323004855. https://doi.org/10.1016/j.immuni.2023.11.004 *contributed equally †contributed equally

Unter Supervision von Prof. Florian Klein, Dr. Christoph Kreer und Dr. Matthias Zehner wurden alle in dieser Arbeit vorkommenden Experimente bis auf die Kristallstruktur von HbnC3t1p1_C6 von mir geplant und durchgeführt sowie alle Ergebnisse durch mich mit Hilfe von Dr. Christoph Kreer und Dr. Matthias Zehner analysiert. Die folgenden Personen haben die vorliegende Arbeit unterstützt: Dr. Hadas Cohen-Dvashi, Aliza Borenstein-Katz und Prof. Ron Diskin haben die Kristallstruktur vom Antikörper HbnC3t1p1_C6 aufgelöst sowie die Ergebnisse analysiert. Hanna Janicki unterstützte diese Studie mit der Herstellung von Antikörpern. Lisa Kottege unterstützte diese Studie mit der Herstellung von Antikörpern sowie mit der Durchführung von Neutralisationsassays. Dr. Henning Grüll und Dr. Kanika Vanshylla unterstützten diese Studie mit der Durchführung von Neutralisationsassays mit SARS-CoV-2 Varianten. Dr. Timm Weber unterstützte diese Studie mit dem Design von Germline Antikörper Varianten. Dr. Christoph Kreer und Dr. Matthias Zehner unterstützen diese Arbeit mit der Herstellung von Antikörpern, der Durchführung von Neutralisationsassays sowie der Analyse der Daten.

Erklärung zur guten wissenschaftlichen Praxis:

Ich erkläre hiermit, dass ich die Ordnung zur Sicherung guter wissenschaftlicher Praxis und zum Umgang mit wissenschaftlichem Fehlverhalten (Amtliche Mitteilung der Universität zu Köln AM 132/2020) der Universität zu Köln gelesen habe und verpflichte mich hiermit, die dort genannten Vorgaben bei allen wissenschaftlichen Tätigkeiten zu beachten und umzusetzen.

Köln, den 18.11.2024

Unterschrift: .....

Acknowledgements

First and foremost, I would like to express my thanks to my supervisor, Prof. Florian Klein, for giving me the opportunity to work on these projects under his tutelage. I am deeply grateful for his continued support and mentorship during my time in his laboratory and beyond. His dedication to science and boundless creativity have been a constant source of inspiration, motivating me to pursue a career in research. Thank you, Florian!

I am also immensely grateful to Dr. Christoph Kreer and Dr. Matthias Zehner, for teaching me the fundamentals and supporting me from the very beginning. Your guidance, encouragement and patience have been instrumental in bringing these projects to live. Christoph, I owe you a special thanks for the time spend helping me find my way through the data and for challenging me to sharpen my critical thinking.

Of course, I also need to extend my gratitude towards all the former and current members of AG Klein, without whom none of these projects could have been completed. I feel incredibly fortunate to have worked alongside such talented, inspiring and kind individuals. A heartfelt thanks goes out to Henning Grüll, Maike Schlotz, Sabrina Dähling, Susanne Detmer, Kanika Vanshylla, Timm Weber, Anna Schmitt, Tina Bresser, Lutz Gieselmann, Hanna Janicki, Lisa Kottege, Johanna Worczinski, Daniela Weiland, Nadine Henn, Seda Ercanoglu, Finn Teipel and Svea Rose. Special recognition goes to my “partners in crime” Nareshkumar Poopalasingam and Artem Ashurov.

I also feel deep appreciation for the support and camaraderie of my friends, who have been a constant source of joy throughout my time in Cologne. Thank you, David, Leo, Janina, Naomi, Helen, and Erik, for your encouragement and the amazing moments we have shared. I want to especially thank you, Noah, for being an inspiration and the best WG buddy I ever had, and you, Lina, for your compassion and kindness that have been invaluable to me – you are truly extraordinary people.

Lastly, and most importantly, I want to express my deepest gratitude to my family—especially Mama, Papa, Leo, and Lena. Mama and Papa, you have raised me with love, care and always stood by me with wisdom and guidance, shaping my path at every step. Your belief in me and your dedication to my education have enabled me to pursue my dreams, and for that, I am endlessly grateful. Though we often joked about the motto “*Kindheit muss schwer sein*” your actions always proved otherwise. Lena, your kindness, empathy, and support have been a cornerstone in my life. I’m deeply grateful for your friendship, love, and irreplaceable presence.

Für Mama und Papa

Table of Contents

List of Abbreviations

ACE2	Angiotensin-converting enzyme 2
AID	Activation-induced cytidine deaminase
API	Application programming interfaces
AUC	Area under the curve
BCR	B cell receptor
C	Cytosine
CD	Cluster of differentiation
cDNA	Complementary deoxyribonucleic acid
CDR	Complementary determining region
CH	Heavy chain constant region
CHE	Central helix
CI	Confidence interval
CL	Light chain constant region
CoV-AbDab	Coronavirus antibody database
COVID-19	Coronavirus disease 2019
DAPI	4’,6-Diamidin-2-phenylindol
DNA	Deoxyribonucleic acid
DZIF	Deutsches Zentrum für Infektionsforschung
E	Envelope protein
EC50	Effective dose 50
ELISA	Enzyme-linked Immunosorbent Assay
Fab	Fragment antigen binding
FACS	Fluorescence-activated cell sorting
Fc	Fragment crystallizable
FDC	Follicular dentritic cell
FP	Fusion peptide
G	Guanin
GC	Germinal Center
GeoMeanID50	Geometric mean of the infectious dose 50
GISAID	Global Initiative on Sharing All Influenza Data
GL	Germline
HCoV	Human coronavirus
HR	Heptad repeat
HRP	Horseradish peroxidase
IC50	Inhibitory dose 50
ID50	Infectious dose 50

Ig	Immunoglobulin
IgG	Immunoglobulin G
IGHV	Immunoglobulin heavy chain variable region
IGKV	Immunoglobulin kappa chain variable region
IGLV	Immunoglobulin lambda chain variable region
IMGT	The international ImMunoGeneTics information system
IQR	Interquartile range
J	Joining chain
J gene	Joining gene
KD	Dissociation constant
kDa	Kilo dalton
LLOQ	Lower limit of quantification
LZ	Light zone
M	Membrane protein
mAb	Monoclonal antibody
MID	Molecular identifier
mRNA	Messenger ribonucleic acid
MT	Mature
N	Nucleocapsid protein
n.n.	No neutralization
NGS	Next-generation sequencing
nm	Nanometers
nsp	Non-structural protein
NTD	N-terminal domain
OD	Optical density
ORF	Open reading frame
PB	Plasma blast
PBMC	Peripheral blood mononuclear cell
PBS	Phosphate-buffered saline
PC	Plasma cell
PCR	Polymerase chain reaction
PDB	Protein data bank
PEI	Polyethylenimine
PES	Polyethersulfone filter
Phe	Phenylalanine
RBD	Receptor binding domain

RBM	Receptor binding motif
RT-qPCR	Reverse transcription real-time polymerase chain reaction
S protein	Spike protein
SARS-CoV-2	Severe acute respiratory syndrome coronavirus type 2
SD1/SD2	Subdomain 1/2
SHM	Somatic hypermutation
SLIC	Sequence and ligation-independent cloning
SPR	Surface plasmon resonance spectroscopy
SS	Signaling sequence
TCID50	50% tissue culture infectious doses
Tfh	T follicular helper cell
TM	Transmembrane domain
TMPRSS2	Transmembrane protease serin 2
U	Uracil
ULOQ	Upper limit of quantification
UMI	Unique molecular identifier
VH	Heavy chain variable region
VL	Light chain variable region

1. Zusammenfassung

Die adaptive Immunantwort auf Krankheitserreger beruht auf neutralisierenden Antikörpern, die durch eine Infektion oder Impfung entstehen. Mit dem Auftreten von SARS-CoV-2 Ende 2019 wurde ein umfassendes Verständnis der menschlichen Antikörperreaktion auf SARS-CoV-2 für die Entwicklung neuer Therapeutika und für die Impfung unerlässlich. Die Untersuchung der Rolle der somatischen Hypermutation (SHM), insbesondere im Zusammenhang mit unterschiedlichen viralen Escape-Varianten und der Prägung des Immunsystems durch wiederholte virale Exposition, ist wichtig in diesen Bemühungen. Zu diesem Zweck untersuchten wir zunächst die SARS-CoV-2 Serum- und B-Zell-Antwort mithilfe von ELISA, Neutralisationstests und einem Hochdurchsatz Einzelzell-Sequenzierungsansatz, bei dem 4.313 B-Zellen von rekonvaleszenten Personen gescreent wurden. Wir konnten zeigen, dass eine reaktive polyklonale B-Zell-Antwort auf das SARS-CoV-2 Spike-Protein in allen 12 Teilnehmern nach der Infektion induziert wird. Aus diesen B-Zellen identifizierten wir 27 potente SARS-CoV-2 neutralisierende monoklonale Antikörper (mAbs) bestehend aus einem breiten Spektrum an V-Gen Segmenten und einem geringen Grad an somatischer Hypermutation (SHM), die eine Virusinfektion mit Konzentrationen von nur 0,04 µg/ml hemmen können. Anschließend analysierten wir die Rolle von SHM für die Funktionalität von Antikörpern, indem wir ein breites Panel von zuvor isolierten SARS-CoV-2 neutralisierenden Antikörpern (n=92) in ihre V-Gen Keimbahnvariante umwandelten. Unsere Ergebnisse zeigen, dass die meisten neutralisierenden SARS-CoV-2 Antikörper (78 von 88) von ihren Mutationen abhängen. Ein Teil der mutierten neutralisierenden SARS-CoV-2-Antikörper (11 von 88), darunter alle Antikörper des öffentlichen Klonotyps VH1-58/VK3-20, band und neutralisierte jedoch unabhängig von den erworbenen Mutationen. Beim Klonotyp VH1-58/VK3-20 zeigte nur eine Untergruppe von Antikörpern (10 von 22) neutralisierende Aktivität gegen Omicron BA.1/BA.2-Subvarianten, obwohl sie vor dem Auftreten von Omicron isoliert wurden. Während Mutationen für die Neutralisation der Varianten Wu01, Alpha, Beta und Delta entbehrlich waren, waren sie für die Neutralisation von Omicron BA.1/BA.2 entscheidend. Schließlich untersuchten wir mit Hilfe von Pseudovirus-Neutralisationstests die Auswirkungen der neuen Virusvarianten (BA.1, BA.1.1, BA.2, BA.2.12.1 und BA.4/5) auf die etablierte humorale Immunität in 50 Proben von geimpften oder rekonvaleszenten Personen sowie in einem 163 monoklonalen Antikörperpanel. Unsere Ergebnisse zeigen, dass die Booster-Impfung mit mRNA (Wu01) eine Neutralisation gegen verschiedene Omicron-Sublinien im Serum hervorruft, was die Bedeutung der Booster-Immunisierung für den Aufbau einer ausreichenden Omicron-Antwort unterstreicht. Darüber hinaus ergab die Analyse der Neutralisationssensitivität im 163-Antikörper-Panel bemerkenswerte Unterschiede in verschiedenen Escape-Mustern innerhalb der Omicron Variante mit einer

gesteigerten Resistenz gegen BA.4/5. Durch das Wissen über Bystander-Mutationen und Antigen-Escape konnten wir den klinischen Antikörper Tixagevimab (VH1-58/VK3-20), der gegen Omicron BA.1/BA.2 unwirksam ist, in einen wirksamen neutralisierenden Antikörper gegen diese Variante umwandeln. Unsere Ergebnisse erweitern unser Verständnis von SHM als einen Mechanismus, der die Affinitätsreifung vorantreibt und durch Bystander-Mutationen zur Diversifizierung von Antikörpern beiträgt und so die Chancen erhöht, virale Escape-Varianten zu neutralisieren.

2. Summary

The adaptive immune response towards pathogens relies on neutralizing antibodies induced by infection or vaccination. With the emergence of SARS-CoV-2 in late 2019, a comprehensive understanding of the human antibody response towards SARS-CoV-2 became essential for developing novel therapeutics and informing vaccination efforts. Studying the role of somatic hypermutation (SHM), especially in the context of antigenically drifted viral escape variants and immune imprinting from repeated viral exposures, is key to advancing these efforts. To address this, we initially investigated the SARS-CoV-2 serum and B cell response using ELISA, neutralization assays, and a high-throughput single-cell sequencing approach screening 4.313 B cells in convalescent individuals. We showed that a SARS-CoV-2 spike protein reactive polyclonal B cell response is readily induced in all 12 participants after infection. From those B cells, we identified 27 potent SARS-CoV-2 neutralizing monoclonal antibodies (mAbs) with a broad spectrum of V gene segments and a low degree of somatic hypermutation (SHM) that can inhibit authentic virus infection at concentrations as low as 0,04 µg/ml. We then analyzed the role of SHM in antibody functionality by reverting a broad panel of previously isolated SARS-CoV-2 neutralizing antibodies (n=92) to their V gene germline variant. Our results illustrate that most SARS-CoV-2 neutralizing antibodies (78 out of 88) depend on their mutations. However, a fraction of mutated SARS-CoV-2 neutralizing antibodies (11 out of 88), including all antibodies from the VH1-58/VK3-20 public clonotype, bound and neutralized independently of acquired mutations. For the VH1-58/VK3-20 public clonotype, only a subset of antibodies (10 out of 22) showed neutralizing activity against Omicron BA.1/BA.2 subvariants despite being isolated before the emergence of Omicron. While mutations were dispensable for Wu01, Alpha, Beta, and Delta variants, they were critical for Omicron BA.1/BA.2 neutralization. Lastly, using pseudovirus neutralization assays, we have examined the impact of emerging viral variants (BA.1, BA.1.1, BA.2, BA.2.12.1, and BA.4/5) on established humoral immunity in 50 samples comprised of vaccinated or convalescent individuals as well as in a 163 monoclonal antibody panel. Our results show that Wu01 mRNA vaccination booster elicits serum neutralization activity against diverse Omicron sublineages, underlining the importance of booster immunization in establishing a sufficient Omicron response. Additionally, the analysis of neutralization sensitivity in the 163-antibody panel revealed notable antigenic differences showcasing distinct escape patterns within the Omicron sublineages with a higher resistance to BA.4/5. Leveraging the knowledge of bystander mutations and antigenic escape, we converted the clinical antibody Tixagevimab (VH1-58/VK3-20), which is ineffective against Omicron BA.1/BA.2, into a potent neutralizer of these viruses. Our findings broaden our understanding of SHM as a mechanism that

drives affinity maturation and contributes to antibody diversification through bystander mutations thus increasing the chances to neutralize viral escape variants.

3. Introduction

3.1. Fundamentals of our immune system

The human immune system consists of cells, proteins, and processes designed to protect us from pathogens such as bacteria, fungi, viruses, toxins, or even cancer cells.[1] Our immune system can be divided into innate and adaptive parts, which are responsible for different functions but are closely linked.[1–3] The innate immune system represents the first line of defense consisting of non-specific mechanisms such as anatomical barriers (epithelial cells, mucus layer, etc.), humoral (complement system, cytokines, etc.), and cellular elements (neutrophile granulocytes, macrophages, dendritic cells, etc.).[1–3] On the other hand, the adaptive immune system develops after several days. It is primarily responsible for a highly specific and antigen-dependent defense mechanism by creating an immunological memory.[1–3] Despite their different mechanisms, innate and adaptive immune systems act together, with components of the innate system playing a crucial role in activating the adaptive system.[3] Consequently, although the innate and adaptive immune responses differ fundamentally in their mechanisms, their synergy is indispensable for a robust and fully effective immune response.[1–3]

3.1.1. Adaptive immune system

The adaptive immune system can be divided into T cell-mediated and antibody-mediated through B lymphocytes.[4] B and T lymphocytes express antigen-recognizing receptors on their surface, which B cells can also secrete as a soluble protein called an antibody.[1,4] T and B cell receptors (BCR) and antibodies can bind to any molecule, like proteins, lipids, or carbohydrates, individually.[4] Since these receptors can distinguish between molecules, the adaptive immune system can recognize different pathogens and respond specifically.[1–4] To cover the vast amount of different antigens, a complex set of gene segment rearrangements (V-(D)-J recombination) is performed to generate various receptor combinations, facilitating an almost endless variety of receptors and antibodies.[4–6] However, since the rearrangements can produce receptors or antibodies that target self-molecules, immunological self-tolerance is ensured through the elimination, inactivation, or suppression of self-reactive B cells via regulatory T cells.[1–4] The interaction of antigens with matching receptors (clonal selection) triggers naïve lymphocytes to proliferate (clonal expansion) and differentiate into effector cells capable of eliminating pathogens.[1–4] Effector B cells, called plasma cells, release antibodies that can neutralize pathogens or toxins over extended distances.[4,7] In contrast, effector T cells can produce cell-surface and secreted co-

stimulatory molecules that help other immune cells eliminate a pathogen or induce infected host cells to undergo apoptosis.[3,4] During the primary response, effector lymphocytes can undergo a process called affinity maturation, enhancing their ability to respond more effectively to the antigen by developing BCRs with a higher affinity towards the selected antigen[8,9] After the primary response, specific effector T and B cells can differentiate into memory cells, enabling a swifter and more effective immune response upon subsequent exposure to the same antigen.[4,10,11]

3.1.2. B-cell development and VDJ-Recombination

B cells differentiate from lymphoid progenitor cells produced by hematopoietic stem cells in the bone marrow.[3,4] The various stages of B cell development can be distinguished by the formation of the BCR, consisting of a heavy and a light chain and different cell surface molecules called cluster of differentiation (CD).[12] The BCR belongs to a class of proteins called immunoglobulins (Ig) and develops by joining genes encoding variable (VH), diversity (VD), and joining (VJ) regions for the heavy chain and variable (VL) as well as joining (VJ) for the light chain in a process mediated by RAG1/2 activity.[5,6,12] By combining 40 VH, 25 VD, and 6 VJ for the heavy and 40 VL with 5 VJ or 30 VL with 4 VJ for the κ or λ light chain, respectively.[4] In principle, 5520 VH regions can be combined with 195 VL regions (175 κ and 120 λ chains), yielding $1{,}5 \times 10^6$ different antigen-binding sites (Figure 1).[4] At joining sites of the different gene segments, specifically the third hypervariable region (complementary determining region), nucleotides can be lost, or a variable number of nucleotides can be inserted in a process called junctional diversification that increases the B cell diversity up to about 10^8-fold.[4–6] The BCR expressed on the surface of B cells can be categorized into five major classes of Ig (IgM, IgD, IgA, IgG, IgE) that each initiates a distinct biological response upon antigen contact.[4,13] Each B cell clone produces a singular type of immunoglobulin with a unique antigen binding site.[1,4,13] The BCR on the surface of immature naïve B cells in the bone marrow is of the IgM class, while a mature naïve B cell in peripheral lymphoid tissue expresses both IgM and IgD class BCRs on its surface.[7,13,14] Upon contact with the matching antigen, mature naïve B cells differentiate into IgM-secreting effector cells with the help of T helper cells so that IgM class antibodies dominate the primary immune response. [4,7,13] As activated B cells undergo affinity maturation in the later stages of the immune response, the combination of antigen and T helper cell-derived cytokines stimulates numerous activated B cells to transition from IgM and IgD to producing IgG, IgE, or IgA in a process called class switching.[4,7,13,14] Some class-switched cells differentiate into memory cells expressing their immunoglobulin as BCRs, while others transform into plasma cells secreting immunoglobulins as antibodies.[4,7,13,14]

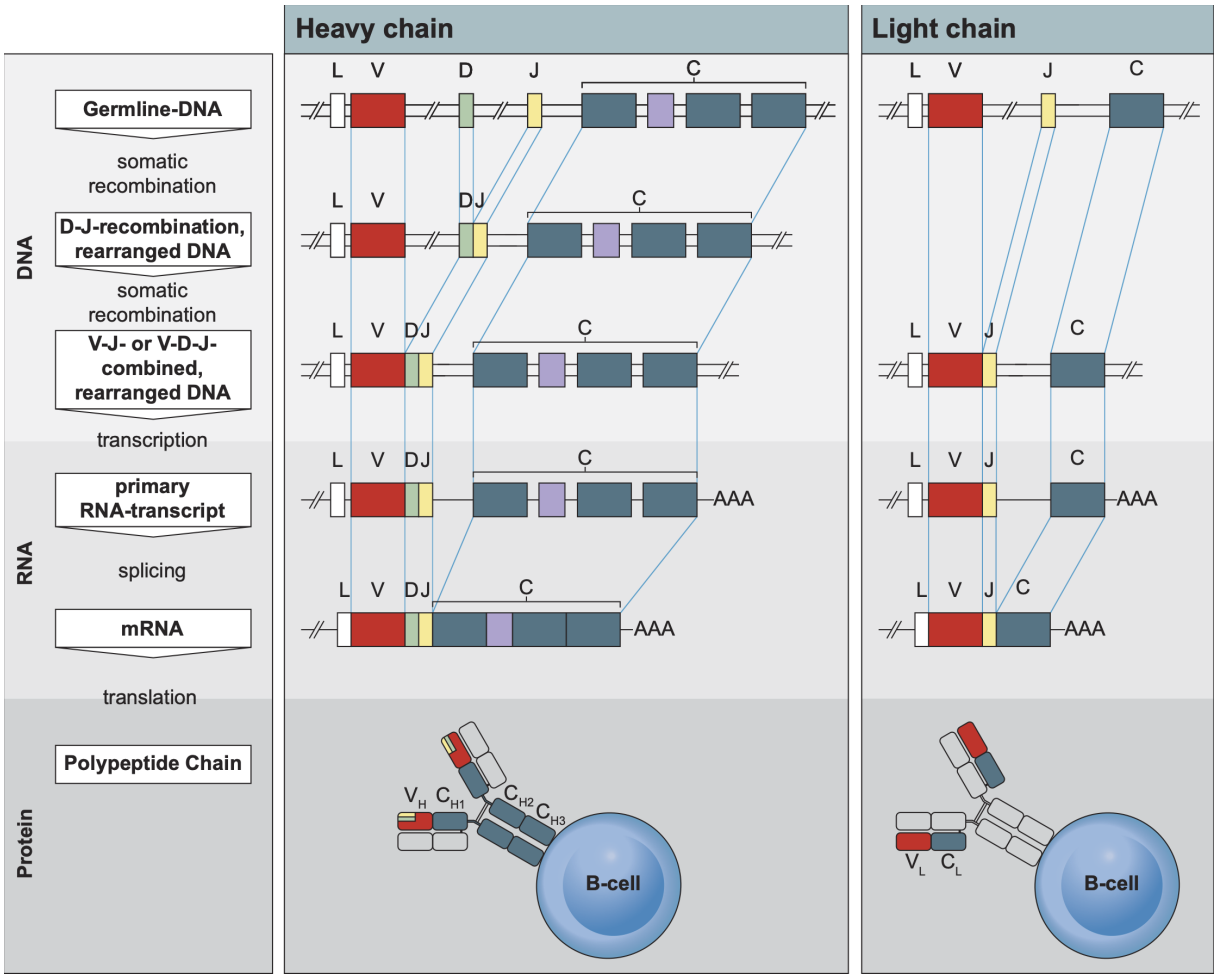

Figure 1. Overview of VDJ-recombination in B cells.

Schematic of the different stages of VDJ-recombination for the variable region of heavy and light chain. The heavy chain is composed of three gene segments (left). First, the D- and J-gene segments are connected and, in the next stage, combined with the V-gene, forming the complete variable gene segment exon. The variable gene segment is transcribed, and the heavy chain constant region (C) exon, as well as the preceding leader peptide (L) exon, is spliced during RNA transcript processing, removing the introns between L and V-segment as well as J-segment and constant region (C). For the light chain (right), V- and J-gene segments are connected, the light chain variable gene segment is transcribed and the leader peptide (L) sequence as well as the constant region (C) are added during splicing. The leader peptide (L) facilitates the secretion of the BCR onto the cell surface. [adapted from *Janeway Immunologie; Abb. 5.3*][1]

3.1.3. Affinity maturation

As time passes following an antigen contact or after repeated exposures to the same antigen a gradual increase in antibody affinity towards that antigen can be observed.[4,15,16] The observed affinity maturation is driven by the accumulation of mutations in the V gene regions of the antibody's heavy and light chains through a process called somatic hypermutation (SHM).[4,15,16] Upon binding to the antigen, B cells with the help of T helper cells undergo rapid proliferation forming structures within secondary lymphoid tissue known as germinal centers (Figure 2A).[9,17,18] Germinal centers are composed of a dark zone primarily

occupied by densely packed, actively dividing B cells known as centroblasts, and a light zone with smaller, non-dividing centrocytes surrounded by a network of follicular dendritic cells, T cells and macrophages (Figure 2A).[9,17,18] Centroblasts in the dark zone diversify their V genes through SHM.[9,17,18] This process primarily introduces single nucleotide changes into the V gene region at a mutational frequency of 10^{-3} per base pair per generation and is triggered by the targeted deamination of the DNA base C (cytosine) to U (uracil) by an enzyme termed activation-induced cytidine deaminase (AID; Figure 2B).[15,17,19] The resulting transformation of C:G (guanin) pairs into U:G mispairs activates different repair pathways such as base excision repair (uracil-DNA glycosylase) or conventional mismatch repair (MSH2/MSH6) leading to various types of mutations introduced into the BCR (Figure 2B).[15,17,19,20] To assess the antigen binding capabilities as well as the self-reactivity of newly generated BCRs on the surface of the centroblasts, a selection process involving follicular dendritic cells and T helper cells occurs in the light zone of the germinal center (Figure 2A).[9,17,21] The positive selection of a B cell clone is based on the affinity of their BCR towards antigens displayed on the surface of follicular dendritic cells combined with the positive interaction between B cells and T follicular helper cells resulting in the survival and proliferation of the B cell clone in question (Figure 2A).[9,17,21] However, in cases where the BCR fails to bind the antigen or when an increased self-reactive is acquired apoptosis of the B cell is triggered (Figure 2A).[9,17,21] After repeated cycles of SHM followed by antigen driven selection B cells with progressively higher affinities become more frequent during the adaptive immune response ensuring increasingly effective protection against pathogens (Figure 2A).[3,4,17] To carry out effector or memory functions, B cells in the germinal center must differentiate into plasma cells or memory B cells, respectively (Figure 2A).[7,9,21] Recently activated B cells at the T-B cell border can choose between differentiating into plasma or memory cells or entering the germinal center for affinity maturation (Figure 2A).[7,9,21] In later stages positively selected germinal center B cells can interrupt the re-entry cycle to exit the germinal center as plasma or memory cells.[7,9,21] However, the mechanism by which affinity shapes the differentiation into plasma or memory B cell is not entirely understood.[7,9,21] Recent studies suggest that high affinity B cells preferentially differentiate into plasma cells, whereas those with low affinity tend to differentiate into memory B cells.[22–24]

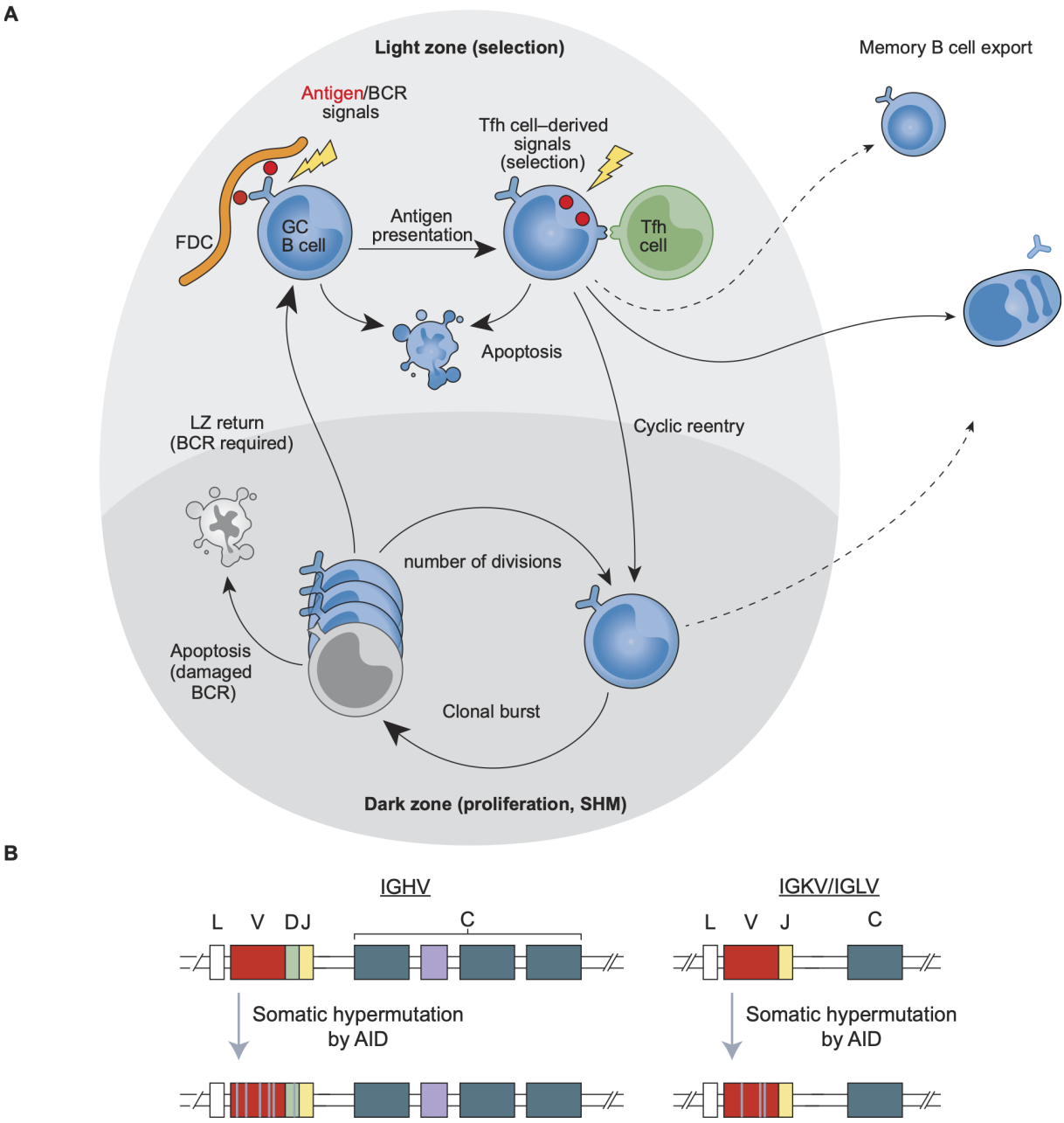

Figure 2. Schematic of germinal center interaction and SHM.

(A) Model depicts key events and decision points in the selection cycle of germinal center B cells. Dotted arrows signify potential transitions. Abbreviations: FDC: follicular dendritic cell, GC: germinal center, SHM: somatic hypermutation, BCR: B cell receptor, LZ: light zone, Tfh: T follicular helper cell, PB: plasma blast, PC: plasma cell. [adapted from *Victora and Nussenzweig, 2022, Annu. Rev. Immunol.*; Figure 2][21] (B) Schematic of AID-dependent SHM in heavy and light chain VDJ-regions. [as described in *Di Noia and Neuberger, 2007, Annu. Rev. Biochem.*][15]

3.1.4. Antibody structure and function

Antibodies are the secreted form of the BCR and belong to the family of immunoglobulins.[4,13,25] They are bivalent, Y-shaped glycoproteins composed of two identical heavy (HC) and light (LC) chains, which are linked by disulfide bridges featuring two identical antigen binding sites (Figure 3A).[4,13,25] Both chains consist of constant (CH or CL for

HC and LC, respectively) and variable regions (VH or VL for HC and LC, respectively).[4,13,25] The N-terminal part of both HC and LC forms the antigen contact side (paratope) in the variable region. At the same time, the C-terminal domain shapes the tail of the constant region, mediating various activities based on the antibody isotype.[4,13,25] A typical HC comprises one VH and up to four CH, weighing approximately 55 kDa, while one VL forms the LC and only one CL, weighing around 25 kDa.[4,13,25] The variable region is created through the process of V(D)J-recombination (see 3.1.2) and refined by affinity maturation (see 3.1.3).[4,13,25] The following description of antibody structure will primarily focus on antibodies of the IgG1 class, one of the four IgG subtypes (IgG1, IgG2, IgG3, IgG4).[4,13,25] The intact antibody comprises two Fragment antigen binding (Fab) regions and one Fragment crystallizable (Fc) region (Figure 3A).[4,13,25] Each Fab, in turn, consists of a pair of VH and VL containing identical paratopes and a pair of CH1 (HC constant region 1) and CL.[4,13,25] The paratope comprises three hypervariable regions known as complementary determining region (CDR), contributed by each VH and VL (Figure 3B).[4,13,25] Among all CDRs, the heavy chain CDR3 region (CDRH3) exhibits the highest variability in length and amino acid sequence as the CDRH3 is positioned at the joining side of the gene segments during VDJ-recombination (Figure 3B). [4,13,25] The three non-hypervariable regions in the VH or VL are termed framework regions (FWR; Figure 3B).[4,13,25] The two Fab regions are coupled by a hinge region, providing the paratope with high conformational flexibility.[4,13,25] In contrast, the glycosylated Fc region is constructed from 2 CH for each HC. It interacts with various receptor molecules, determining how the antibody interacts with different adaptive and humoral immune system components.[4,13,25] The Fc region can mediate antibody-dependent cellular toxicity, antibody-dependent cellular phagocytosis, complement-dependent cytotoxicity, and numerous other effector functions, all achieved by engaging with Fc gamma receptors and a subcomponent of the C1 complement complex.[4,13,25,26] CH can be one of five isotypes (IgM, IgD, IgA, IgG, IgE), with three constant regions for IgA, IgD, and IgG and four for IgE and IgM (Figure 3C).[13,27] An additional J chain is present in IgA and IgM isotypes, allowing the formation of dimers and pentamers, respectively, while the other isotypes remain monomeric (Figure 3C).[13,27] CL, on the other hand, can exist either as κ or λ isotypes.[13,27] IgM antibodies are the first to arise during the adaptive immune response, characterized by lower affinity but high avidity due to multimeric interaction between the IgM pentamer and the antigen (Figure 3C).[13,27] Circulating IgD is seldom found in the serum, and its function remains unclear; however, membrane-bound IgD is thought to influence B cell fate decisions (Figure 3C).[13,28] IgA is present in serum, mucosal surfaces, and secretions such as saliva or breast milk, playing a crucial role in safeguarding mucosal surfaces from bacteria, viruses, or toxins (Figure 3C).[13,27] Although IgE is only found in low quantities in the serum, it plays a major role in hypersensitivity and allergic reactions by binding to receptors

expressed on basophils and mast cells, triggering degranulation and an allergic response (Figure 3C).[13,27] Additionally, IgE contributes to the immune response against parasitic work infections.[13,27] Lastly, IgG, the most prevalent isotype in the serum, has the longest half-life.[13,27] The IgG isotype can activate Fc receptor functions and directly participates in the immune response by binding and neutralizing pathogens (Figure 3C).[4,13,25,26]

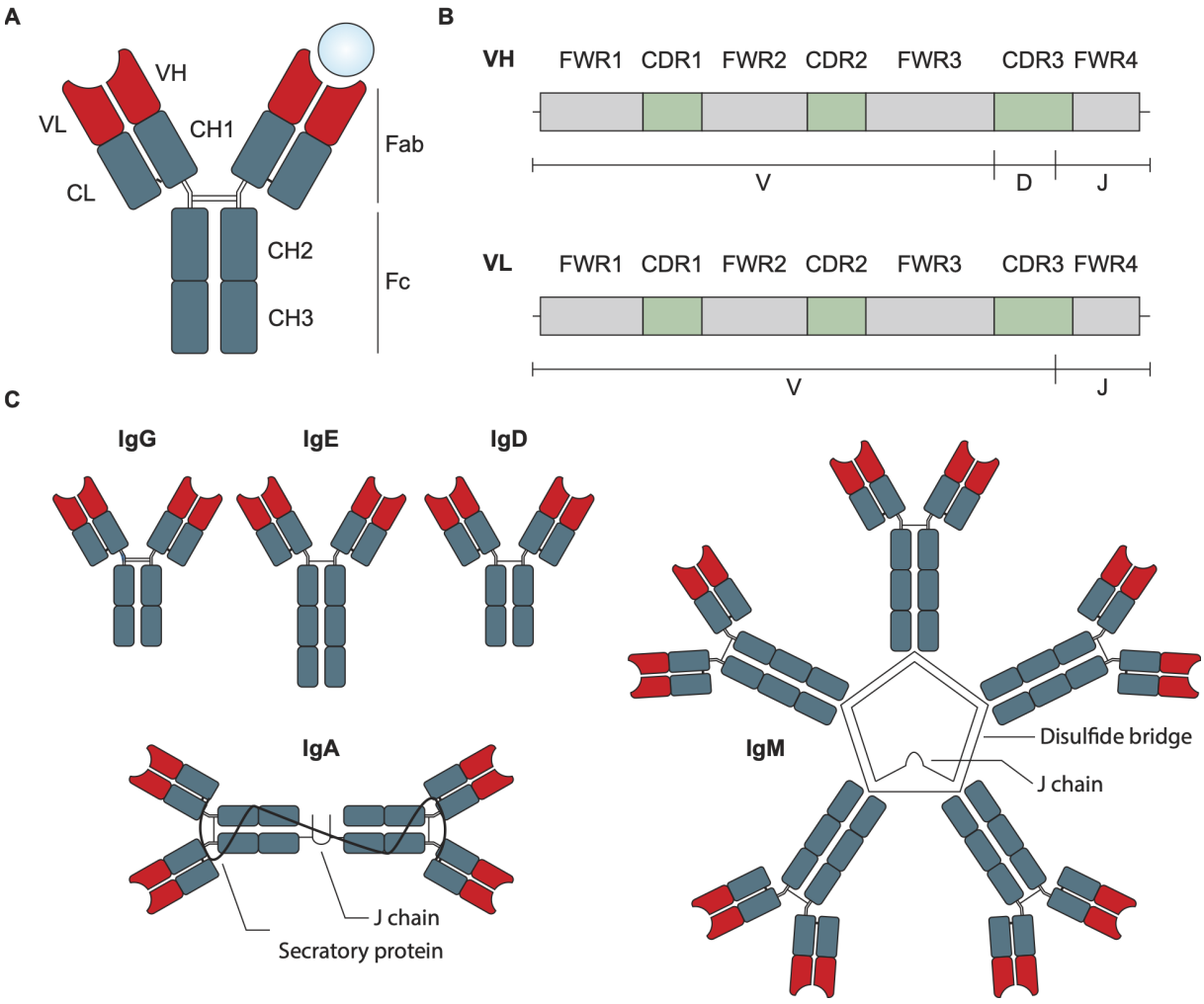

Figure 3. Overview of antibody structure and isotypes.

(A) Antibody structure of IgG isotype with two identical heavy (VH) and light (VL) chain variable regions forming the fragment antigen binding (Fab) along with the first heavy chain constant region (CH1) and the light chain constant region (CL). The fragment crystallizable (Fc) region forms the antibody tail and consists of the heavy chain constant regions two and three (CH2-3). (B) Overview of the variable region for heavy (VH) and light chain (VL), including the framework regions (FWR1-4) and the complementary determining region (CDR1-3). The VH region comprises VDJ segments, while the VL region is only composed of VJ segments. (C) Representation of the five different antibody isotypes. Antibody isotypes may exist in dimeric (IgA) or pentameric (IgM) states linked by a joining chain (J), feature four constant regions (IgE) or be predominantly expressed at the surface of naïve B cells (IgD). [based on *Chiu et al., 2019, Antibodies*][25]

3.2. Severe acute respiratory syndrome coronavirus 2 (SARS-CoV-2)

The severe acute respiratory syndrome coronavirus 2 (SARS-CoV-2) is an enveloped, positive-stranded RNA virus with a 60-140 nm diameter belonging to the coronaviridae family.[29,30] Coronaviruses are widespread pathogens affecting humans and animals. They can be categorized into alpha, beta, gamma, and delta coronaviruses, with the predominant human pathogenic species being NL63 (alpha), 229E (alpha), HKU1 (beta), and OC43 (beta).[31–33] These human coronaviruses can infect the upper and lower respiratory tract, leading to common cold symptoms.[33,34] While most infections with these viruses take a mild course, three life-threatening viral diseases due to the zoonotic spillover of coronaviruses have been recorded in the last two decades.[33–35] This includes the SARS-CoV epidemic that originated in China in 2003, infecting 8094 individuals with 774 related deaths, and the intermittent outbreaks of Middle East respiratory virus (MERS-CoV) in the Middle East with a total of 2.617 confirmed cases and 947 recorded deaths.[36–39] The latest recorded zoonotic spillover was first detected in late 2019 in a market in Wuhan, China, where an outbreak of severe pneumonia of unknown origin hospitalized 41 people by January 2020.[40] These initial cases were confirmed to suffer from COVID-19, a viral pneumonia caused by SARS-CoV-2.[30,41,42] SARS-CoV-2 rapidly spread worldwide and was declared a pandemic on the 11th of March 2020.[43] As of the time of writing this thesis (08.12.2023), 772.138.818 confirmed cumulative cases and 6.985.964 cumulative deaths were recorded by the WHO.[44]

3.2.1. SARS-CoV-2 biology

SARS-CoV-2 is a betacoronavirus that shares a 79% genome sequence similarity with SARS-CoV and 50% with MERS-CoV.[45,46] A phylogenetic analysis performed on the whole genome shows that SARS-CoV-2 clusters with SARS-CoV and SARS-CoV related coronaviruses found in bats with its closest relatives being isolated from horseshoe bats (RaTG13, BANAL-52).[42,46,47] Like other betacoronaviruses SARS-CoV-2 has six functional open reading frames coding for four structural proteins envelope (E), membrane (M), nucleocapsid (N) and spike (S), as well as non-structural proteins ORF1a/ORF1b (open reading frame) which can be proteolytically cleaved into 16 non-structural proteins (nsp) that are essential for replication and viral RNA transcription (Figure 4A).[48] Additionally, seven putative open reading frames encoding accessory proteins are dispersed among the structural genes (Figure 4A).[48] The different structural proteins are responsible for various processes such as viral assembly, genome packaging and viral release, with the S protein specifically facilitating host cell attachment (Figure 4A).[49] The SARS-CoV-2 S is a homotrimeric glycoprotein spanning 1.273 amino acids and is located on the virion's surface giving the virus its crown like shapes (Figure 4B).[46,50] It consists of an S1 subunit, which is

responsible for viral attachment, and an S2 subunit, which facilitates the fusion of viral and host cell membranes (Figure 4C).[51] In its prefusion state, the S1 subunit can be divided into the receptor binding domain (RBD), two C-terminal domains, and the N-terminal domain (NTD), all of which encircle the prefusion S2 subunit.[52] The three RBDs of the trimeric S protein constitute the top of the S protein and can adopt either an receptor-accessible "up" conformation, or a receptor-inaccessible "down" conformation.[52] A polybasic cleavage site (PRRA) located between the S1 and S2 subunits enables efficient cleavage by furin and other proteases such as transmembrane protease serin 2 (TMPRSS2) which is essential for cell-cell fusion and entry into human cells (Figure 4C).[53,54] For cell entry the receptor binding motif (RBM) located in the RBD mediates contact with angiotensin converting enzyme 2 (ACE2), the same receptor as SARS-CoV (Figure 4C).[52] This receptor is also found in different animals including dogs, cats, civets and rhesus monkey suggesting a broad host range.[55] The binding of the S protein to the ACE2 receptor triggers a conformational change in both subunits, bringing the viral and cell membranes closer together.[52] This results in the formation of a fusion pore, allowing the viral genome to enter the cell cytoplasm.[52] Once the viral genome enters the cell ORF1a/ORF1b is translated and proteolytically cleaved into 16 non-structural proteins (nsp) by two cysteine proteases, nsp3 and nsp5.[56] Nsp1 can bind to the human 40S ribosomal subunit and blocking mRNA translation effectively inhibiting the immune response.[57] Nsp2-16 collectively constitute the viral replication and transcription complex, which is responsible for RNA replication and the transcription of subgenomic RNA.[56,58] This subgenomic RNA functions as messenger RNA (mRNA) for both structural and accessory genes.[56,58] The structural proteins along with the genomic RNA are assembled in the endoplasmic reticulum – Golgi intermediate compartment followed by their transport to the cell surface where new virus particles are released through exocytosis.[52,56]

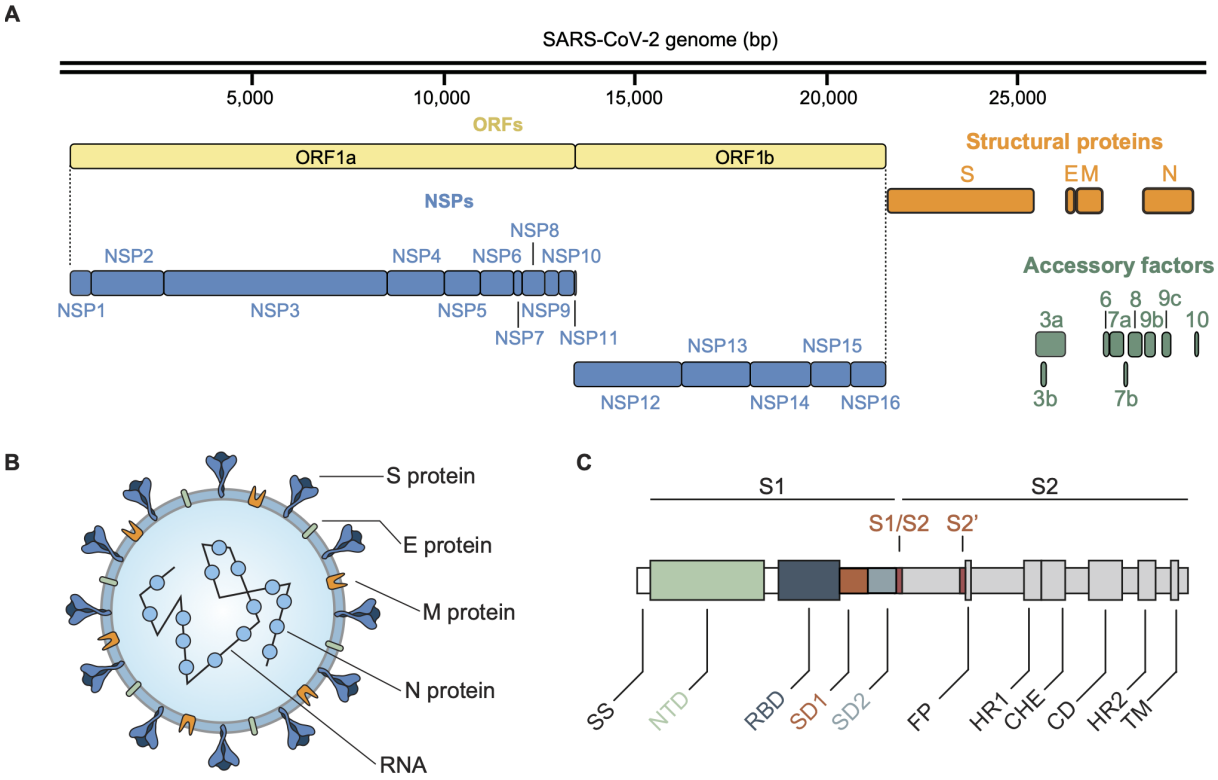

Figure 4. Representation of SARS-CoV-2 genome, virion and S protein structure.

(A) Representation of the SARS-CoV-2 genome including the open reading frames (ORFs) and its non-structural proteins (NSPs), structural, and accessory factors [adapted from *Gordon et al., 2020, Nature; Figure 1*][59] (B) Schematic of a full SARS-CoV-2 virion with the spike (S), envelope (E), membrane (M), and nucleocapsid (N) proteins. [based on *Arya et al., 2021, Journal of Molecular Biology*][49] (C) Schematic of the SARS-CoV-2 S protein. Cleavage cite by host proteases are marked in red. SS: signaling sequence, NTD: N-terminal domain, RBD: receptor-binding domain, SD1/SD2: subdomain 1/2, FP: fusion peptide, HR: heptad repeat, CHE: central helix, CD: connector domain, TM: transmembrane domain, RBM: receptor-binding motif. [adapted from *Gruell et al., 2022, Immunity; Figure 2B*][60]

3.2.2. COVID-19 disease, treatment and prevention

Viral transmission can mainly occurred through liquid droplets expelled during speech or through airborne transmission via aerosol particles emitted by an infected person.[61,62] The high transmissibility of SARS-CoV-2 may be attributed to active viral replication in the upper respiratory tract early during infection.[63] Individuals are presumed to be infectious one to three days before symptom onset and the duration extending several days after infection depending on symptoms.[64–66] Of note, SARS-CoV-2 transmissions exhibit overdispersion, with most individual not contributing to transmissions but rather superspreader events playing a major role in virus spread.[67] SARS-CoV-2 can be diagnosed using reverse transcription real time polymerase chain reaction (RT-qPCR) of viral nucleic acid or by detecting the N protein in a lateral flow immunochromatographic assay commonly known as rapid antigen tests.[68] Additionally, serological test to detect antibodies against the SARS-CoV-2 structural proteins can inform about past virus or antigen exposure.[68] COVID-19

clinical manifestation varies dependent on age and comorbidities.[46] Typically, older men with comorbidities have a higher likelihood of developing severe pneumonia while young individuals and children tend to only experience a mild disease with some being completely asymptomatic.[69,70] Upon infection, the incubation period ranged from two to 14 days, with 5 days being the most frequently observed duration.[71] Predominant symptoms include fever, fatigue and a dry cough with less common symptoms including sore throat, chills, hemoptysis, headache, sputum production, chest pain, anorexia, nausea, diarrhea, and vomiting.[69,70,72] The case fatality rate ranged between 0,1% for South Korea up to 4,9% for Peru.[73] For specific COVID-19 treatment, at the time of writing this thesis, eight options are authorized by the European Medicines Agency consisting of therapies targeting the host immune response (Tozilicumab, Anakinra, Barcitinib), antiviral therapies (Remdesivir, Paxlovid), and neutralizing monoclonal antibodies (Sotrovimab, Casirivimab/Imdevimab, Regdanvimab).[74,75] As for COVID-19 prevention, seven vaccines, two mRNA based vaccines (Comirnaty and Spikevax), two viral vector vaccines (Vaxzevria, Jcovden), and three protein subunit vaccines (Bimervax, VidPrevtyn Beta, Nuvaxovid), are currently authorized by the European Medicines Agency.[74]

3.2.3. SARS-CoV-2 evolution

Similar to many RNA viruses, coronaviruses can undergo rapid evolution with genomic changes taking place over a period of months.[76,77] This evolution is propelled by the generation and dissemination of mutations within the virus population.[76,77] Advantageous and disadvantageous mutations are then filtered by natural selection.[76,77] The speed of viral evolution is fundamentally influenced by the mutation rate and is dependent on the fidelity of the virus polymerase enzyme.[78] Unlike other RNA viruses such as the hepatitis C virus or human immunodeficiency virus, SARS-CoV-2 has a lower mutation rate due to the proofreading mechanism present in the replication machinery of coronaviruses.[78] In the first months of the pandemic SARS-CoV-2 showed only limited adaptation with a single spike substitution, D614G, being the only noticeable evolutionary change in April 2020.[78,79] This virus lineage B.1 (PANGO lineage), characterized by the D614G mutation, rapidly become dominant in Europe, underscoring the heightened fitness of the virus conferred by the D614G mutation.[79–81] From October 2020 divergent SARS-CoV-2 lineages, later termed Alpha (B.1.1.7), Beta (B.1.351), and Gamma (P1), emerged independently in different countries and became dominant variants regionally.[78,79] In May 2021 the World Health Organization (WHO) defined the newly emerged Delta variant (B.1.617.2) as a variant of concern.[82] Delta quickly became the dominant variant globally responsible for wave of transmission and mortality in India in 2021.[82] In late November 2021 the Omicron variant (B.1.1.529) was first discovered in South Africa and rapidly outcompeted the Delta

variant.[78,83] Since its emergence Omicron gave rise to divergent Omicron sublineages (BA.1, BA.2, BA.3, BA.4/5) marking the start of global dominance by successive sweeps of different Omicron sublineages.[78,84] All these variants were distinguished by a higher number of non-synonymous mutations, especially in the spike protein (Figure 5).[79] These mutations resulted in distinct phenotypic properties, such as altered transmissibility and antigenicity, which enhanced viral fitness.[79]

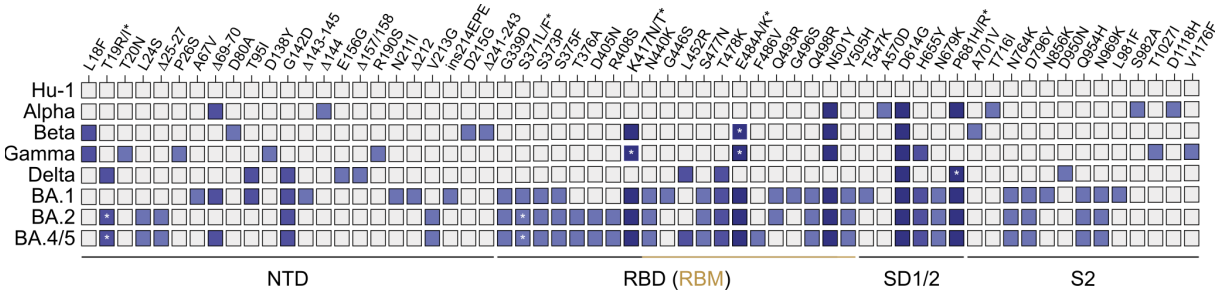

Figure 5. Overview of SARS-CoV-2 variants with highlighted mutations.

Map illustrating SARS-CoV-2 S protein changes in variants of concern related to the ancestral Wu-01 strain. Changes were identified based on prevalence among sequence variants deposited at GISAID[85–87] and aggregated at outbreak.info[88]. Colors indicate the frequency of changes in SARS-CoV-2 variants (light blue for one, blue for two, dark blue for three or more variants with identical changes). Omicron sublineages BA.1, BA.2, and BA.4/5 are represented as one single variant. Amino acid polymorphisms are marked as asterisks. [adapted from *Gruell et al., 2022, Immunity; Figure 2F*][60]

3.3. SARS-CoV-2 humoral immunity

Systemic and mucosal immunity plays a crucial role in combating SARS-CoV-2 infection.[89] Typically, within two to three weeks of symptom onset, nearly all immune-competent individuals infected with SARS-CoV-2 undergo seroconversion, producing antibodies primarily targeting S and N proteins.[90,91] Indicative of protection against COVID-19 are the neutralizing antibody titers, which can block the virus from entering the host cells.[92] Additionally, current vaccines are effective in generating a robust neutralizing antibody response, protecting against hospitalization and death.[93] However, the declining antibody levels over time, coupled with the emergence of viral variants such as Delta and Omicron, contribute to a reduction in vaccine efficacy.[89,94] To enhance the immune response and counteract the decreased antibody levels booster immunization with updated variants are imperative.[93] They can restore disease protection and broaden the immune response, ensuring a sustained defense against SARS-CoV-2.[93]

3.3.1. Antibody response to SARS-CoV-2 infection or vaccination

SARS-CoV-2 infection induced a polyclonal serum response, typically developing 7-14 days after symptom onset.[60,95] Similarly, seroconversion occurs within 14 days of vaccination with any available vaccine.[60,95] However, in some asymptomatic cases, seroconversion might be absent.[60,95] The serum response's main target are the virus's N and S proteins.[60,95] S protein reactive IgG in convalescent and vaccinated individuals is mainly directed against epitopes outside the RBD, with many mAbs being unable to neutralize the virus.[60,95] Serum Ig levels plateau between two to four weeks after infection, after which IgM and IgA levels decline to preinfectional levels while neutralizing mAb titers plateau at three to six weeks post-infection.[60,95,96] The serum neutralization activity is highly dependent on disease severity and response duration.[97] Patients with severe COVID-19 showed elevated titers of RBD binding mAbs and demonstrated strong serum neutralization activity, likely attributed to prolonged and heightened antigen exposure.[97–99] About 1%-5% of infected individuals, so-called “elite neutralizers”, can generate an exceptionally potent neutralizing serum response with broad cross-reactivity towards other betacoronaviruses independently of disease severity.[100,101] In contrast, up to 20% of individuals with mild disease or asymptomatic infection do not exhibit detectable neutralization.[60,98,100] The serum response induced by mRNA vaccination, on the other hand, leads to a more consistent development of a robust immune response.[102,103] Reduced immunogenicity of vaccination can be observed in immunocompromised or elderly patients, while vector-based SARS-CoV-2 vaccines tend to elicit lower titers of neutralizing mAbs.[104,105] A heterologous vaccination with mRNA or protein subunit vaccines can increase the neutralizing serum response.[106,107] With the emergence of viral escape variants displaying a heightened resistance to neutralization, breakthrough infections could be observed.[108] This has prompted the initiation of booster vaccine campaigns and the development of variant-adjusted vaccines to counter infection with immune escape SARS-CoV-2 variants.[109]

3.3.2. Monoclonal SARS-CoV-2 antibodies

SARS-CoV-2 neutralizing antibodies play a pivotal role in providing protection against infection.[92] To treat severe COVID-19 convalescent plasma therapy has been investigated in clinical trials but mostly failed to reduce mortality.[110–112] However, monoclonal antibodies (mAbs), isolated from convalescent or vaccinated individuals, present an attractive option for potential SARS-CoV-2 therapeutics or prophylactics due to their high specificity and neutralization ability.[113] Beyond virus neutralization, mAbs can also engage immune effectors via their Fc domains (see) contributing to disease protection.[114] A multitude of mAbs have been isolated from SARS-CoV-2 convalescent individuals, contributing to a better understanding of the humoral immune response.[115–119] As described in 3.2.2 three of

these mAbs were authorized for clinical use by the European Medicines Agency at the time of writing this thesis.[74] Neutralizing mAbs predominantly target the S protein expressed on the virions surface, with most of them specifically targeting the RBD.[60,120] The most commonly referenced system for RBD targeting mAbs is the Barnes classification, grouping mAbs into four classes based on their S protein binding mode (Figure 6A).[60,120] Class one mAbs bind to the RBM but can only interact with their epitope when the RBD is in an "up" conformation (see 3.2.1; Figure 6A).[60,120,121] Their high neutralization potency is achieved by blocking the S protein from binding to the ACE2 receptor preventing viral entry into the host cell or by mimicking the receptor interaction triggering a conformational change in the S protein from pre- to postfusion state (Figure 6B).[60,120,121] Class two mabs also interact with the RBM, however they are able to bind both "up" and "down" RBD conformations with some able to lock the S protein trimer in an closed "all-RBD-down" state (Figure 6A&B).[60,120,121] Class three mAbs engage with epitopes located distally to the RBM showing no or minimal overlap and are able to bind both "up" and "down" RBD conformations (Figure 6A&B).[60,120,121] While some class three mAbs block ACE2 interactions others hinder binding through steric overlap (Figure 6A&B).[60,120,121] Finally, non-ACE2-competing RBD mAbs targeting a conserved epitope on the RBD fall into class four (Figure 6A).[60,120,121] These mAbs showed broad cross-reactivity but limited neutralization potency as neutralization is achieved through S protein disruption like premature S1 shedding rather than ACE2 blocking (Figure 6B).[60,120,121] Neutralizing mAbs can also target a vulnerable site in the NTD, located in the S1 subunit of the S protein, that can block conformational changes required for virus entry.[60,120] Lastly, the more conserved S2 subunit of the S protein can also be targeted by broadly neutralizing mAbs, preventing the fusion of viral and cellular membrane.[60,120] While the observed antibody response to SARS-CoV-2 infection or vaccination is typically polyclonal, there are instances of a convergent antibody response with public clonotypes utilizing IGHV3-30, IGHV3-53/66, or IGHV1-58 V gene segments observed in different individuals (Figure 6C).[60,122] Interestingly, some isolated mAbs acquired little to no somatic mutations while demonstrating potent SARS-CoV-2 neutralizing activity.[60,118,119,122] Nevertheless, continued SHM has been reported even in the absence of antigen re-exposure as well as the dependence on certain mutations for neutralization activity in some antibodies (Figure 6C).[123–126] Finally, S protein mutations in viral variants play an important role in the antibody response, as mutations in key epitopes can confer antibody resistance, potentially offering a fitness advantage.[79] Consistently, emerged viral variants with mutations in the RBD and the NTD showed reduced sensitivity towards neutralization by mAbs when compared to the ancestral strain.[60]

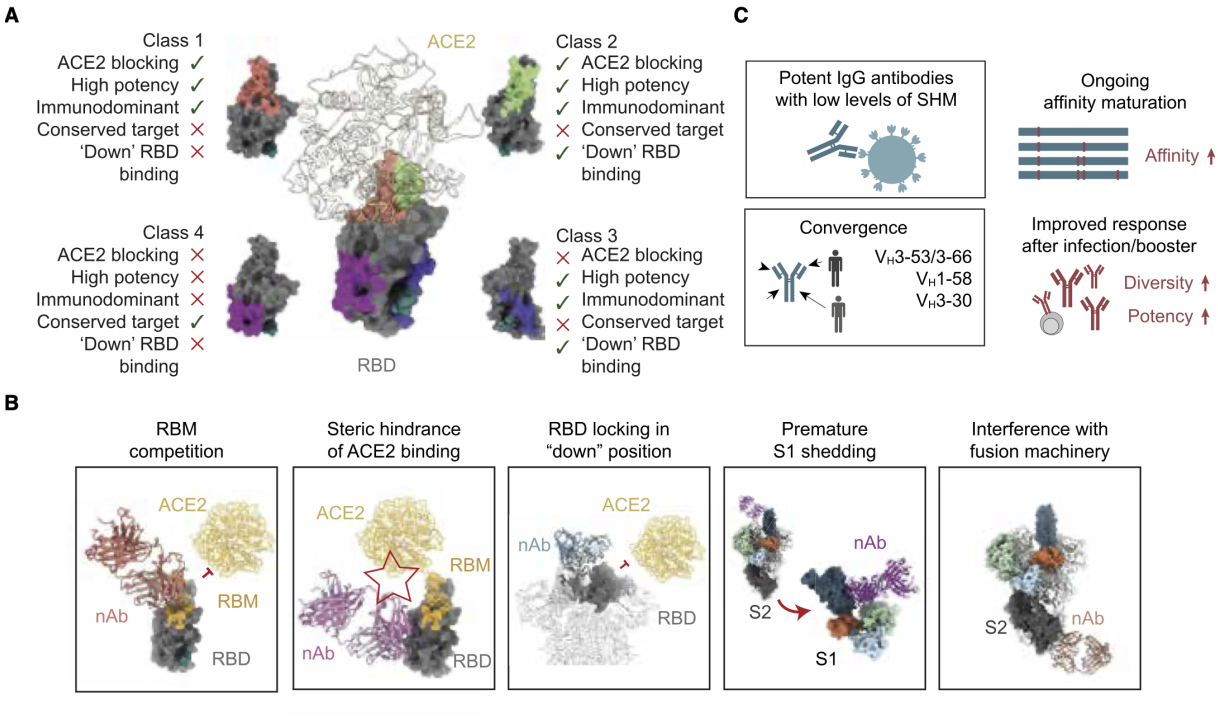

Figure 6. SARS-CoV-2 monoclonal antibody classification and modes of neutralization.

(A) Proposed antibody classification system with 4 classes defined in *Barnes et al., 2020, Nature*.[121] Green ticks represent key features of different RBD targeting antibodies, whilst red crosses mark their absence. [published in *Gruell et al., 2022, Immunity; Figure 2D*][60] (B) SARS-CoV-2 S protein trimeric structure with bound antibodies highlighting the main targets of neutralization activity (RBD, NTD, and S2 domain). [published in *Gruell et al., 2022, Immunity; Figure 2C*][60] SD1/2: subdomain 1/2. (C) Modes of SARS-CoV-2 antibody neutralization. [published in *Gruell et al., 2022, Immunity; Figure 2E*][60] (D) Depiction of several features of the monoclonal antibody response towards SARS-CoV-2 infection. [adapted from *Gruell et al., 2022, Immunity; Figure 1*][60]

3.4. Objective of this thesis

As SARS-CoV-2 spread rapidly, understanding the immune response became crucial for comprehending the disease and developing effective vaccines and treatments. This thesis evaluates the impact of SHM on antibody functionality against SARS-CoV-2 and its effects on different viral escape variants. We first described the longitudinal B cell immune response towards SARS-CoV-2 infection in 7 infected individuals and isolated potent neutralizing mAbs from 12 individuals. We then focused on the impact of SHM on SARS-CoV-2 binding and neutralization in a representative panel of 92 previously isolated mAbs. Lastly, we aimed to investigate the antibody escape profile of several Omicron sublineages (BA.1, BA1.1, BA.2, BA.2.12.1, and BA.4/5) to further guide antibody and vaccine development.

4. Materials and Methods

4.1. Identification of SARS-CoV-2 neutralizing mAbs

Methods and materials described in the following section are adapted from *Kreer et al., 2020, Cell*.[127]

4.1.1. Donors and sampling

The study protocol (protocol 16-054) was approved by the Institutional Review Board of the University of Cologne and the local institutional review boards.[127] Samples from 6 female and 6 male participants (Table S1) were obtained after written informed consent was provided for either a single blood draw or longitudinal follow-up.[127] Recruitment sites were Munich Clinic Schwabingen (IDMnC1, IDMnC2, IDMnC4, IDMnC5), the University Hospital of Frankfurt (IDFnC1-2), the University Hospital Cologne (IDCnC2) and as outpatients in the county Heinsberg (IDHbnC1-5).[127] Estimation of sample size to inform on B cell receptor repertoires and yield neutralizing antibodies was based on previous studies.[128–130]

4.1.2. PBMCs, plasma, and IgG isolation

Blood draws were conducted using EDTA tubes and/or syringes filled with heparin. Using Leucosep centrifuge tubes (Greiner Bio-one) containing density gradient separation medium (Histopaque; Sigma-Aldrich), plasma and peripheral blood mononuclear cells (PBMCs) were isolated as per the manufacturer's instruction.[127] To isolate IgG, 1 ml of heat-inactivated plasma (56°C for 40 minutes) was incubated overnight at 4°C with Protein G Sepharose (GE Life Sciences).[127] Following incubation, the Protein G suspension was transferred to chromatography columns (BioRad) and washed with phosphate-buffered saline (PBS).[127] Elution of IgGs was done using 0,1 M glycine (pH3) into 0,1 M Tris (pH8) for buffering.[127] Amicon spin membranes (30kDa; Millipore) were used for buffer exchange to PBS.[127] A UV/Vis Spectrophotometer (NanoDrop One; Thermo Fisher Scientific) was used with the Protein A280 method to measure the purified IgG concentration.[127] Samples were stored at 4C°.

4.1.3. SARS-CoV-2 S protein expression and purification

The SARS-CoV-2 S ectodomain construct (amino acids 1-1208 of SARS-CoV-2 S; GenBank: MN908947) was generously provided by Jason McLellan (Texas, USA).[51,127] In detail, to stabilize the prefusion state, two proline substitutions were made at residues 986 and 987, the furin cleavage site was replaced with a "GSAS" substitution at residues 682-685, and a C-terminal T4 fibritin trimerization motif was introduced.[127] A C-terminal

TwinStrepTag and 8XHisTag were added to purify the S protein. The S protein was produced by transient transfection of 1 µg DNA per 1 ml of FreeStyle 293 medium (Thermo Fisher Scientific) using polyethylenimine (PEI; Sigma-Aldrich) at a medium cell density of $0{,}8x10^6$ cells/mL.[127] After 7 days of culture at 5% CO_2 and 37C°, the supernatant was collected and filtered through a 0,45µm polyethersulfone filter (PES; Thermo Fisher Scientific).[127] Strep-Tactin affinity chromatography (IBA Lifescience) separated the targeted protein from the harvested supernatant per the manufacturer's instructions.[127] In brief, the filtered supernatant was adjusted to pH 8 using 100ml of 10x Buffer W (1 M Tris/HCl, pH 8, 1,5 M NaCl, 10 mM EDTA; IBA Lifescience) and loaded on a column with 5ml bed volume of Strep-Tactin resin (IBA Lifescience) using a low-pressure pump adjusted to 1ml/min.[127] The column was washed with 15 column volumes of 1x Buffer W (IBA Lifescience) after the filtered supernatant passed through and then eluted with 6x2,5 ml of 1x Buffer BXT (IBA Lifescience).[127] Finally, the buffer was exchanged for PBS (Thermo Fisher Scientific) using a 100 kDa cut-off cellulose centrifugal filter (Merck).[127]

4.1.4. Production of SARS-CoV-2 S protein subunits and EBOV glycoprotein

The plasmid of SARS-CoV-2 S protein RBD (amino acids 319-541 of SARS-CoV-2 S; GenBank: MN908947) fused to a 6xHisTag was kindly provided by Florian Krammer.[131] For protein production, HEK293-T cells were transiently transfected using calcium phosphate.[127] Culture supernatant was harvested and filtered through a 0,45µm PES filter (Thermo Fisher Scientific) filter after 7 days of culture at 37C° and 5% CO_2.[127] The target protein was purified from the harvested supernatant using Ni-NTA agarose (Macherey-Nagel).[127] In brief, Ni-NTA beads were equilibrated with NPI10 (1xNPI10 buffer: 50mM NaH2PO4, 300mM NaCl, 10mM imidazole, pH8) and added to the harvested supernatant (1ml bed volume per 1000ml original culture supernatant), which was previously mixed with 2x NPI10 buffer in a 1:1 ratio.[127] The beads were incubated at 4C° overnight under constant rotation. For the harvest, beads were centrifuged at 500 g for 5 min at 4C°, washed twice in NPI10 (100ml per 1000ml original culture supernatant), and centrifuged again at 500g for 5 min at 4C°.[127] After washing the beads three times in NPI20 (50 mM NaH2PO4, 300mM NaCl, 20mM imidazole, pH8), they were transferred to Polyprep chromatography columns (BioRad) and washed with 10ml NPI20.[127] 5ml of NPI250 (50mM NaH2PO4, 300mM NaCl, 250mM imidazole, pH8) was used for elution. The buffer was exchanged to PBS using 10 kDa Amicon spin columns (Millipore).[127]

The SARS-CoV-2 S ectodomain monomer lacking the trimerization domain (amino acids 1-1207 of SARS-CoV-2 S; GenBank: MN908947) and the SARS-CoV-2 S1 subunit (amino acids 14-529 of SARS-CoV-2 S; GenBank: MN908947) were amplified by PCR from the

SARS-CoV-2 S ectodomain (amino acids 1-1208 of SARS-CoV-2 S; GenBank: MN908947) plasmid described in 4.1.3.[51,127] The amplified PCR product was then cloned into a modified sleeping beauty transposon expression vector, which included a C-terminal thrombin cleavage site and a TwinStrepTag.[127] Stable HEK293 EBNA cell lines were generated using the sleeping beauty transposon system for recombinant protein production.[127,132] In brief, HEK293 EBNA cells were transfected with the expression plasmids using FuGENE HD transfection reagent (Promega).[127] Following puromycin selection, the transfected cells were induced with doxycycline.[127] The supernatant was then collected and filtered, and the target protein was isolated using StrepTactin resin (IBA Lifescience).[127] Isolated proteins were eluted from the resin using biotin-containing TBS buffer (IBA Lifescience), and the buffer was exchanged for TBS by dialysis.[127] The EBOV protein (amino acids 1-651 of EBOV Makona; GenBank: KJ660347) and the HIV-1 gp140 (amino acids 1-683 of HIV-1 strain YU2; GenBank: M93258), both without a transmembrane domain but including a GCN4 trimerization domain[130] were expressed by transient transfection following the same protocol described in 4.1.3.[127] For protein purification with Ni-NTA agarose (Macherey-Nagel), the same protocol described in 4.1.4 was used.[127]

4.1.5. Isolation of SARS-CoV-2 S protein reactive B-cells

CD19-microbeads (Miltenyi Biotec) were used to isolate B cells following the manufacturer's instructions.[127] Using a fluorescence staining mix containing 4',6-diamidino-2-phenylindole (DAPI; Thermo Fisher Scientific), anti-human CD20-Alexa Fluor 700 (Becton Dickinson), anti-human IgG-APC (Becton Dickinson), anti-human CD27-PE (Becton Dickinson) and DyLight488-labeled SARS-CoV-2 S protein (10µg/mL) B cells were stained on ice for 20 min.[127] With a FACSAria Fusion (Becton Dickinson) $Dapi^-$, $CD20^+$, IgG^+, SARS-CoV-2 S protein positive B cells were sorted into 96-well plates prefilled with 4µl lysis buffer consisting of 10 mM DTT (Thermo Fisher Scientific), 0,5 U/µL RNAsin (Promega), 0,5x PBS, and 0,5 U/µL RNaseOUT (Thermo Fisher Scientific).[127] Plates were immediately stored at -80C° until subsequent processing.[127]

4.1.6. Amplification and analysis of antibody sequences

The amplification protocol of antibody heavy and light chains can be found in previous publications.[128,133,134] In brief, RT-PCR was performed with Random Hexamers (Invitrogen), Superscript IV (Thermo Fisher Scientific), RNaseOUT (Thermo Fisher Scientific), and RNasin (Promega).[127] An optimized V gene primer set was used for a sequential semi-nested amplification of antibody chains from cDNA using a PlatinumTaq HotStart polymerase (Thermo Fisher Scientific) with a 6% KB extender.[127,133] Gel electrophoresis was performed to identify PCR products with the correct size.[127] Sanger sequencing of PCR

product with the correct size was done by Eurofins PlateSeq Service.[127] Sequence chromatograms passed quality control with a minimal sequence length of 240 nucleotides and a mean Phred score of 28.[127] Subsequently, the sequences were annotated using IgBLAST, and the variable region from FWR1 to the end of the J gene was extracted.[127,135] Base calls with a Phred score below 16 within the variable region were masked.[127] Sequences were omitted from subsequent analysis if stop codons, frameshift mutations, or more than 15 masked nucleotides were detected.[127] For clonal assessment, productive heavy chain sequences were categorized individually for each patient based on matching VH/VJ gene pairs.[127] Levenshtein distances were calculated pairwise for their CDRH3s, and clonal members were identified based on a minimum CDRH3 amino acid identity of ≥75%, beginning from a randomly selected sequence.[127] The clonal assignment was conducted 100 times, and the outcome with the fewest remaining unassigned (non-clonal) sequences was chosen for further analysis.[127] The study investigators independently validated all identified clones.

4.1.7. NGS sequencing of naïve control B-cell repertoire

The amplification protocol using an unbiased template-switch based approach for the B cell receptor repertoire sequencing can be found in.[127,128,130] In brief, CD19+ cells from 48 healthy individuals (samples were collected at the Transfusion Medicine department of the University Hospital of Cologne under protocol 16-054) were enriched with CD19-microbeads (Miltenyi Biotec).[127] Using a FACSAria Fusion (Becton Dickinson), 100.000 $CD20^{+}IgG^{+}$ and 1.000.000 $CD20^{+}IgD^{+}IgM^{+}CD27^{-}IgG^{-}$ B cells were sorted into FBS (Sigma-Aldrich) for each of the 48 individuals. RNA was isolated using the RNeasy Micro Kit (Qiagen) on a QiaCube instrument (Qiagen), and according to the SMARTer RACE 5'/3' manual, cDNA was synthesized by template-switch reverse transcription.[127] This process utilized SMARTScribe Reverse Transcriptase (Takara) with a template-switch oligo that included an 18-nucleotide unique molecular identifier (UMI).[127] The variable regions of antibody heavy and light chains were amplified using a constant region-specific nested PCR.[127] Following library preparation, sequencing was performed on the Illumina MiSeq platform with read lengths of 300 bp.[127] The raw NGS reads were then pre-processed and assembled using an in-house pipeline, which used IgBLAST[136], Clustal Omega[137], and the pRESTO toolkit[138] with a custom Python script as previously described.[127,130] In brief, raw reads with a sequence length of ≥ 250 bp and a mean Phred score of ≥ 25 were filtered, and UMIs were extracted.[127] Paired reads were pre-annotated using IgBLAST[135]. An additional molecular identifier (MID) was created by taking 18 nucleotides, starting with 12 nucleotides downstream of the end of framework region 3 (FWR3).[127] Raw reads with the same UMIs were grouped for error correction.[127] Reads were excluded from their UMI group if their V

gene call did not match the most common V gene or had ≥1 nucleotide difference compared to other reads.[127] The remaining single reads, as well as the excluded ones, were regrouped using their MID, as errors in RT, PCR, or sequencing within the UMI could account for ungrouped or excluded reads.[127] New UMI groups were established based on MID groups with a unique V gene and no more than 1 nucleotide difference among included UMIs.[127] All reads within a corrected UMI group were aligned using Clustal Omega[137] and collapsed to form a consensus read.[127] The consensus was determined by selecting base calls with the highest quality-weighted (1 – error probability) frequencies.[127] Paired consensus reads were then assembled using the pRESTO AssemblePairs module[138], with a minimal overlap set to 6 nucleotides, and annotated with IgBLAST[135].[127] Only productive sequences were saved for downstream analysis.[127] NGS-derived sequences with ≥3 reads in a UMI group were used in the analysis to minimize the effect of sequencing and/or PCR errors.[127] A maximum of one amino acid length difference and ≤3 amino acid differences in the CDR3s were considered similar for identifying overlapping clonotypes.[127]

4.1.8. Cloning and expression of mAbs

The protocol for antibody cloning from 1st PCR products by sequence and ligation independent cloning (SLIC) can be found in.[127,128,139,140] In brief, Q5 Hot Start High Fidelity DNA Polymerase (New England Biolabs) was used to amplify the DNA, using 1µl of the first PCR product along with specific forward and reverse primers that include overhangs for subsequent SLIC into expression vectors (IgG1, Igλ, Igκ).[127,139] The second amplification for SLIC assembly was carried out using extended forward primers that cover the endogenous leader sequence of all V genes, along with reverse primers targeting the 5' end of the constant regions from an optimized primer set.[127,133] The PCR cycle included 98C° for 30s, 35 cycles at 98C° for 10s each, 72C° for 45s and 72C° for 2min.[127] Using the NucleoSpin 96 PCR Clean-up kit (Macherey Nagel), PCR products were purified and cloned into expression vectors by SLIC using T4 DNA polymerase (New England Biolabs) and competent Escherichia coli DH5a.[127] After colony PCR, gel electrophoresis of colony PCR fragments and subsequent Sanger sequencing positive clones were inoculated with 50ml LB-Medium (1L distilled water, 10g tryptone (Carl Roth), 5g yeast extract (Carl Roth), 5g NaCl (Carl Roth)) and plasmids isolated using the NucleoBond Xtra Midi kit (Macherey Nagel) as per manufacturers instruction.[127] Purified expression plasmids of the heavy and light chains were transiently co-transfected with PEI (Sigma-Aldrich) into HEK293-E cells maintained in FreeStyle 293 Expression Medium (Thermo Fisher Scientific) supplemented with 0,2% penicillin/streptomycin (Thermo Fisher Scientific) for mAb production.[127] Cells were cultivated at 37°C, 6% CO2, and kept under constant shaking at 90-120 rpm for 7 days.[127] The supernatant was collected by centrifugation after 7 days.[127] To purify mAbs, the

harvested supernatant was incubated overnight with Protein G-coupled Sepharose beads (GE Life Sciences).[127] The supernatant was transferred onto Polyprep chromatography columns (BioRad) and washed with DPBS (Thermo Fisher Scientific).[127] Antibodies were then eluted from the resin using 0,1 M glycine (pH3) and buffered with 1 M Tris (pH8).[127] The buffer was exchanged to PBS using Amicon spin membranes (Millipore) (Thermo Fisher Scientific).[127] Purified mAb concentration was measured using a UV/Vis Spectrophotometer (NanoDrop One; Thermo Fisher Scientific) with the Protein A280 method, and samples were stored at 4°C.[127]

4.1.9. SARS-CoV-2 S protein ELISA

For ELISA, 2µg/ml of SARS-CoV-2 protein (S protein trimer, RBD, N-terminal truncated S1) in PBS (Thermo Fisher Scientific) or in 2M Urea (spike ectodomain monomer) were coated on ELISA microplates (Corning 3369) overnight at 4°C.[127] For the SARS-CoV-2 spike ectodomain ELISA, 5% BSA in PBS (Thermo Fisher Scientific) was used for blocking at room temperature for 60min.[127] Plates were then incubated with primary antibody diluted in 1% BSA in PBS for 90 min and washed 3 times with T-PBS containing 0,02% Tween (Carl Roth).[127] Washed Plates were incubated with anti-human IgG-HRP (Southern Biotech 2040-05) diluted 1:2500 in 1% BSA in PBS for another 60min at room temperature.[127] ELISA plates were washed a final time and developed using ABTS solution (Thermo Fisher Scientific).[127] An ELISA microplate reader (Thermo Fisher Scientific) was used to measure absorbance at 415 and 695 nm.[127] Using a non-linear fit model (agonist vs. response – variable slope [four parameters]) in Prism (GraphPad), EC_{50} values were calculated from the absorbance data.[127] An OD>0,25 and an EC_{50}<30 µg/ml were defined as positive binding. ELISA for the SARS-CoV-2 subunits was done following a published protocol.[127,131] Using the automated platform Euroimmun Analyzer 1 with the commercial anti-SARS-CoV-2 ELISA kit for immunoglobulin class G provided by Euroimmun (Euroimmun Diagnostik), antibody detection was performed per the manufacturer's instruction.[127] A concentration of 50 µg/ml for mAb and 2 mg/ml for plasma IgG was used for detection.[127]

4.1.10. SARS-CoV-2 virus neutralization test

Live SARS-CoV-2 neutralization assays with poly-IgG or mAbs samples were done based on a published protocol for MERS-CoV.[127,141] In brief, samples were serially diluted in 96 well plates following a 1h incubation at 37°C together with 100 50% tissue culture infectious doses ($TCID_{50}$) of SARS-CoV-2 (BavPat1/2020 isolate, European Virus Archive Global #026V-03883).[127] A 1500 µg/ml starting concentration was used for plasma IgG and 100 µg/ml for mAbs.[127] Cytopathic effects were analyzed after 4 days of incubation with VeroE6 cells (ATCC CRL-1586).[127] Neutralization was defined as the complete absence of

cytopathic effects compared to virus controls.[127] A neutralizing COVID-19 patient plasma was used in duplicates as a positive control for the inter-assay neutralization standard.[127]

4.1.11. Surface plasmon resonance measurements

Using a Superdex200 10/300 column (GE Healthcare) for size exclusion chromatography, the RBD was purified for surface plasmon resonance (SPR) measurement.[127] With a Biacore T200 instrument (GE Healthcare), the binding of antibodies to the RBD was measured in single-cycle kinetics experiments.[127] Purified mAbs were immobilized on a series S sensor chip protein A (GE Healthcare) in PBS and 0,02% sodium azide buffer at coupling densities of 800-1200 response units.[127] A series of soluble RBD in PBS was injected at different concentrations (i.e., 0,8, 4, 20, 100, and 500 nM) into the flow cells on the sensor chip at a flow rate of 60 µl/min.[127] From four flow cells on the sensor chip, one was empty to serve as a blank.[127] Regeneration of the sensor chip was done using 10 mM Glycine-HCL pH1,5 buffer.[127] To describe the experimental data and to derive antibody kinetic parameters, a 1:1 binding model was used.[127] In cases where a 1:1 binding model did not adequately describe the binding kinetics of a mAb, a two-state binding model assuming two binding constants due to conformational change was used.[127] Only the first binding constants (K_D^1) were reported in these cases.[127]

4.1.12. HEp-2 cell assay

mAbs were tested using the NOVA Lite HEp-2 ANA Kit (Inova Diagnostics) at 100 µg/ml concentration in PBS with positive and negative kit controls on each substrate slide according to the manufacturer's instructions.[127] For additional controls, antibodies with known reactivity profiles targeting HIV-1 were included.[127] Using a DMI3000 B microscope (Leica), images were acquired at an exposure time of 3,5 s, intensity of 100%, and a gain of 10.[127]

4.1.13. Quantification and statistical analysis

FlowJo10 was used for flow cytometry analysis and quantification. Statistical analyses were done using Python (v3.6.8)[142], R (v.4.0.0)[143], GraphPad Prism (v7), and Microsoft Excel for Mac (v14.7.3).[127] Linear Mixed Effects Model (R-function nlme::lme())[144] was applied to the combination of all longitudinal data points with individuals having their own intercept to test for a significant increase in S-reactive B cells over time (Figure 9C).[127] Antibody characteristics, including V gene usage, V gene germline identity distribution for clonal sequences, CDRH3 length, and CDRH3 hydrophobicity using the Eisenberg scale,[145] were determined for all input sequences without further clonal collapsing (Figure 9E).[127]

D'AgostinoPearson normality test (Prism, GraphPad) was used to test for normality before a Wilcoxon matched-pairs signed rank test (Prism, GraphPad) on κ/λ ratios of each subset to test for a significant difference of κ/λ ratios between clonal versus non-clonal sequences (Figure 10).[127] Collapsed clonal sequences were used for V gene analysis between neutralizer and non-neutralizer (Figure 11G).[127] Spearman's rank correlation coefficients were calculated in Prism (GraphPad) for correlation analysis (Figure 11E and Figure 12).[127] Using standard parameters, a multiple sequence alignment for the longitudinal analyses on mutation frequencies of recurring B cell clones (Figure 15A) was calculated with Clustal Omega (version 1.2.3; Figure 15A)[137].[127] From the multiple sequence alignment, a phylogenetic tree was built with RAxML through the raxmlGUI (version 2.0.0-beta.11)[146] using the GTRGAMMA substitution model (RAxML version 8.2.12)[147].[127] All variants of a clone at a time point were paired with variants at consecutive time points based on the phylogenetic tree distances and the slope between the pairs computed.[127] Hamming distances between pairs were calculated and normalized for sequence length and time difference to calculate the mean mutation frequency per day.[127] A one-sided Wilcoxon Signed Rank Test was used to test if the slopes are equal to zero, given the median slope per clone and the alternative hypothesis that the slopes are smaller than zero.[127] For visualizing VH gene germline identity change over time, the identity of each clone was normalized by its median value at the first-time measurement, and the median slope was plotted (Figure 15A).[127] D'Agostino-Pearson normality test (Prism, GraphPad) was used, followed by a two-tailed unpaired Mann-Whitney U test (Prism, GraphPad) to test for a difference in VH gene germline identity between neutralizing antibodies isolated at early or late time points (8-17 and 34-42 days).[127]

4.2. Impact of SHM on SARS-CoV-2 neutralizing mAbs

Methods and materials described in the following section 4.2 are adapted from *Korenkov et al., 2023, Immunity*.[148]

4.2.1. mAb selection

SARS-CoV-2 neutralizing mAbs were randomly selected from the Coronavirus Antibody Database (CoV-AbDab; i.e., 319 SARS-CoV-2 neutralizing antibodies with complete heavy and light chain sequences from human B cell; retrieved on 20.01.2021)[149] as well as from previously isolated antibodies.[127,148] Antibodies were tested in a Wuhan-Hu1 S protein pseudo-typed lentivirus neutralization assay (see 4.2.8) and included in further analyses if antibodies achieved an IC_{50} of at least 20 µg/ml.[148] This yielded a final set of 92 antibodies.[148] 17 additional antibodies from the CoV-AbDab (retrieved on 09.09.2021) and

our own study have been selected for an in-depth analysis of the IGHV1-58 public clonotype.[101,148,149]

4.2.2. Reversion of SHM

Amino acid sequences of selected antibodies were annotated using igblastp (igblast v1.16.0) and reverse translated using the reverse translate tool from the Sequence Manipulation Suite.[135,148,150] Downloaded sequences were codon optimized using Geneious Prime (Biomattes) and stored for further processing. Germline reversion of mAbs was done using the most probable V gene derived from igblastp (igblast v1.16.0)[135] as a template while adding the original CDR3 and FWR4 regions to the germline V gene sequence.[148]

4.2.3. Sequence analysis

Mutations were counted from FWR1 to FWR3, excluding any mutations in the CDR3 and FWR4 regions based on the most probable V gene derived from igblastp (igblast v1.16.0)[135] results.[148] Mature and germline antibody sequences were aligned using the PairwiseAligner object implemented in biopython (v1.77)[151] using the BLOSUM62 substitution matrix, an open_gap_score of -10 and extend_gap_score of -0.5.[148] Mutations were defined as all alignment mismatches, including deletions or insertions. Antibody mutations were matched to their respective CDR or FWR region according to the boundaries annotated by igblastn (igblast v1.16.0).[135,148] For clonal analysis, sequences were grouped according to the same VH gene and a minimal CDRH3 identity (Levenshtein distance in relation to the length of the shorter CDRH3 identity) of ≥75%.[148] Using the Eisenberg scale, CDRH3 hydrophobicity was calculated.[145,148] Multiple sequence alignments were created with Clustal Omega (v1.2.3) and logo plots drawn using a custom python script with Matplotlib (v3.3.4).[137,148,152]

4.2.4. Cloning and production of mAbs

Antibody heavy and light chain sequences, including overhangs designed for subsequent cloning into expression vectors (IgG1, Igλ, Igκ), were ordered as eBlocks gene fragments (IDT).[148] Detailed methods on mAbs cloning and production are described in 4.1.8 or in Korenkov et al., 2023, Immunity.[148] In contrast to the method described in 4.1.8 a murine leader sequence encoded in the vector was used for secretion instead of the endogenous leader.[148]

4.2.5. SARS-CoV-2 spike protein production

The following coronavirus proteins were cloned into a modified Sleeping Beauty transposon expression vector[132]: Wu01 S protein (GenBank: MN908947; amino acids: 1-1207; RRAR to

GGGG; K986P; V987P; C-terminal T4 foldon – Twin-Strep-tag; 139 kDa); SARS-CoV-2 HexaPro BA.1 S protein (GenBank: MN908947; amino acids: 16-1208, furin site: RRAR to GSAS, A76V, delta69-70, T95I, G142D, delta143-145, N211I, delta212, 215EPEins, G339D, S371L, S373P, S375F, K417N, N440K, G446S, S477N, T478K, E484A, Q493R, G496S, Q498R, N501Y, Y505H, T547K, D614G, H655Y, N679K, P681H, N764K, D796Y, N856K, Q954H, N969K, L981F, including the stabilizing mutations: F817P, A892P, A899P, A942P, K986P, V987P, N-terminal BM40 signal peptide, C-terminal T4 foldon followed by a Twin strep tag, 139 kDa); SARS-CoV-2 Delta S protein (GenBank: MN908947; amino acids:1-1207; RRAR to GGSG; T19R, G142D, R156G, delta157-158, L450R, T476K, D612G, P679R, D948N, K986P, V987P, N-terminal BM40 signal peptide, C-terminal T4 foldon followed by a Twin strep tag, 139 kDa); OC43 S protein (GenBank: AAX84792; amino acids: 1-1300; RRSRR to GSAS; A1078P; L1079P; C-terminal T4 foldon – Twin-Strep-tag; 150 kDa); 229E S1 protein (GenBank: BAL45639; amino acids: 22-539, N-terminal BM-40 signal peptide – Twin-Strep-tag; 61 kDa) HKU1 S1 protein (GenBank: YP_173238; amino acids: 14-612, N-terminal BM-40 signal peptide – Twin-Strep-tag; 72 kDa) and NL63 S1 protein (GenBank: AKT07952; amino acids: 16-619, N-terminal BM-40 signal peptide – Twin-Strep-tag; 71 kDa).[148] Stable HEK293 EBNA cell lines were generated using the sleeping beauty transposon system for recombinant protein production.[132,148] HEK293 EBNA cells were co-transfected with the expression- and a transposase plasmid (10:1) using FuGENE® HD transfection reagent (Promega) in DMEM/F12 supplemented with 6% FBS.[148] Cells were expanded in triple flasks after high puromycin selection (3 µg/ml; Sigma-Aldrich).[148] Protein production was induced using doxycycline (0,5 µg/ml; Sigma-Aldrich).[148] After 3 days, supernatants were harvested, and protein was purified via a Strep-Tactin®XT (IBA Lifescience) resin according to the manufacturer's instruction.[148] After elution with biotin-containing buffer (IBA Lifescience), proteins were dialyzed against TBS and stored at 4°C or -80°C.[148]

4.2.6. ELISA

Methods on ELISA can be found in 4.1.9 or in *Korenkov et al., 2023, Immunity*.[148] For SARS-CoV-2 S protein ELISA, AUC values were calculated using Prism 9 (total peak area above baseline; GraphPad) and normalized to the AUC of a control antibody (HbnC3t1p2_B10) running on every plate.[148] Normalization of human coronavirus ELISA AUC was done using the AUC of Streptactin-HRP (IBA Lifescience) running on every plate.[148]

4.2.7. SARS-CoV-2 pseudovirus cloning and production

SARS-CoV-2 Wu01 S protein (GISAID: EPI_ISL_406716) was codon optimized and cloned into a pCDNA3.1/V5-HisTOPO vector (Thermo Fisher Scientific) as described

previously.[100,101,148] S protein variants were cloned by introducing mutations in the Wu01 S protein expression vector using the Q5® Site-Directed Mutagenesis Kit (New England Biolabs) and/or the NEBuilder HiFi DNA Assembly Kit (New England Biolabs) as per the manufacturer's instructions.[148] The following amino acid changes relative to Wu01 were included: Alpha (B.1.1.7): D69-70, D144, N501Y, A570D, D614G, P681H, T716I, S982A, D1118H.[148] Beta (B.1.351): D80A, D215G, D242-244, K417N, E484K, N501Y, A570D, D614G, A701V.[148] Delta (B.1.617.2): T19R, G142D, D156-157, R158G, L452R, T478K, D614G, P681R, D950N.[148] Omicron sublineage (BA.1): A67V, D69-70, T95I, G142D, D143-145, N211I, D212, ins215EPE, G339D, S371L, S373P, S375F, K417N, N440K, G446S, S477N, T478K, E484A, Q493R, G496S, Q498R, N501Y, Y505H, T547K, D614G, H655Y, N679K, P681H, N764K, D796Y, N856K, Q954H, N969K, and L981F.[148] Omicron sublineage (BA.2): T19I, D24-26, A27S, A67V, G142D, V213G, G339D, S371F, S373P, S375F, T376A, D405N, R408S, K417N, N440K, S477N, T478K, E484A, Q493R, Q498R, N501Y, Y505H, D614G, H655Y, N679K, P681H, N764K, D796Y, Q954H, N969K.[148] Expression plasmid for Wu01, BA.2.12.1, and BA.4/5 had a C-terminal deletion of 21 cytoplasmic amino acids for increased pseudovirus titers.[148] All plasmid sequences were verified by Sanger sequencing.[148] A lentivirus construct was used to produce pseudovirus particles, as described previously.[100,148,153,154] In brief, for the pseudovirus production individual plasmids encoding SARS-CoV-2 spike construct, HIV-1 Tat, HIV-1 Gag/Pol, HIV-1 Rev and firefly luciferase IRES-ZsGreen were co-transfected in HEK293-T cells using FuGENE 6 Transfection Reagent (Promega) in Dulbecco's Modified Eagle Medium (DMEM; Thermo Fisher Scientific).[148] After 48h and 72h post-transfection, culture supernatant was harvested, centrifuged, clarified using a 0,45 µm filter, and stored at -80°C until further use.[148] The harvested pseudovirus supernatant batches were titrated by infecting ACE2-expressing HEK293-T cells.[148] After 48h of incubation at 37°C and 5% CO2, the luciferase activity was determined by the addition of luciferin/lysis buffer (10 mM MgCl2, 0,3 mM ATP, 0,5 mM coenzyme A, 17 mM IGEPAL CA-630 (all Sigma-Aldrich), and 1 mM D-Luciferin (GoldBio) in Tris-HCL) using a microplate reader (Berthold).[148] A detailed description of SARS-CoV-2 pseudovirus constructs and pseudovirus production can be found in the previously published work.[100,101,148,155]

4.2.8. Pseudotyped neutralization assay

A lentivirus-based pseudotype neutralization assay was performed using published protocols.[100,148,153,154] In brief, neutralization assays for serially diluted mAbs (starting at 10 µg/ml) were prepared in culture medium and then incubated for one hour at 37°C and 5% CO2 with the harvested pseudoviruses.[148] The luciferase activity was measured after adding ACE2 expressing HEK293-T cells and a 48h incubation period at 37°C and 5% CO2 using a

microplate reader as described in 4.2.7.[148] For antibody IC_{50} calculation, the antibody concentration that resulted in a 50% reduction in relative light units compared to the average of virus-infected untreated control cells was determined after subtracting the average background relative light units of non-infected cells.[148] To calculate the IC_{50}s, a non-linear fit model plotting an agonist vs. normalized dose-response curve with variable slope utilizing the least squares fitting method in Prism 9 (GraphPad) was used.[148] All neutralization assays with monoclonal antibodies (mAbs) were performed in duplicates or triplicates.[148]

4.2.9. Structural analysis of HbnC3t1p1_C6

HbnC3t1p1_C6 IgG heavy and light chain plasmids were co-transfected in HEK293-F suspension cells (Thermo Fisher Scientific) using PEI-MAX (Polysciences).[148] After 6 days of incubation, culture supernatant was harvested, and IgG was purified using protein-A affinity chromatography (GE Healthcare).[148] Purified IgG was digested with Papain (Sigma-Aldrich) with a 1:1000 enzyme-to-protein ratio for generating the Fab fragment.[148] The digestion was carried out overnight at 16°C in a buffer containing 20 mM Cysteine-HCl (Sigma-Aldrich) and 10 mM EDTA titrated to pH7.[148] Fabs underwent size exclusion chromatography on a Superdex 200 10/300 column (GE Healthcare), and the Fc fragment was removed by protein A chromatography.[148] His-tagged SARS-CoV-2 RBD plasmid (Genbank: MN908947; amino acids 319-541) was kindly provided by Florian Krammer.[148] SARS-CoV-2 RBD was transfected in HEK293-F cells as described in 4.1.4.[148] The His-tagged RBD protein was purified using a HiTrap IMAC FF Ni^{2+} (GE Healthcare) affinity column, followed by size exclusion chromatography purification with a Superdex 200 10/300 column.[148] Protein complexes of HbnC3t1p1_C6 Fab and SARS-CoV-2 RBD were created by mixing both proteins at a 1:1,2 molar ratio, respectively.[148] A mosquito crystallization robot (TTP Labtech) set to vapor diffusion sitting drops with 96-well iQ plates (TTP Labtech) was used for crystallization.[148] Three protein (80, 120, and 160 nl) to reservoir (120 nl) ratios were tested for each well.[148] To identify initial hits obtained for apo-Fab HbnC3t1p1_C6 and Fab HbnC3t1p1_C6 bound to RBD PEGrx-HT screen (Hampton Research) and ProPlex screen-HT (Molecular Dimensions) were used.[148] Apo-Fab HbnC3t1p1_C6 protein concentrations of 10,7 mg/ml and a protein reservoir ratio of 1:1 were used to obtain crystal hits. For optimal conditions, 12% isopropanol, 0,08 M sodium citrate tribasic dihydrate, and 22% polyethylene glycol 3350 were used.[148] Crystal hits for Fab HbnC3t1p1_C6 bound to RBD were obtained in 0,1 M Tris pH=8,5, 20% polyethylene glycol 6000 using 14 mg/ml protein in a 1,3:1 protein to reservoir ratio.[148] As a cryo-protectant, 25% and 33% of ethylene glycol reservoir solution was used for apo-Fab HbnC3t1p1_C6 and Fab HbnC3t1p1_C6 bound to RBD, respectively.[148] All crystals were incubated at 20°C.[148] Using Rigoku R-axis IV++ home source at 3 Å resolution, X-ray diffraction data from a crystal of Fab

HbnC3t1p1_C6 in complex with SARS-CoV-2 RBD belonging to an orthorhombic space group was collected.[148] Collected data was further indexed, integrated, and scaled using HKL2000.[148,156] Phaser was used to obtain a molecular replacement solution with a structure of a Fab (PDB 6XUK), and of the SARS-CoV-2 RBD (PDB 6M17) search models.[148] With Coot[157] the model was manually traced into the electron density maps and refined with Phenix Refine[158].[148] The following PDB files were used for the Figure 22 overlay structures: 7B0B, 7E3K, 7E3L, 7BEN, 7P40, 7EZV, 7LRS.[148]

4.2.10. Quantification and statistical analysis

For statistical analyses, Prim 9.0 (GraphPad), Microsoft Excel for Mac (v14.7.3), and Python (v3.6.8)[142] were used.[148] Amino acid sequence alignment of coronavirus spike proteins for the phylogenetic analyses in Figure 23 and Figure 19 were done using Geneious Prime (Biomatters) and a tree build using PhyML implemented in Geneious Prime (Biomatters).[148] A p-value below 0.05 was considered significant.[148] Further details on statistical analyses used can be found in the corresponding legends of Figures 12 to 16.[148]

4.3. Antibody escape properties of the SARS-CoV-2 omicron lineage

Methods and materials described in the following section 4.3 are adapted from *Gruell et al., 2022, Cell Host & Microbe*.[155]

4.3.1. Donors and sampling

Serum samples of 20 COVID-19 convalescent individuals were collected under study protocols approved by the ethics committee of the Medical Faculty of the University of Cologne (16-054 and 20-1187).[155] Individuals with a prior SARS-CoV-2 infection confirmed by RT-qPCR and documented in a test certificate or self-reported were enrolled within eight weeks of symptom onset and/or diagnosis between April and May 2020.[155] Since all participants were enrolled prior to the emergence of variants of concern (as defined by the WHO), most individuals were likely infected by an early viral strain similar to Wu01.[155] To enable the study of long-term immunity to SARS-CoV-2 participants, the study was conducted longitudinally.[155] Samples after booster immunization were collected between May and August 2021.[155] Between sampling points, the study participants reported no SARS-CoV-2 reinfection.[155] Serum samples from 30 vaccinated individuals were collected at the Charité – Universitätsmedizin Berlin under protocols approved by the local ethics committee (EICOV, EA4/245/20) as well as the ethics committees of the Federal State of Berlin and the Paul Ehrlich Institute (COVIM, EudraCTNo. 2021-001512-28).[155] Healthcare workers vaccinated at Charité – Universitätsmedizin Berlin were enrolled in the study

irrespective of medical history.[155] If individuals had a history of SARS-CoV-2 infection, had a positive polymerase chain reaction test performed at sampling, or had detectable antibodies against SARS-CoV-2 nucleocapsid, the individuals were excluded from the vaccinated group.[155] All serum samples were tested for SARS-CoV-2 nucleocapsid targeting antibodies using the SeraSpot Anti-SARS-CoV-2 IgG microarray-based immunoassay (Seramun Diagnostica).[155] After two vaccinations, serum samples from 29 individuals were collected in February and March 2021 (one serum sample from one participant was obtained in July 2021), and samples after booster vaccination were collected in December 2021 and January 2022.[155] All serum samples were collected after centrifugation and stored at -80°C.[155] Participant and sample selection was based on comparable sampling time points relative to vaccination and identical vaccine used.[155] Further details concerning individual study cohorts, gender distribution, and age can be found in Supplementary Table 9.[155] All study participants provided written informed consent.[155]

4.3.2. SARS-CoV-2 pseudovirus constructs

Methods used for cloning of SARS-CoV-2 spike proteins expression plasmids can be found in 4.2.7 or in *Gruell et al., 2022, Cell Host & Microbe*.[155] On top of the described viral variants in 4.2.7, Omicron sublineage BA.1.1 was cloned based on BA.1 with an additional R346K mutation, Omicron sublineage BA.2.12.1 was cloned based on BA.2 with an additional L452Q and S704L mutations, and Omicron sublineage BA.4/5 was cloned based on BA.2 with an additional D69-70, L452R, and F486V mutations but without Q493R mutation.[155]

4.3.3. Selection and production of mAbs

The mAb panel investigated here consisted of mAbs obtained from convalescent individuals by single cell-sorting of S reactive B cells and subsequent cloning as described in 4.1.5 and 4.1.8 or in previously published work[127,153] or from mAbs derived from the CoV-AbDab[149] with methods on selection, cloning, and production found in 4.2.1 and 4.2.4 or in previously published work.[148,155] eBlocks (IDT) of nucleotide sequences for antibodies COV2-2130 (cilgavimab), ADG-2, COV2-2381, MAD0004J08, P2C-1F11 (BRII-196), and COV2-2196 (tixagevimab) published in GenBank were ordered and cloned as described in 4.2.4.[155] For antibodies CT-P59 (regdanvimab), C135 and LY-CoV1404 (bebtelovimab) eBlocks (IDT) of codon-optimized (IDT Codon Optimization Tool) nucleotide sequences based on mAb structures deposited in the Protein Data Bank (accession nos. 7K8Z, 7CM4, and 7MMO) were ordered and cloned as described in 4.2.4.[155] eBlocks (IDT) of codon-optimized (IDT Codon Optimization Tool) nucleotide sequences for antibodies BD-368-2, 47D11, C144, and P2B-2F6 derived from amino acid sequences found in the CoV-AbDab[149] were ordered and cloned as described in 4.2.4.[155] Methods on mAbs production can be found in 4.1.8.[155]

Aliquots from clinical stocks were used for antibodies bamlanivimab, casirivimab, DZIF-10c, etesevimab, imdevimab, and sotrovimab.[155] A more detailed description can be found in previously published work.[155]

4.3.4. Pseudovirus neutralization assay

Methods for producing pseudovirus particles and the pseudovirus assay can be found in 4.2.7 and 4.2.8, respectively, or in previously published work.[153,155] For neutralization assays with serum samples, serial dilutions of heat-inactivated serum (56°C for 45min) starting at 1:10 were prepared in a culture medium and then incubated with the harvested pseudovirus for one hour at 37°C and 5% CO2.[155] Following the addition of HEK293-T ACE2 expressing cells and a 48h incubation period at 37°C and 5% CO2, the luciferase activity was measured by adding luciferin/lysis buffer using a microplate reader as described in 4.2.7.[155] For the luciferase signal evaluation, serum ID_{50}s were determined as the serum, resulting in a 50% relative light unit reduction compared to the average of virus-infected untreated control cells after subtracting the average background relative light units of non-infected cells.[155] A non-linear fit model plotting an agonist vs. normalized dose-response curve with variable slope using the least squares fitting method in Prism 9 (GraphPad) was used to calculate ID_{50}s.[155] All neutralization assays with serum samples were done in duplicates or triplicates.[155] For further details and imputation rules for samples with values outside the limits of quantification, see 4.3.8.

4.3.5. Sequence analysis

Sequence analysis in Figure 30 is based on 67 randomly selected human SARS-CoV-2 neutralizing antibodies from the CoV-AbDab[149] (accessed on 01st January 2021), 12 antibodies in clinical use or development, and 79 antibodies obtained in our previous work. Five mAbs in clinical development shown in Figure 32 were not included in the analysis as they were isolated from immunized mice with human immunoglobulin gene repertoires (47D11, casirivimab), individuals infected with SARS-CoV (ADG-2, sotrovimab) or by using phage display technology as information on heavy and light chain pairing is lost (regdanvimab).[155] Annotation of antibody amino acid sequences were done using igblastp (igblast v1.16.0)[135] based in the IMGT database[159].[155] For sequence analysis, CDR3 lengths were determined using the IMGT numbering scheme, V genes were counted without the individual alleles, and the number of V gene mutations was determined in reference to the top V gene call from igblastp (igblast v1.16.0)[135].[155] The phylogenetic analysis of the VH3-53/3-66|VK1-9 public clonotype was done using the the MAFFT algorithm[160] implemented in the EMBL-EBI search and sequence analysis tools API.[155,161] The phylogenetic tree was built in Geneious Prime (Biomatters) using the Jukes-Cantor distance model for tree building with

the neighbor-joining method without resampling.[155] Data aggregation and visualization was done using the Python libraries pandas (v1.1.5)[162], NumPy (v1.19.2)[163], SciPy (v1.5.2)[164], and Matplotlib (v3.3.4)[152] with Python (v3.6.8)[142], and GraphPad Prism (v7).[155]

4.3.6. Distribution of SARS-CoV-2 variants

Data on weekly SARS-CoV-2 cases (COVID-19 Data Repository) curated by the Center for Systems Science and Engineering (CSSE) at Johns Hopkins University[165] were downloaded from http://ourworldindata.org (accessed on 20.06.2022).[155] Clade and linage statistics of sequences submitted to the GISAID database[85–87] were retrieved from GISAID (accessed on 20.06.2022).[155] Individual variant frequencies were illustrated as a fraction of all sequences submitted to GISAID per week and variant.[155] Except for BA.1.1 and its sublineages, all BA.1 sublineages were classified as BA.1, except for BA.2.12.1, all BA.2 sublineages were classified as BA.2, and all BA.3 sublineages were classified as BA.3.[155]

4.3.7. Visualization of SARS-CoV-2 S protein change

SARS-CoV-2 S protein amino acid changes relative to the Wu01 S protein were visualized with ChimeraX (v1.3)[166,167] using a 3D reconstruction of the S protein obtained by cryo-electron microscopy (PDB: 6XR8)[168].[155]

4.3.8. Quantification and statistical analysis

Serum samples and mAbs were subjected to duplicate or triplicate testing.[155] The average ID_{50} for serum samples was determined from 2-3 single dilution series experiments (except for one sample tested in technical duplicates).[155] An ID_{50} value equal to the limit of quantification (ID_{50}=10) was assigned to samples with low-level serum neutralization (ID_{50}>10) determined in a single run.[155] Technical duplicates within the same experiments were tested for antibodies in clinical use or under investigation.[155] Two or three single-dilution experiments were used for additional antibodies included in the panel, and average IC_{50}s were computed.[155] In Figure 28 and Figure 29, samples with less than 50% inhibition tested at the lowest dilution of 10 (lower limit of quantification, LLOQ) were assigned to ½ x LLOQ (ID_{50}=5), and serum samples with ID_{50}s>21,870 (upper limit of quantification) were assigned to ID_{50}=21,871.[155] In Figure 30 and Figure 31, samples with IC_{50}<0,005 µg/ml (LLOQ) were assigned to ½ x LLOQ (IC_{50}=0,0025 µg/ml), and IC_{50}>10 µg/ml were assigned to 2 x LLOQ (IC_{50}=20 µg/ml).[155] Friedman test with Dunn's multiple comparison post-hoc test implemented in Prim 7.0 (GraphPad) was used to test for significant differences in serum neutralization against different variants/sublineages.[155] Spearman's rank correlation coefficients (Rho) were calculated using Prism 7.0 (GraphPad).[155] A two-sided Mann-

Whitney U test using Prism 7.0 (GraphPad) was computed to compare several amino acid mutations relative to germline for antibodies only neutralizing Wu01 and those neutralizing any Omicron sublineage.[155] A p-value below 0,05 was considered statistically significant.[155] Further details are provided in the Figure legends.[155] The cohort size of convalescent and vaccinated participants was based on sample availability and criteria mentioned in 4.3.1.[155]

5. Results

5.1. Isolation of potent SARS-CoV-2 neutralizing mAbs from convalescent individuals

All results, including figures and tables in section 5.1, are adapted from *Kreer et al., 2020, Cell*.[127]

5.1.1. SARS-CoV-2 convalescent individuals exhibit a polyclonal memory B cell response towards the S protein

Blood samples from seven COVID-19 patients aged between 38 and 59 years were collected 8 and 36 days after diagnosis to study the humoral response against SARS-CoV-2 (Figure 7A; Supplementary Table 1).[127] Of the recruited individuals, five patients reported mild symptoms, including dry cough, fever, and dyspnea.[127] Two patients reported no symptoms (Supplementary Table 1). Plasma IgGs were purified from all seven individuals, and plasma binding was tested using ELISA against the SARS-CoV-2 full trimeric S ectodomain protein.[127] All individuals tested showed binding activity with EC_{50}s ranging between 3,1 to 96,1 µg/ml (Figure 7B; Supplementary Table 2).[127] Purified IgG samples were also tested in an authentic SARS-CoV-2 live virus neutralization assay.[127] Five of seven patients showed 100% inhibitory concentrations (IC_{100}) between 78,8 and 1500 µg/ml (Figure 7B; Supplementary Table 2).[127] Single-B-cell sorting and subsequent sequence analysis were performed for every individual to investigate the molecular characteristics of the underlying B-cell response after SARS-CoV-2 infection.[127] IgG^+ B cells reacting with the S ectodomain were detected between 0,04% (±0,06) and 1,02% (±0,11) in flow cytometry analysis (Figure 7C; Figure 8).[127] From the SARS-CoV-2 S protein reactive B cells, 1751 single B cells were isolated using an optimized PCR protocol to amplify corresponding heavy and light chain sequences (Figure 7C; Supplementary Table 3) and subsequent Sanger sequencing.[127] Heavy and light chain sequence analysis revealed a polyclonal antibody response towards SARS-CoV-2 S protein with 22% to 45% clonally related sequences per individual and 2–29 members per identified B cell clone (Figure 7D; Supplementary Table 3).[127] Here, we show that a polyclonal B cell response towards SARS-CoV-2 S protein was present in all study participants.[127]

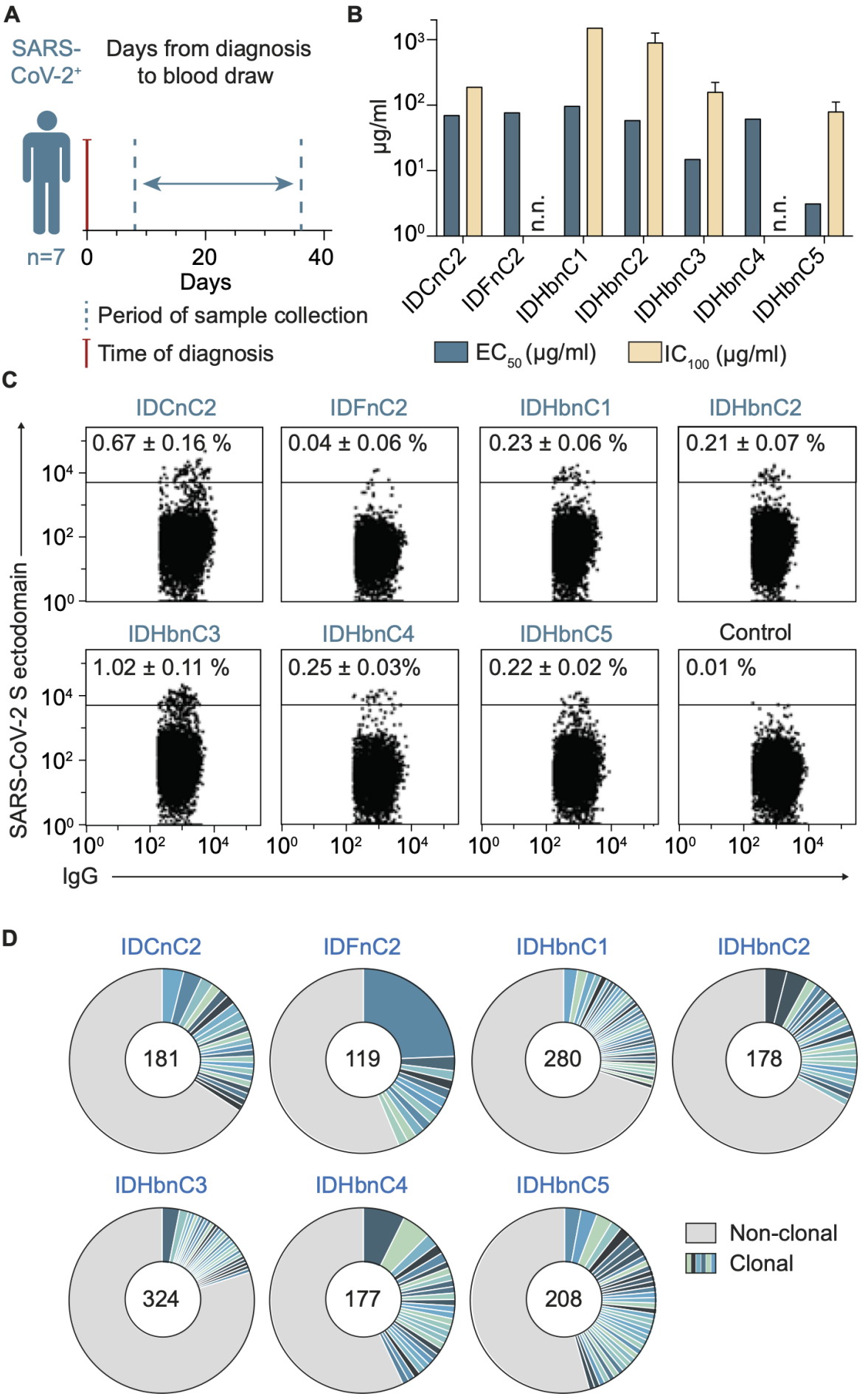
A
SARS-CoV-2+
Days from diagnosis to blood draw
n=7
0
20
40
Days
Period of sample collection
Time of diagnosis
B
µg/ml
n.n.
n.n.
IDCnC2
IDFnC2
IDHbnC1
IDHbnC2
IDHbnC3
IDHbnC4
IDHbnC5
EC50 (µg/ml)
IC100 (µg/ml)
C
IDCnC2
IDFnC2
IDHbnC1
IDHbnC2
0.67 ± 0.16 %
0.04 ± 0.06 %
0.23 ± 0.06 %
0.21 ± 0.07 %
IDHbnC3
IDHbnC4
IDHbnC5
Control
1.02 ± 0.11 %
0.25 ± 0.03%
0.22 ± 0.02 %
0.01 %
SARS-CoV-2 S ectodomain
IgG
D
IDCnC2
IDFnC2
IDHbnC1
IDHbnC2
181
119
280
178
IDHbnC3
IDHbnC4
IDHbnC5
324
177
208
Non-clonal
Clonal

Figure 7. A polyclonal B cell and antibody response is induced in SARS-CoV-2 infected individuals.
(A) Sample collection scheme (details in Supplementary Table 1). (B) Bar charts depict binding to the S protein (ELISA, EC_{50}) and authentic SARS-CoV-2 neutralization potency (VeroE6 cell infection inhibition, IC_{100}) of cross-sectional purified IgG samples. Arithmetic or geometric means ± SD of duplicates or quadruplicates for EC_{50} and IC_{100} are shown. (n.n: no neutralization defined as IC_{100} > 1.500 g/mL IgG). (C) Flow cytometry data of IgG+ B cells. Average frequencies of S protein reactive B cells are shown in percent ±SD (see also Supplementary Tables 2 and 3; Figure 8). (D) Pie charts of clonal relationship among S protein reactive B cells. The total number of productive heavy-chain sequences is depicted in the center. Clone sizes correlate with the total number of productive heavy chains per clone. Shades of blue and green are used for individual clones. [published in *Kreer et al., 2020, Cell; Figure 1*][127]

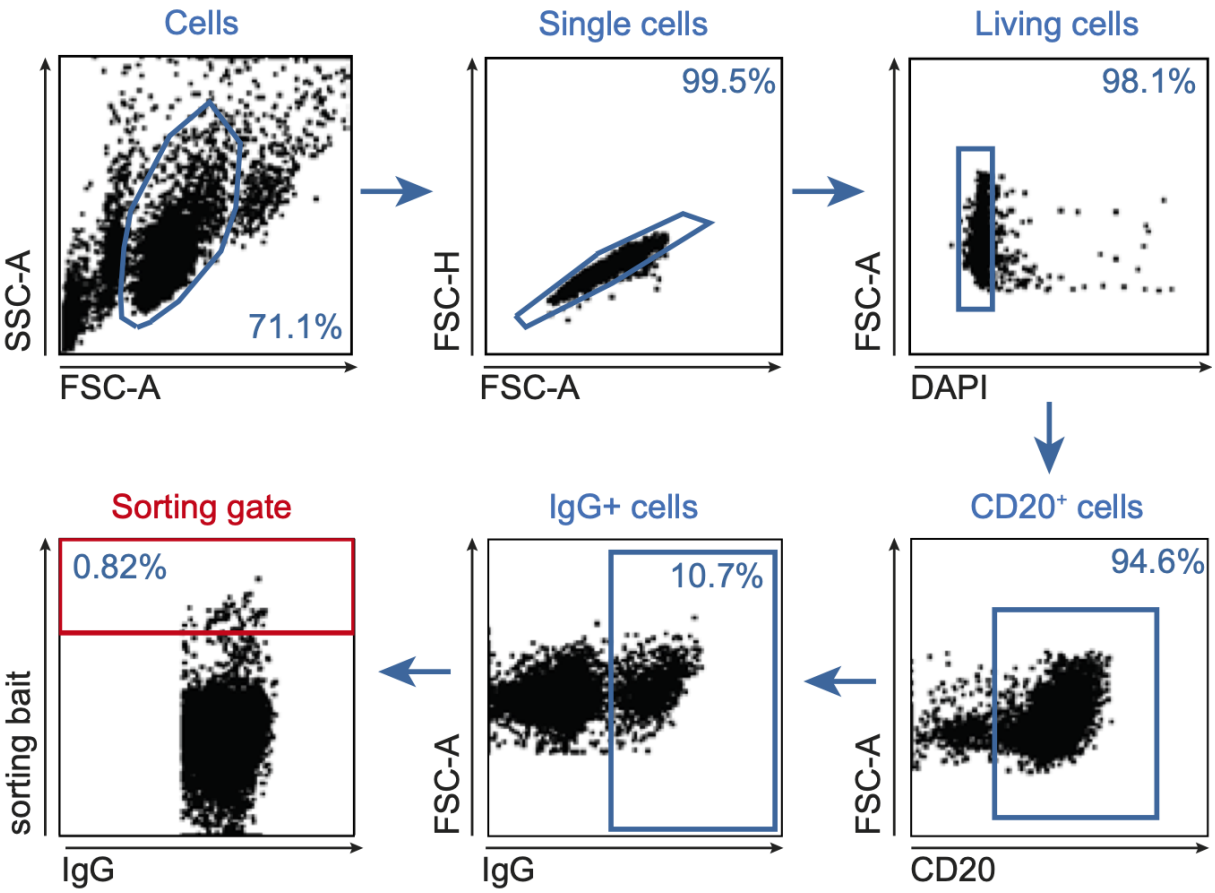

Figure 8. Single cell sort gating strategy.
CD19+ B cells were used after enrichment by MACS. Cell aggregates were excluded by FSC. Living CD20+ IgG+ cells with a positive SARS-CoV-2 S ectodomain staining were selected for single-cell sort. [published in *Kreer et al., 2020, Cell; Figure S1*][127]

5.1.2. A B cell response against SARS-CoV-2 develops after infection and can be detected over time

Five additional samples from infected individuals at three different time points between 8 to 69 days after diagnosis were collected and analyzed for binding and neutralization activity to

explore the longitudinal dynamics of the SARS-CoV-2 humoral response (Figure 9A; Supplementary Table 1).[127] EC_{50} values of plasma IgG detected in the S protein ELISA ranged from 1,54-129 µg/mL, and IC_{100} detected in SARS-CoV-2 live virus neutralization ranged from 78,8-1.500 µg/mL across different individuals.[127] However, each individual's antibody response remained almost unaffected (Figure 9A and B).[127] Additionally, 2.562 SARS-CoV-2 S ectodomain reactive IgG^+ B cells of samples from all five subjects and from different time points (t1, t2, and t3) were sorted with the same FACS strategy to examine B cell clonality and antibody characteristics on a single cell level.[127] This revealed up to 0,65% of SARS-CoV-2 S protein reactive B cells, with frequencies tending to be higher at later time points and time after diagnosis.[127] Furthermore, 254 B cell clones (Supplementary Table 3) were identified, and 129 (51%) were detected recurrently.[127] This finding suggests that over the study period of 2,5 months, SARS-CoV-2 S protein reactive B cells can persist in infected individuals.[127] Across patients, the percentage of clonally related sequences ranged from 18% to 67% and remained steady or showed only moderate reduction over time when examined at individual time points (Figure 9D).[127] When analyzing 6.587 productive SARS-CoV-2 S protein reactive heavy and light chain IgG^+ B cell sequences of all 12 patients, clonal and non-clonal sequences exhibited normally distributed CDRH3 lengths and a symmetrical CDRH3 hydrophobicity distribution with a predominance of the IgG1 isotype as well as a broad spectrum of VH gene segments used (Figure 9E).[127] In comparison to repertoire data from healthy individuals, IGVH3-30 was overrepresented, and κ light chains were more common than λ light chains in clonally related sequences, accounting for 76% in clonal vs. 62,5% in non-clonal sequences (p=0,0029; Figure 9F and Figure 10).[127] Finally, on average, S-reactive B cells showed less somatically hypermutation with a median identity of 98,3% versus 94,3% compared to the healthy IgG^+ repertoire (p<0,0001; Figure 9E and Figure 10).[127] Here, we show that SARS-CoV-2 S reactive IgG+ B cells are present after SARS-CoV-2 infection with the same B cell clones detected over time. Additionally, a preference for the IGHV3-30 segment was observed.[127]

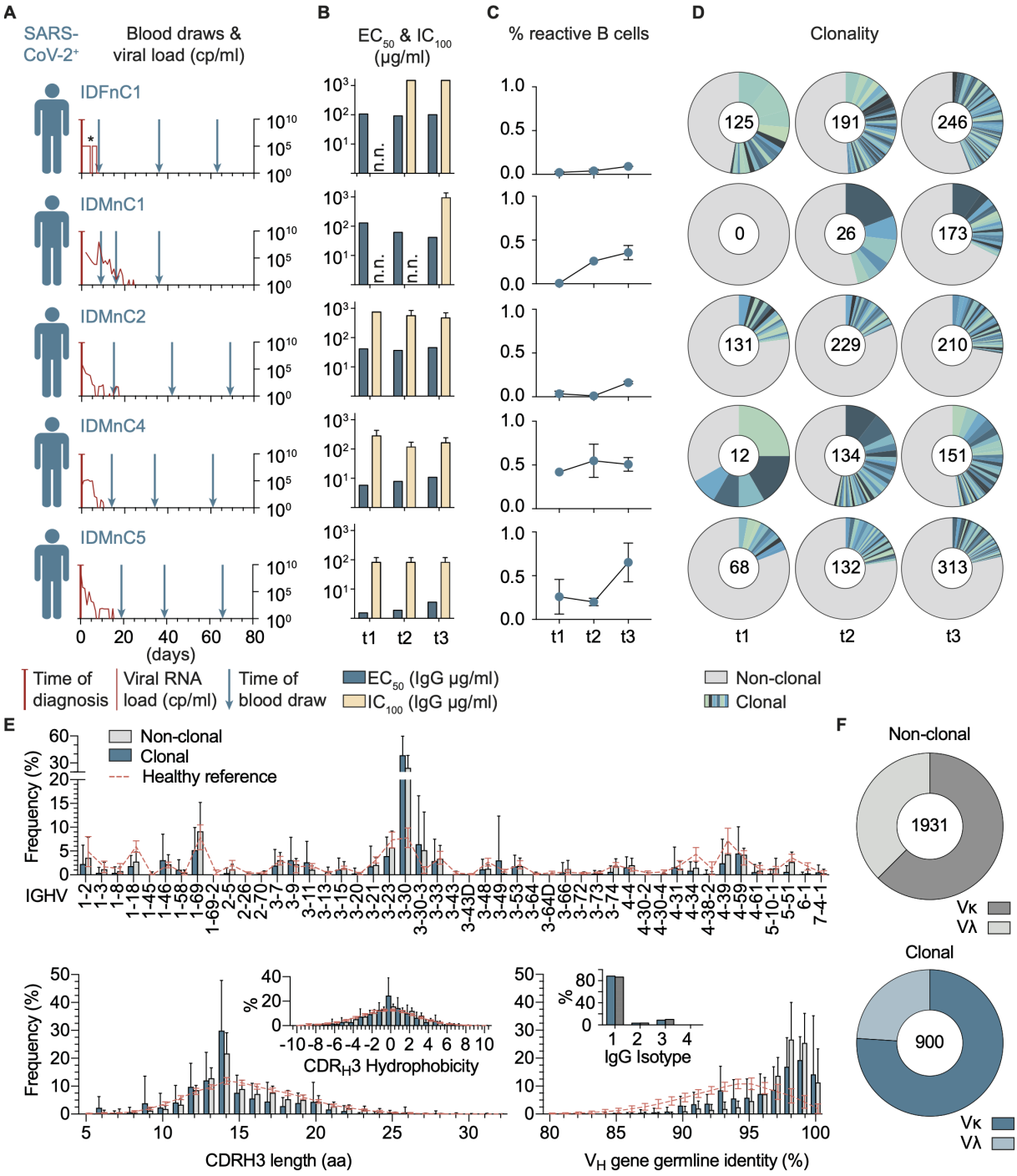

Figure 9. IgG⁺ S reactive B cells rapidly form after SARS-CoV-2 infection with recurring B cell clones and a preference for IGHV3-30 gene segment.

(A) Longitudinal sample collection for individual study participants. Viral RNA load from samples collected by nasopharyngeal swabs is shown in red (copies [cp]/ml, right y-axis). IDFnC1 viral load only has a positive or negative result (see Supplementary Table 1). (B) Bar charts depict binding to the S protein (ELISA, EC_{50}) and authentic SARS-CoV-2 neutralization potency (VeroE6 cell infection inhibition, IC_{100}) of longitudinal purified IgG samples. The bar plots show the arithmetic or geometric means ± SD of duplicates or quadruplicates for EC_{50} and IC_{100}. (n.n: no neutralization defined as IC_{100} > 1.500 g/mL IgG). (C) The percentage of IgG⁺ S protein reactive B cells is depicted over time (mean ± SD; see also Supplementary Tables 2 and 3; Figure 8). (D) Pie charts of clonal relationship among S protein reactive B cells depicted over different time points with shades of blue and green used for individual clones. A total number of productive heavy-chain sequences is depicted in the

center. (E) From all 12 subjects, frequencies of VH gene segments (top), CDRH3 length and hydrophobicity (bottom left), VH gene germline identity, and IgG isotype of clonal and non-clonal sequences (bottom right) are shown. Reference NGS repertoire data of 48 healthy individuals (samples taken prior to SARS-CoV-2 emergence) are depicted in red (see also Supplementary Tables 1 and 2). Line and bar plots depict mean ±SD. (F) Pie charts show the ratio of κ and λ light chains in non-clonal (top, gray) and clonal (bottom, blue) sequences (see also Figrue 10). [published in *Kreer et al., 2020, Cell*; Figure 2][127]

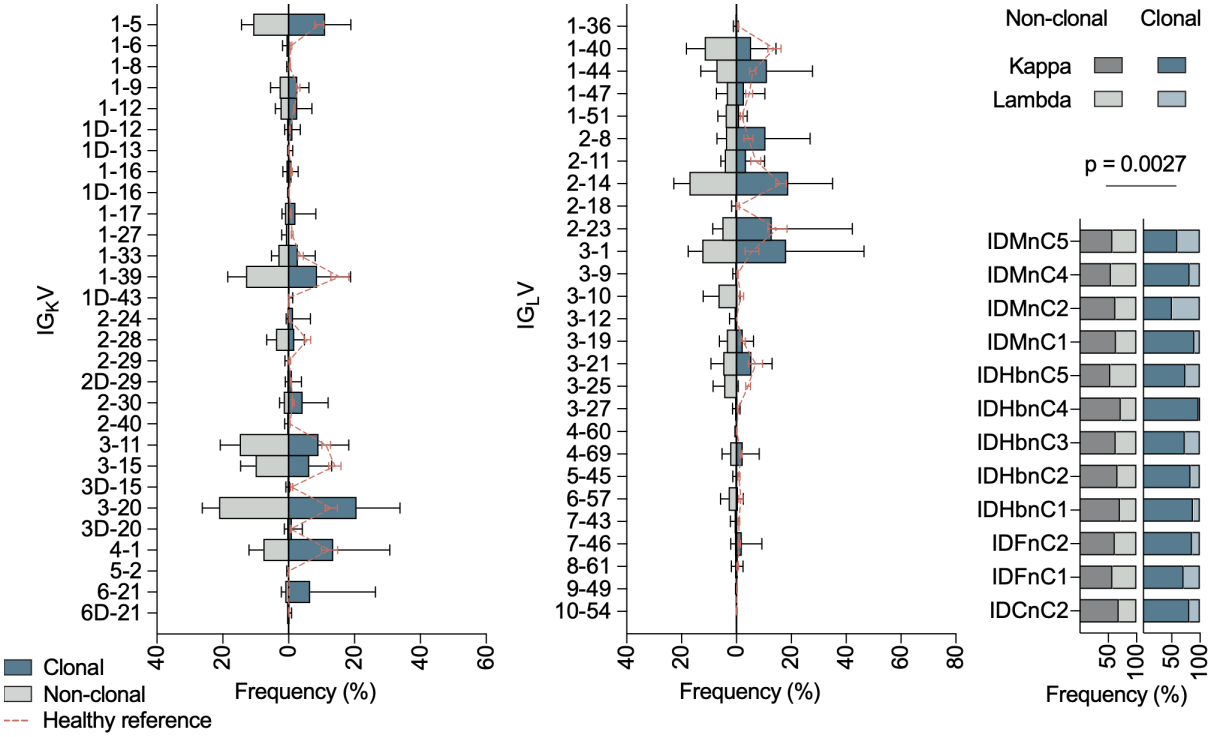

Figure 10. V gene segment usage and clonality of light chains from single B cells.

Frequencies and clonality of κ (left) and λ chain (middle) gene segments are shown. For individual sample sets κ to λ ratios are displayed on the right. A two-tailed Wilcoxon matched-pairs signed rank test was performed on κ/λ ratios to test for significance. [published in *Kreer et al., 2020, Cell; Figure S2*][127]

5.1.3. Isolation of potent SARS-CoV-2 neutralizing mAbs are promising candidates for clinical use

To examine antibody properties and isolate potent neutralizing antibodies, 312 mAbs from all 12 patients were selected based on clonality with at least one clonal member of at least three clones per individual and cloned into expression vectors (Supplementary Table 3).[127] In addition, we included about 1/3 randomly selected non-clonal sequences (83 antibodies) for production as the measured antibody response was highly polyclonal with a median clone size of 2 (Supplementary Table 3), and the presence of weakly expanded clones in the non-clonal fraction suggested by the absence of differences between clonal and non-clonal sequences.[127] From 255 IgG1 antibodies that were successfully produced and tested in ELISA against the SARS-CoV-2 S protein, 79 (31%) showed binding activity with EC_{50} values ranging between 0,02 µg/ml and 5,20 µg/ml (Figure 11A) and 30 antibodies were

reactive to SARS-CoV-2 in the commercial Euroimmun IgG detection kit (Figure 11A and B; Supplementary Table 4).[127] Of the SARS-CoV-2 S protein binding antibodies, SPR analyses with RBD as an analyte were carried out for 13 mAbs, showing dissociation constant (K_D) values as low as 0,02 nM (Supplementary Table 4).[127] All SARS-CoV-2 S protein binding mAbs were tested using an authentic SARS-CoV-2 virus neutralization assay to determine neutralization potency.[127] Of those, 27 neutralizing antibodies were identified from 9 out of 12 individuals with IC_{100} values ranging between 100 µg/ml (assay limit) and 0,04 µg/ml (Figure 11C and D).[127] Interestingly, neutralization activity was preferably detected among high-affinity antibodies, with a positive correlation between neutralization and binding (Spearman's correlation coefficient [rs]=0,429; p=0,023; Figure 11E).[127] To better understand the binding interaction of S protein reactive antibodies, ELISAs were performed with a truncated N-terminal S1 subunit, including the RBD, the isolated RBD, and a monomeric S protein.[127] Out of 27 neutralizing antibodies, 26 were binding to the RBD compared to only 27,5% of the non-neutralizing antibodies, suggesting that the RBD is a major side of vulnerability on the SARS-CoV-2 S protein.[127] Non-neutralizing antibodies targeted the N-terminal S1 domain and other conformational epitopes (Figure 11F; Supplementary Table 4).[127] Notably, a broad distribution of VH and VL gene segments with a preference towards κ light chains was observed for neutralizing and non-neutralizing antibodies (Figure 11G; Figure 13).[127] Surprisingly, high germline identities of 99%-100% were observed for 31 of 79 binding and 11 of 28 neutralizing antibodies, with no correlation between the amount of SHM and neutralization activity (Figure 11G; Supplementary Table 4; Figure 12).[127] Finally, to test for autoreactivity in the SARS-CoV-2 neutralizing antibodies, Hep-2 cell autoreactivity assays were performed.[127] Out of 27 antibodies, 4 showed moderate levels of autoreactivity (Figure 14; Supplementary Table 4), and 2 also reacted with envelope proteins from other viruses (i.e., Ebola glycoprotein and HIV-1 gp140; Supplementary Table 4).[127] In summary, highly potent neutralizing SARS-CoV-2 antibodies that are promising candidates for preventing or treating SARS-CoV-2 infection were isolated.[127] Furthermore, these antibodies are marked by a low amount of SHM and develop from a broad set of different V genes.[127]

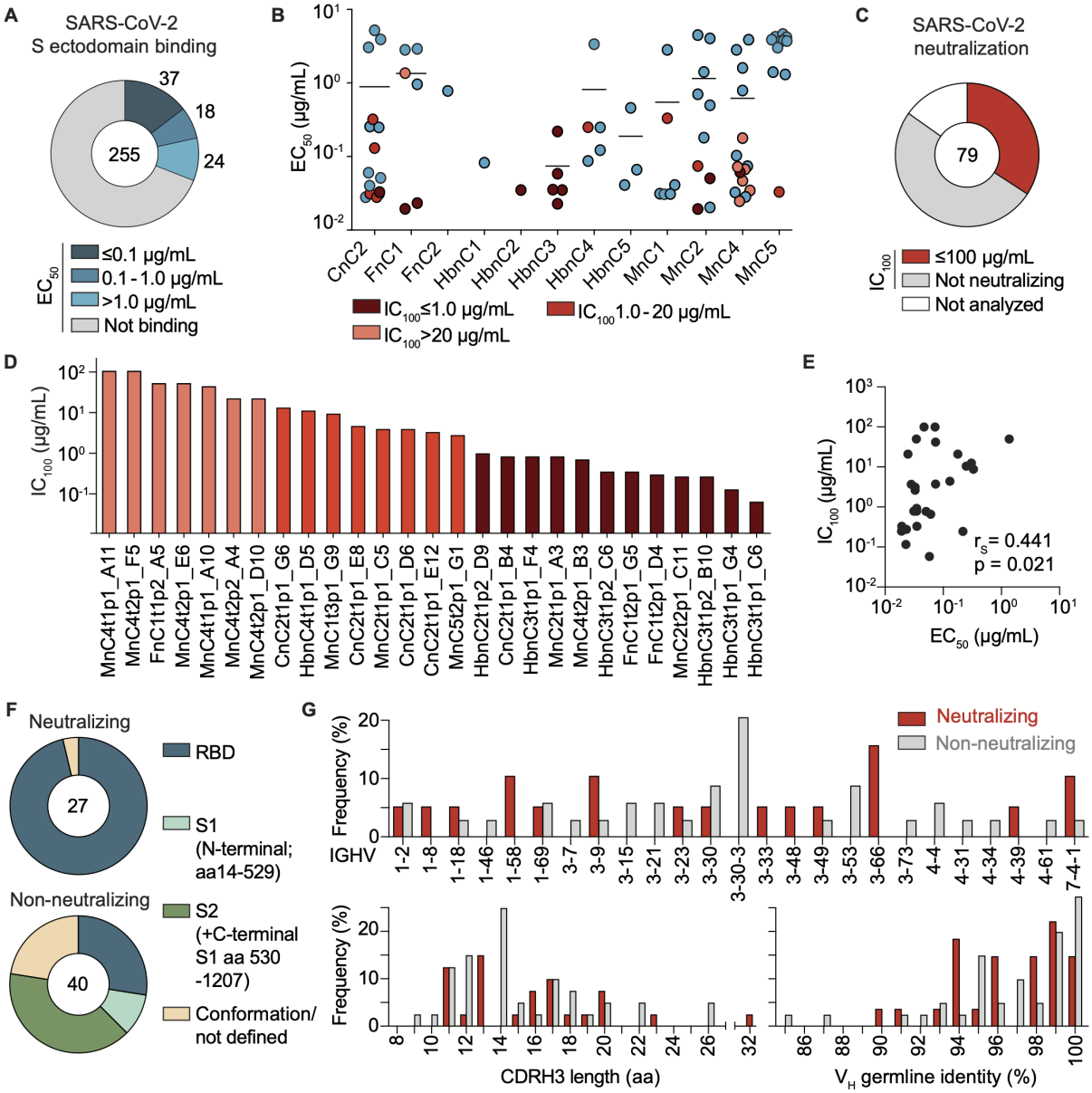

Figure 11. Infected individuals develop potent near-germline RBD binding SARS-CoV-2 neutralizing antibodies.

(A) Pie chart of antibody binding affinity (ELISA, EC_{50}) towards SARS-CoV-2 S protein. Binding (blue) was defined as an EC_{50} <30 µg/ml and an optical density 415-695 nm ($OD_{415-695}$) of >0,25 (data not shown). (B) EC_{50} values (average of duplicates) of SARS-CoV-2 S protein binding antibodies per individual. Antibodies neutralizing SARS-CoV-2 are labeled in shades of red (see also Figure 14 and Supplementary Table 4). (C) Pie chart of S protein-specific monoclonal antibodies (red) neutralizing authentic SARS-CoV-2 virus (complete inhibition of infection in VeroE6 cells, IC_{100}, in quadruplicates). (D) The geometric mean of neutralization potency (IC_{100}) of all neutralizing monoclonal antibodies. (E) S protein binding (EC_{50}) and neutralization potency (IC_{100}) correlate. Spearman's rank order was used to calculate the correlation coefficient rS and approximate p value (see also Figure 12). (F) Pie charts of epitopes including RBD, truncated N-terminal S1 subunit (aa 14-529), and monomeric S protein targeted by SARS-CoV-2 S protein binding antibodies grouped by neutralization. Binding S2 was defined as a measured interaction with the monomeric S protein but not S1 or RBD. Antibodies not targeting any measured subdomain were declared as targeting conformational epitopes or a not-defined epitope. (G) VH gene segment frequencies for neutralizing and non-neutralizing antibodies are shown at the top. For frequency calculation, clonal sequences were collapsed and counted as one sample. VH gene germline

identity (right) and CDRH3 length (left) of neutralizing and non-neutralizing antibodies are shown on the bottom (see also Figure 13). [published in *Kreer et al., 2020, Cell; Figure 3*][127]

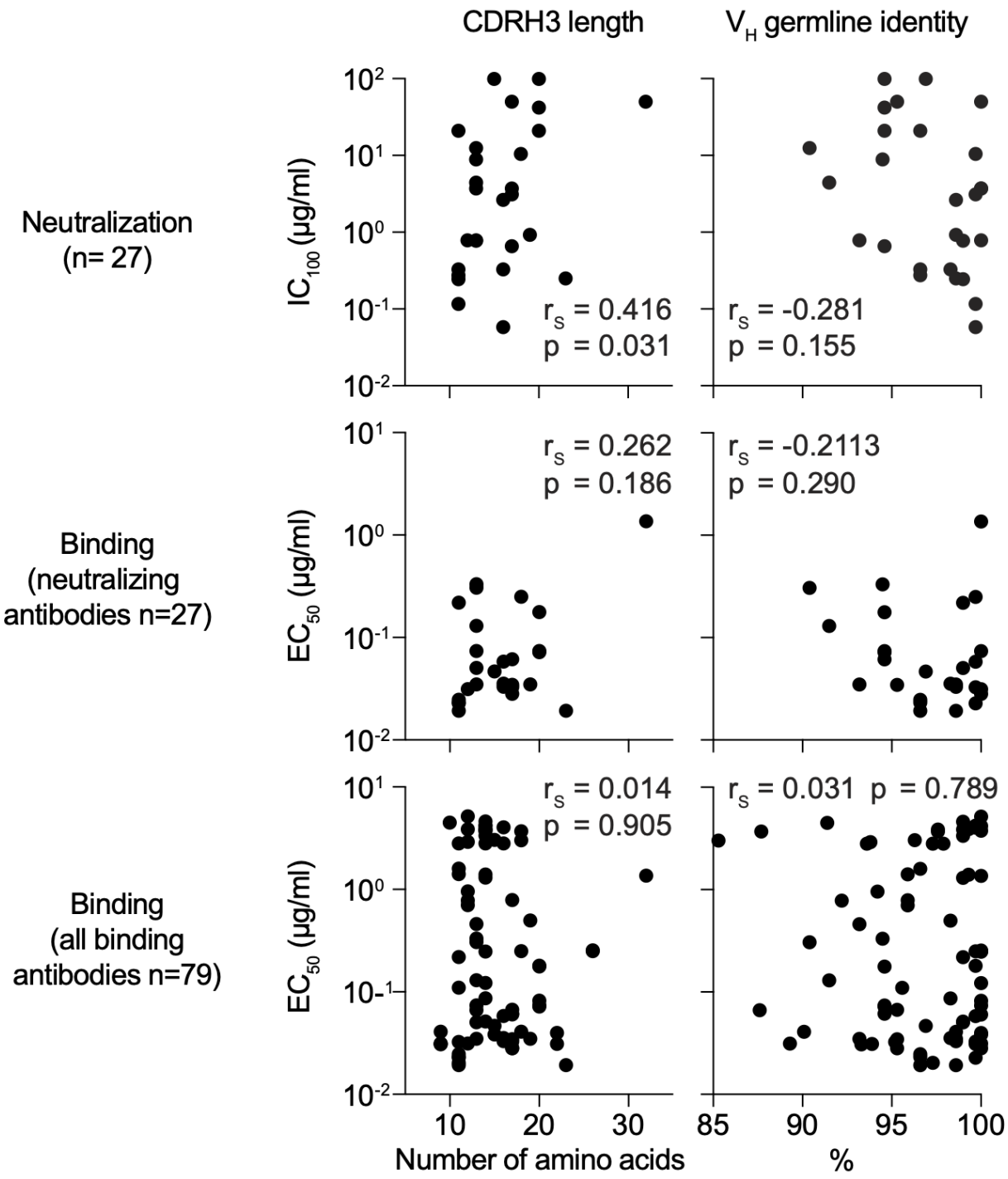

Figure 12. Correlation of VH gene segment characteristics with binding and neutralization.
EC_{50} values of binding or neutralizing antibodies or IC_{100} values of neutralizing antibodies are correlated with CDRH3 lengths or VH germline identities. Spearman correlation coefficient rS and approximate p values were calculated. [published in *Kreer et al., 2020, Cell; Figure S3*][127]

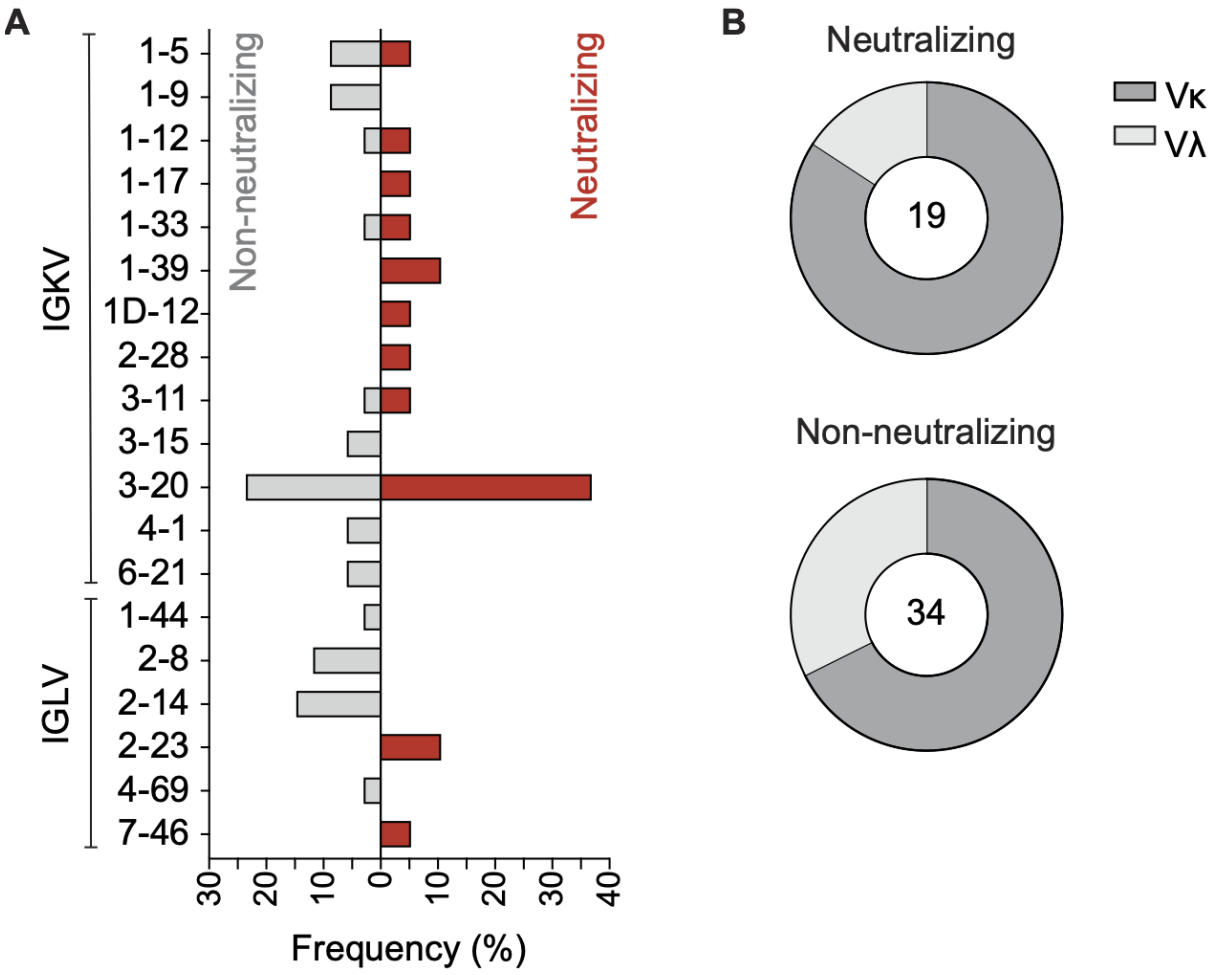

Figure 13. Distribution of light chain V gene segment grouped by neutralization.

(A) VL gene segment frequencies for neutralizing (right, red) and non-neutralizing (left, gray) antibodies. Clonal groups were collapsed and treated as only one sample for frequency calculation. (B) λ and κ LC ratios for neutralizing (top) and non-neutralizing S protein specific antibodies (bottom). [published in *Kreer et al., 2020, Cell; Figure S4*][127]

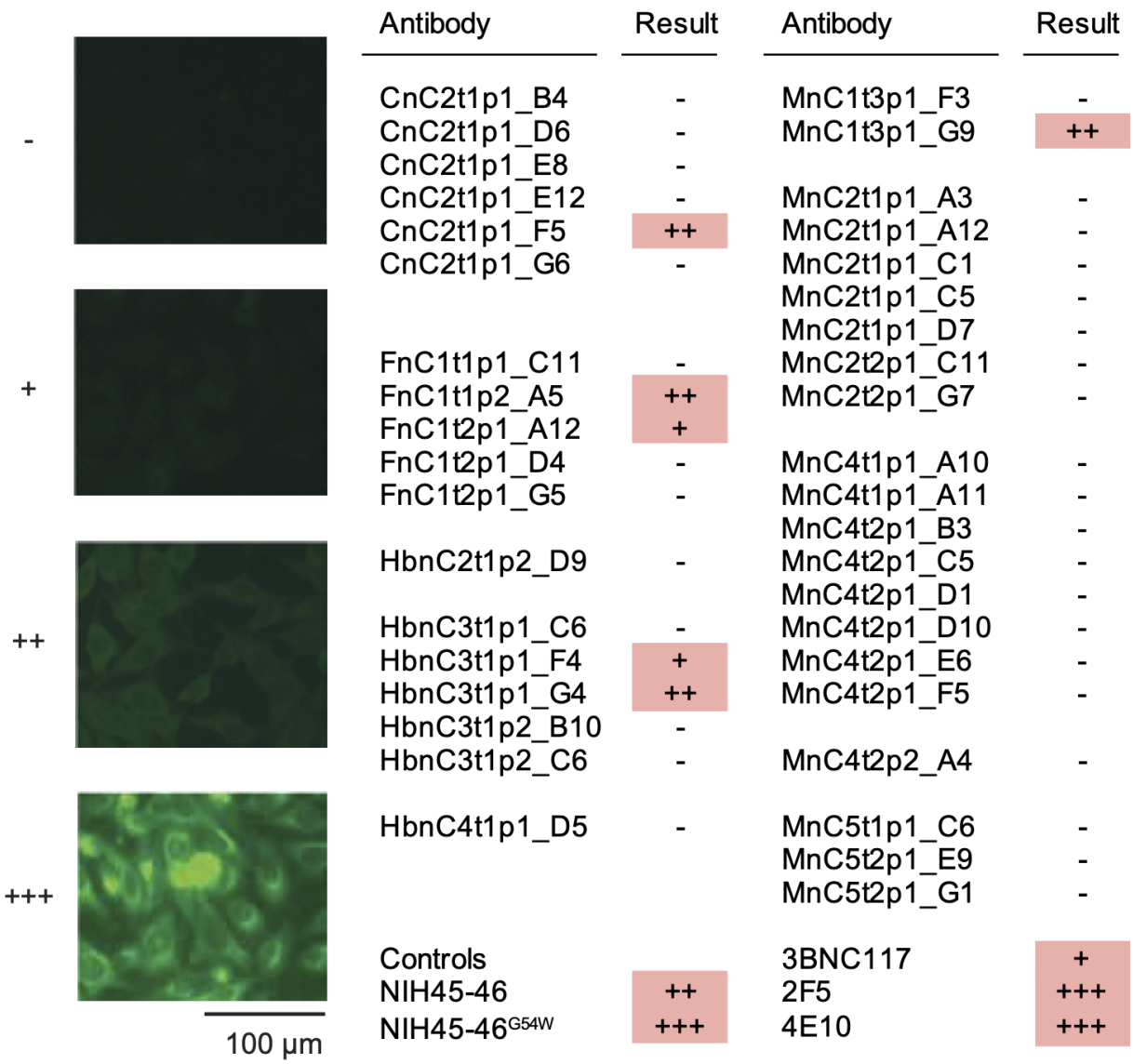

Figure 14. Autoreactivity tested in selected SARS-CoV-2 binding and neutralizing antibodies.
HEp-2 cells were incubated with the antibodies in question at 100 µg/ml and analyzed using indirect immunofluorescence. Representative pictures of the scoring system are used. [published in *Kreer et al., 2020, Cell; Figure S5*][127]

5.1.4. Potent SARS-CoV-2 neutralizing mAbs show low levels of SHM between different isolation timepoints

To investigate the dynamics of SHM over time, 129 recurring B cell clones comprising 17 binding and 6 neutralizing antibodies were longitudinally analyzed.[127] To this end, members of a B cell clone at a given time point were phylogenetically matched to the most closely related member at a consecutive time point (331 pairings in total).[127] Calculated mean mutation frequencies per week measured either towards higher or lower V gene germline identities were 0,51% ± 0,61%, 0,08% ± 0,51% for binding, and 0,01% ± 0,19% per week for neutralizing clonal members (Figure 15A).[127] A moderate increase in SHM could be observed over time when VH gene germline identities of matching clonal members were

averaged.[127] Similar changes in SHM were observed for binding and neutralizing antibodies, with one exception being the neutralizing antibody subset, which showed a decrease in germline identity of 5% over the investigated period (Figure 15A).[127] In agreement with this finding, neutralizing antibodies isolated on days 8-17 after diagnosis showed VH gene germline identities of 97,5%, whereas antibodies isolated on days 34-42 had identities of 97,0% (Figure 15B).[127] These analyses show that SARS-CoV-2 neutralizing antibodies have similar levels of SHM between times of isolation.[127]

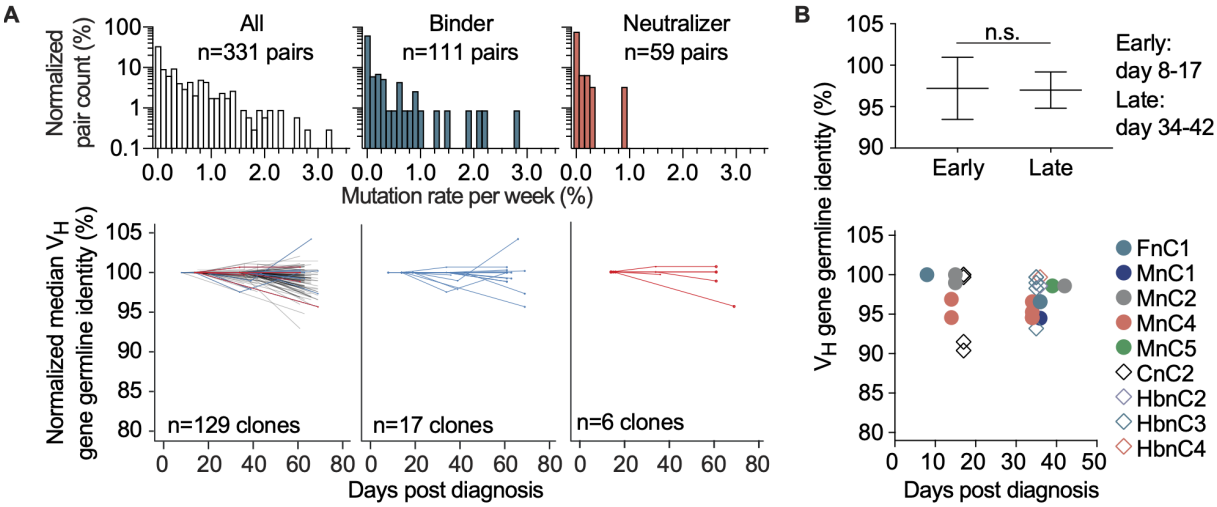

Figure 15. SARS-CoV-2 neutralizing antibodies exhibit similar SHM levels at different isolation timepoints.

(A) Mutation rates per week among clonal members (top) and median change in VH germline identity normalized to the initial measurement for each longitudinal clone (bottom). (B) Mean ±SD of VH germline identity for neutralizing antibodies grouped by early or late time points (top; two-tailed Mann-Whitney U test) and VH germline identities for all neutralizing antibodies grouped by the time from diagnosis to blood sample collection (bottom; see also Supplementary Table 4). [published in *Kreer et al., 2020, Cell; Figure 4*][127]

5.1.5. Identification of potential precursor sequences of SARS-CoV-2 neutralizing mAbs among healthy individuals

The high germline identities in many binding and neutralizing antibodies highlight the importance of distinct germline recombination present in the naïve human B cell repertoire.[127] Therefore, we performed unbiased NGS of heavy- and light chains from naïve B cell receptor repertoires from 48 healthy donors with samples collected prior to the SARS-CoV-2 pandemic (Supplementary Table 5).[127] The NGS analysis yielded 455.423 unique heavy, 170.781 κ, and 91.505 λ chain clonotypes (identical V and joining (J) gene segment with same CDR3 amino acid sequence) from 1,7 million collapsed reads.[127] The NGS sequences were searched for heavy and light chains resembling 79 binding antibodies (Figure 16A).[127] For 14 antibodies, 61 heavy chain clonotype matches from 28 healthy individuals with identical V/J pairs and similar CDRH3s (±1 amino acid length difference and

±3 amino acid total difference), including one exact CDRH3 match (MnC2t1p1_C12) were found (Figure 16B and C).[127] For 41 out of 62 κ light chains and 7 out of 17 λ light chains, 1.357 κ chain and 109 λ chain precursors with exact CDR3 matches were identified, respectively.[127] In every one of 48 healthy B cell repertoires, at least one κ and one λ chain precursor could be found.[127] Both heavy and light chain precursor sequences of 9 binding antibodies were found in 14 healthy individuals.[127] Notably, among these precursor sequences, close similarities to three potent SARS-CoV-2 neutralizing antibodies, HbnC3t1p1_G4, CnC2t1p1_B4, and HbnC3t1p2_B10, were found.[127] Despite that, NGS repertoire data did not include information on native heavy and light chain pairing matched heavy and light chain sequences that could be identified regardless of the small sample size of, on average, 9.500 heavy and 2.000-3.500 light chain clonotypes per individual.[127] In conclusion, potential SARS-CoV-2 binding and neutralizing antibody precursor sequences can be readily identified in naïve B cell repertoires.[127]

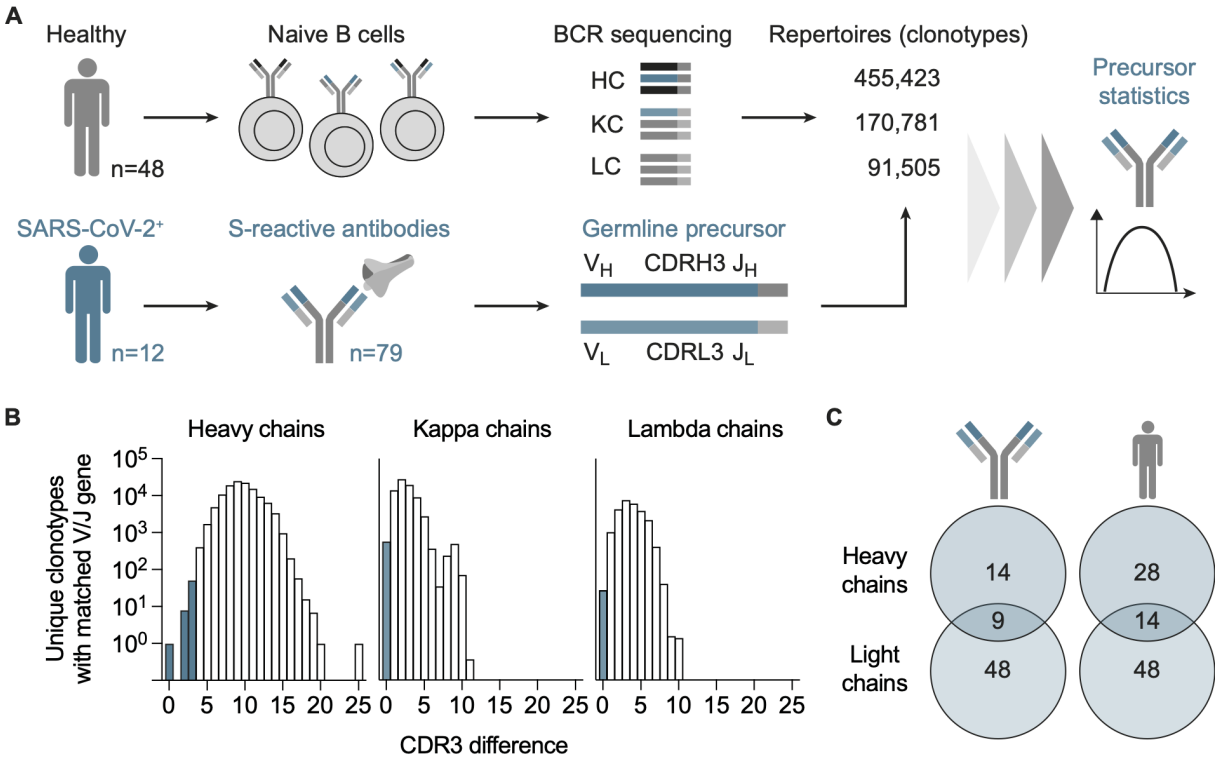

Figure 16. SARS-CoV-2 S reactive antibody sequence precursors found in naïve repertoires of healthy individuals.

(A) Schema for the identification of precursors in healthy naïve BCR repertoires. (B) Bar plot depicting the number of clonotypes found in healthy naïve BCR repertoires (n=48) with matched V/J genes from SARS-CoV-2 S protein binding antibodies (n=79) plotted against the CDR3 difference. Shades of blue are used to highlight potential precursors. Only heavy chain CDR3 differences of 1 aa in length and up to 3 aa mutations were allowed for precursors. Light chain CDR3 had to be identical. (C) Venn diagram of precursors identified in different individuals' antibody heavy and light chains. Numbers from the overlapping circles show the frequency of heavy and light chains being detected (see also Supplementary Table 5). [published in *Kreer et al., 2020, Cell*; Figure 5][127]

5.2. Investigating the impact of SHM on SARS-CoV-2 neutralization and viral escape

All results, including figures and tables in section 5.2 are adapted from *Korenkov et al., 2023, Immunity*.[148]

5.2.1. A subset of SARS-CoV-2 neutralizing mAbs can act irrespective of acquired mutations

To investigate the role of SHM in SARS-CoV-2 neutralizing antibodies, 92 mAbs were selected from the CoV-AbDab, which were isolated from at least 31 SARS-CoV-2 and 2 SARS-CoV convalescent individuals in 16 distinct studies published between 2020 and 2021.[148] This antibody panel comprised 62 unique VH/VL pairings and 86 unique CDRH3 sequences (Figure 17A, Supplementary Table 6).[148] Of the selected antibodies, 90 targeted the RBD and 2 the N-terminal domain with fewer overall mutations than the average memory B cell IgG repertoire (median of 3,5 [IQR: 2-6], 2 [IQR: 0-3], and 3 [IQR: 1-4] vs 10 [IQR: 6-14], 5 [IQR: 3-8], 6 [IQR: 3-8] amino acid substitutions in heavy, κ, and λ chains, respectively; Figure 17B, Supplementary Table 6).[148] Mutations were typically found within the CDR1 and CDR2 antibody regions (Figure 17B).[148] The distribution of heavy, κ, and λ chain variable (IGHV, IGKV, and IGLV) gene segments in this antibody panel showed a SARS-CoV-2 characteristic overrepresentation of distinct V genes such as IGHV3-53, IGHV3-66, IGKV3-20, and IGLV6-57 with 2:1 κ to λ ratio and CDR3 lengths comparable to the reference memory B cell IgG repertoire (Figure 18).[148] To dissect the impact of SHM, all 92 original mature (MT) as well as 88 possible VH/VL region germline reverted (GL) versions (four antibodies had no V gene mutations and were used as internal controls) were recombinantly expressed.[148] Both binding and neutralization activity of MT and GL antibody versions were determined by Wu01 S protein ELISA and pseudo-typed lentivirus neutralization assay.[148] Reversion of SHM either had no effect or decreased binding and neutralization activity up to a complete loss (Figure 17C, left panel).[148] A modest correlation between the total number of reverted mutations and the log fold changes in EC_{50} and IC_{50} values between MT and GL variants was identified, meaning antibodies with more mutations tended to lose functionality upon germline reversion more strongly (Figure 18).[148] For instance, antibodies with 1-5 mutations decreased on average by 1,2 $\log_{10}$ fold in neutralization, while antibodies with 6-10 mutations decreased 2,4 $\log_{10}$ fold (Figure 17C, right panel).[148] Interestingly, from the 88 neutralizing antibodies with one or more mutations, we identified 37 antibodies that had no relevant change in EC_{50} and 10 antibodies that had no relevant change in IC_{50} after germline reversion (Figure 17C), implying that these

antibodies have only acquired mutations that are neglectable for Wu01 binding and neutralizing activity.[148] Additionally, no binding activity of MT or GL antibody variants against human coronavirus S proteins (HCoV; OC43, HKU1, NL63, and 229E) could be detected in ELISA (Figure 19).[148] In summary, the importance of SHM for potent binding and neutralization of the ancestral Wu01 strain is increasing with the number of mutations present in an antibody.[148] However, some distinct antibodies remain unaffected by the reversion of SHM and, therefore, act independently of their mutations, relying on either germline V gene or CDR3 encoded sequence features for their activity.[148]

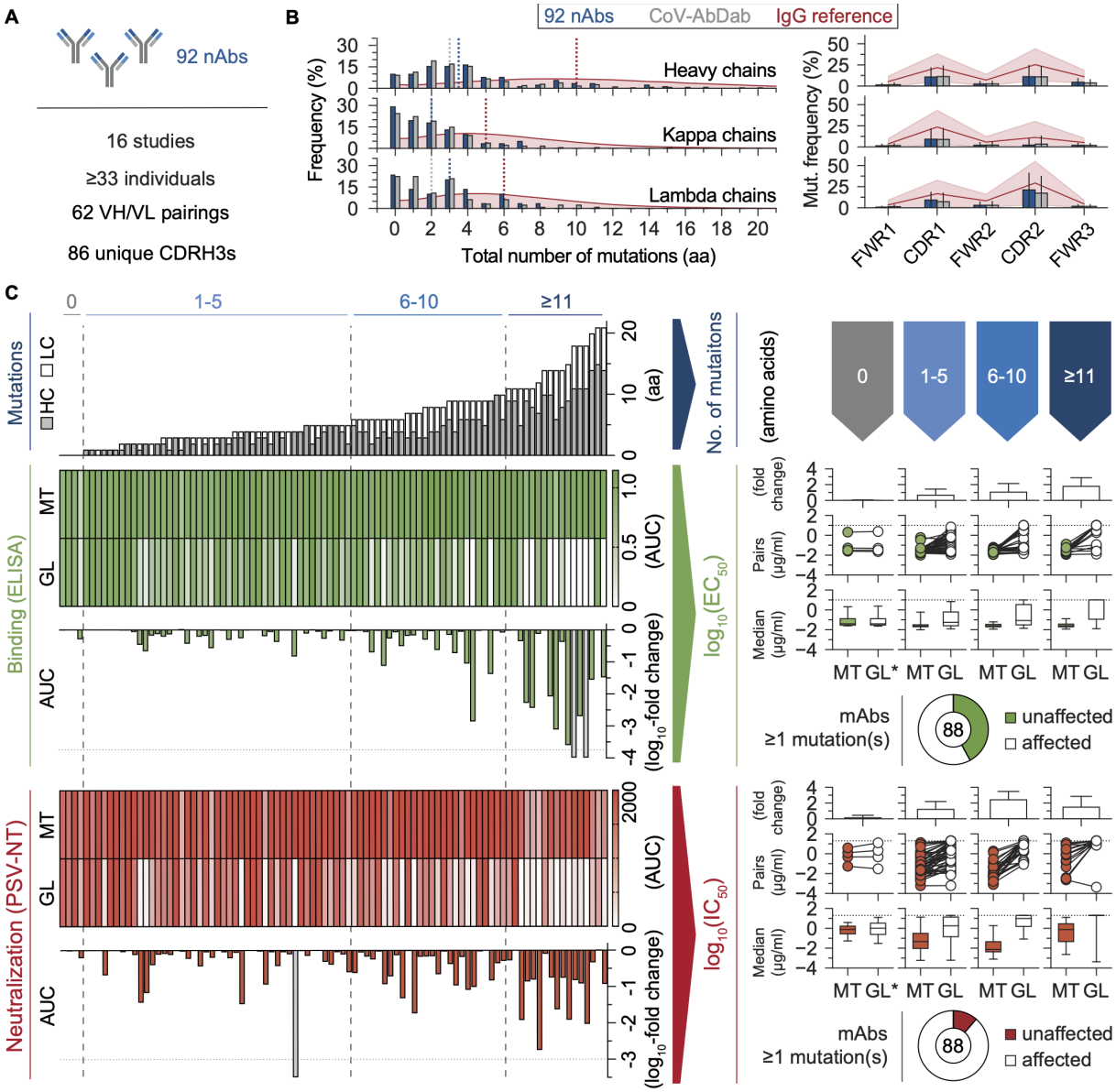

Figure 17. Most somatic mutations play an important role in antibody functionality.

(A) Schema of antibodies selected from the CoV-AbDab[149] for this study. (B) Frequency of V gene segment mutations (FWR1 to FWR3) in the selected antibodies compared to all human SARS-CoV-2 neutralizing antibodies found in the CoV-AbDab[149] (access date: 20.01.2021) and reference sequences from 57 healthy naïve BCR repertoires. The absolute number of mutations is shown in the left panel with dotted lines depicting the median. The relative frequency of SHM within antibody regions is shown in the right panel as bars with SD

depicted as error bars (mAbs) or as a line with the shaded area (IgG reference). (C) Binding (AUC/EC_{50}) and neutralization (AUC/IC_{50}) data were compared between MT and GL antibodies grouped by the total number of amino acid mutations. Individual fold changes in AUC (log_{10}; left panel) and the geometric mean of fold changes in the EC_{50}/IC_{50} values (log_{10}; right panel) are provided. Fold changes above the dashed line (open grey bars; left panel) represent a complete loss of potency following germline reversion. For EC_{50} and $IC_{50,}$ upper limits of quantification (ULOQ) are represented by dotted lines (right panel). Pie charts show the fraction of antibodies with conserved potency after germline reversion. GL*: no mutations, i.e., MT and GL sequences are identical. [published in *Korenkov et al., 2023, Immunity; Figure 1*][148]

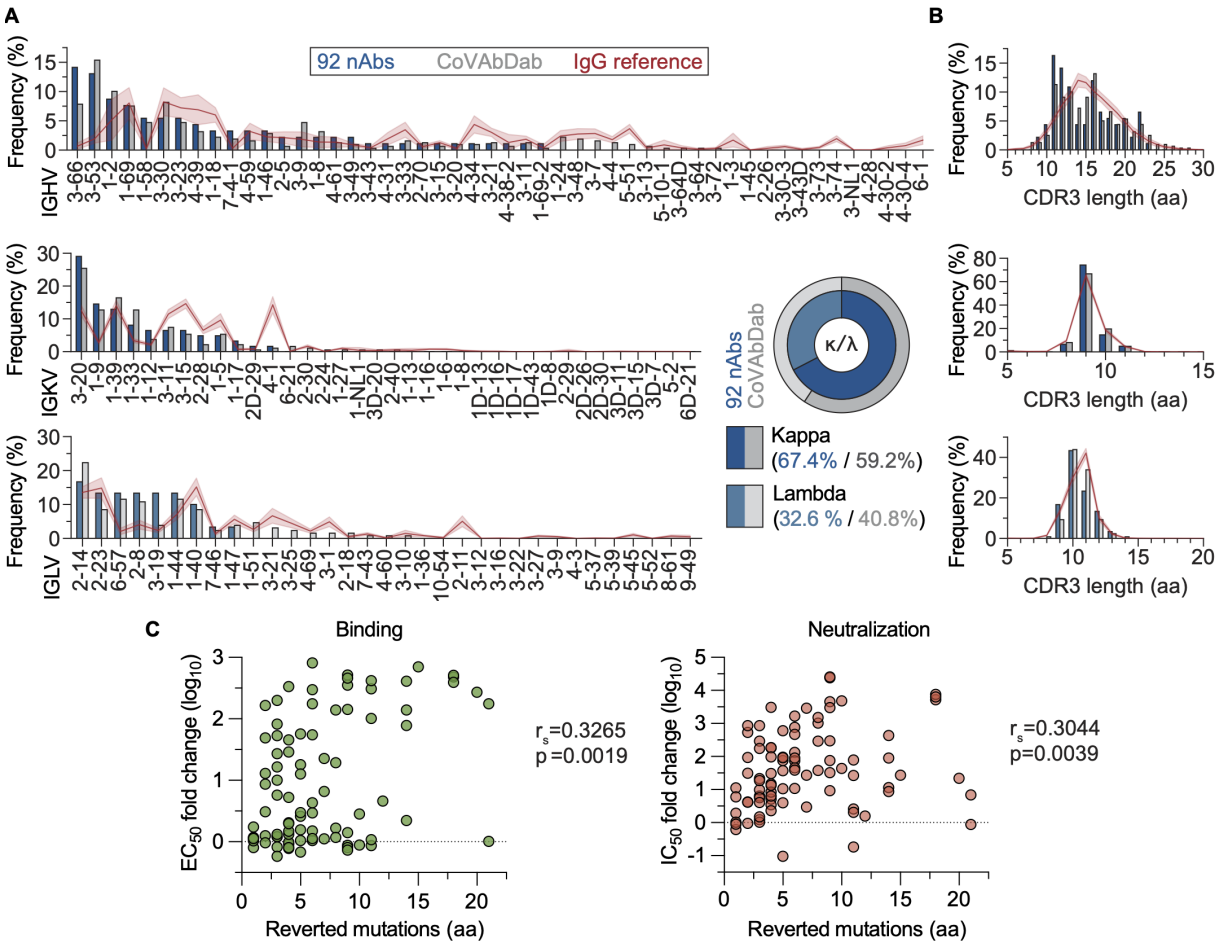

Figure 18. Sequence characteristics of the selected antibodies and correlation of reverted mutations with changes in antibody functionality.

(A) V gene segment usage for HC and LC and CDR3 length distribution for the selected 92 antibodies compared to 319 antibodies from the CoV-AbDab[149] and an IgG reference repertoire from 57 healthy individuals[127] as well as κ/λ ratios between selected antibodies and the CoV-AbDab[149]. IgG reference data is shown as the frequency mean (red solid line) with the SD (shaded area) (B) Length distribution of CDR3 for different V gene segments, including the selected 92 antibodies, the CoV-AbDab[149] and the IgG reference repertoire (as described in (A)). (C) A total number of reverted HC and LC mutations are correlated with the log_{10}-fold changes in EC_{50} or IC_{50} after germline reversion. Spearman correlation coefficients rs and corresponding p values are shown. [published in *Korenkov et al., 2023, Immunity; Supplementary Figure 1*][148]

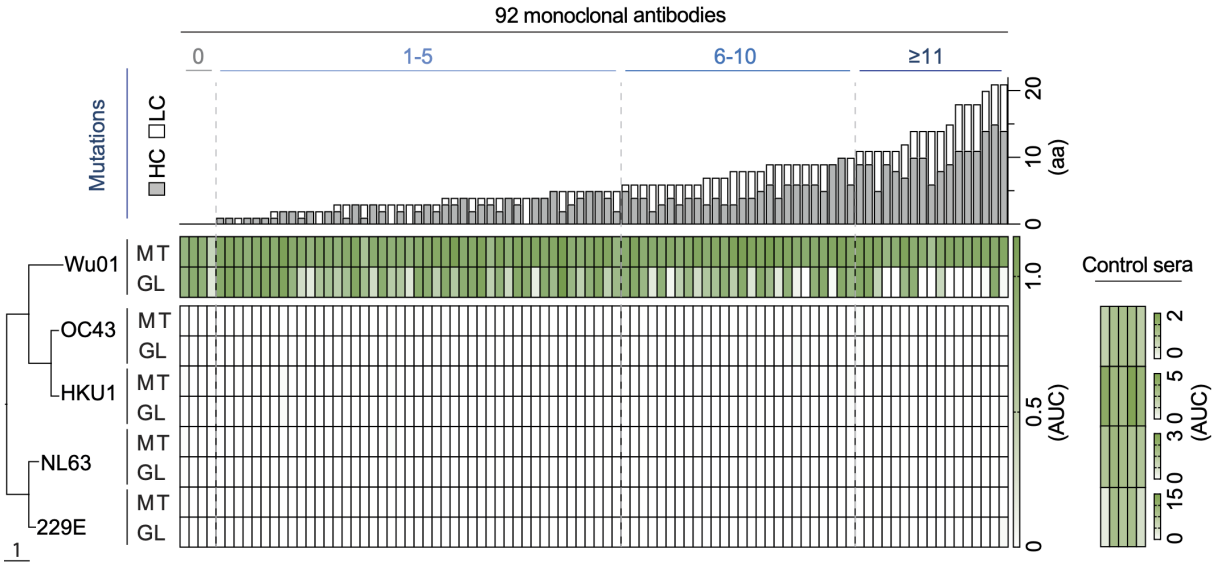

Figure 19. Cross reactivity of mature and germline reverted SARS-CoV-2 binding antibodies against endemic human coronavirus S proteins.

The heatmap shows the area under the curve (AUC) calculated from ELISAs of 92 antibodies against Wu01, OC43, HKU1, 229E, and NL63 S proteins. A phylogenetic tree is depicted with one amino acid substitution scale per side. Human coronaviruses were ordered according to their phylogenetic distance. Five control sera of healthy individuals were taken as controls for human coronavirus S protein binding activity. The mutation count and Wu01 data for MT and GL antibodies were taken from Figure 12C for comparison. [published in *Korenkov et al., 2023, Immunity; Supplementary Figure 2*][148]

5.2.2. SARS-CoV-2 Wu01 is neutralized by the VH1-58/VK3-20 public clonotype independently of SHM

To further investigate the importance of distinct sequence features that facilitate SHM-independent SARS-CoV-2 neutralization defined as ≤0,3 IC_{50} log_{10} fold change between MT and GL antibody versions, the correlation of IC_{50} log_{10} fold change with CDRH3 length, hydrophobicity, and V gene segment usage was calculated.[148] On average, SHM-independent neutralizing antibodies exhibited slightly but not significantly longer (p=0,2731) and more hydrophobic (p=0,0099) CDRH3 regions (Figure 20A).[148] Grouping all 10 SHM-independent neutralizing antibodies by V gene segments revealed that these antibodies are distributed across seven different VH/VL gene combinations (Figure 20B), with most antibodies belonging to commonly described public VH gene groups such as IGHV3-53/3-66, 3-30, and 1-69 dropping substantially in the mean neutralization after germline reversion (Figure 21A).[148] However, antibodies belonging to the IGHV1-58 group were among the most potent neutralizers and showed no dependence on the few mutations they acquired (Figure 21A, highlighted in green).[148] Antibodies belonging to this previously described public clonotype were exclusively paired with an IGKV3-20 κ light chain and were characterized by a highly convergent 16 amino acid CDRH3 region, including a double cysteine motif (Figure 21B).[148] Interestingly, the VH1-58 class public clonotype accounted

for 95 (79%) out of 119 IGHV1-58 antibody sequences reported to neutralize the ancestral SARS-CoV-2 Wu01 isolate deposited in the CoV-AbDab.[148] A solved crystal structure of HbnC3t1p1_C6 belonging to the VH1-58 public clonotype classified these antibodies as class 1 binders according to the classification scheme proposed by Barnes et al. (Figure 22A).[121] The structure revealed contact sides between all heavy and light chain CDRs and some residues at the RBD ridge, namely a long loop connecting β-strands 5 and 6 of the RBD (residues 473-489; PDB: 7B0B, Figure 22B and C, Supplementary Table 7).[148] While several RBD residues contribute to the epitope, Phe486 holds a central position as it is tightly packed in a hydrophobic pocket formed at the interface between the heavy and light chains and is central to the interaction (Figure 22D).[148] The CDRH3 double cysteine motif forms a disulfide bridge, critically contributing to the binding and neutralization activity of the antibody (Figure 22E and F).[148] In line with the sequence similarity, the binding mechanism within the VH1-58 public clonotype seems highly convergent as the structure of HbnC3t1p1_C6 is almost identical in an overlay with 7 solved structures of VH1-58 class members (Figure 22G).[148] In conclusion, potent SARS-CoV-2 neutralizing antibodies that act independent of SHM can arrive from different V(D)J recombination events and heavy and light chain pairings.[148] Within SHM-independent neutralization, the VH1-58 public clonotype displayed remarkable convergence across many individuals.[148]

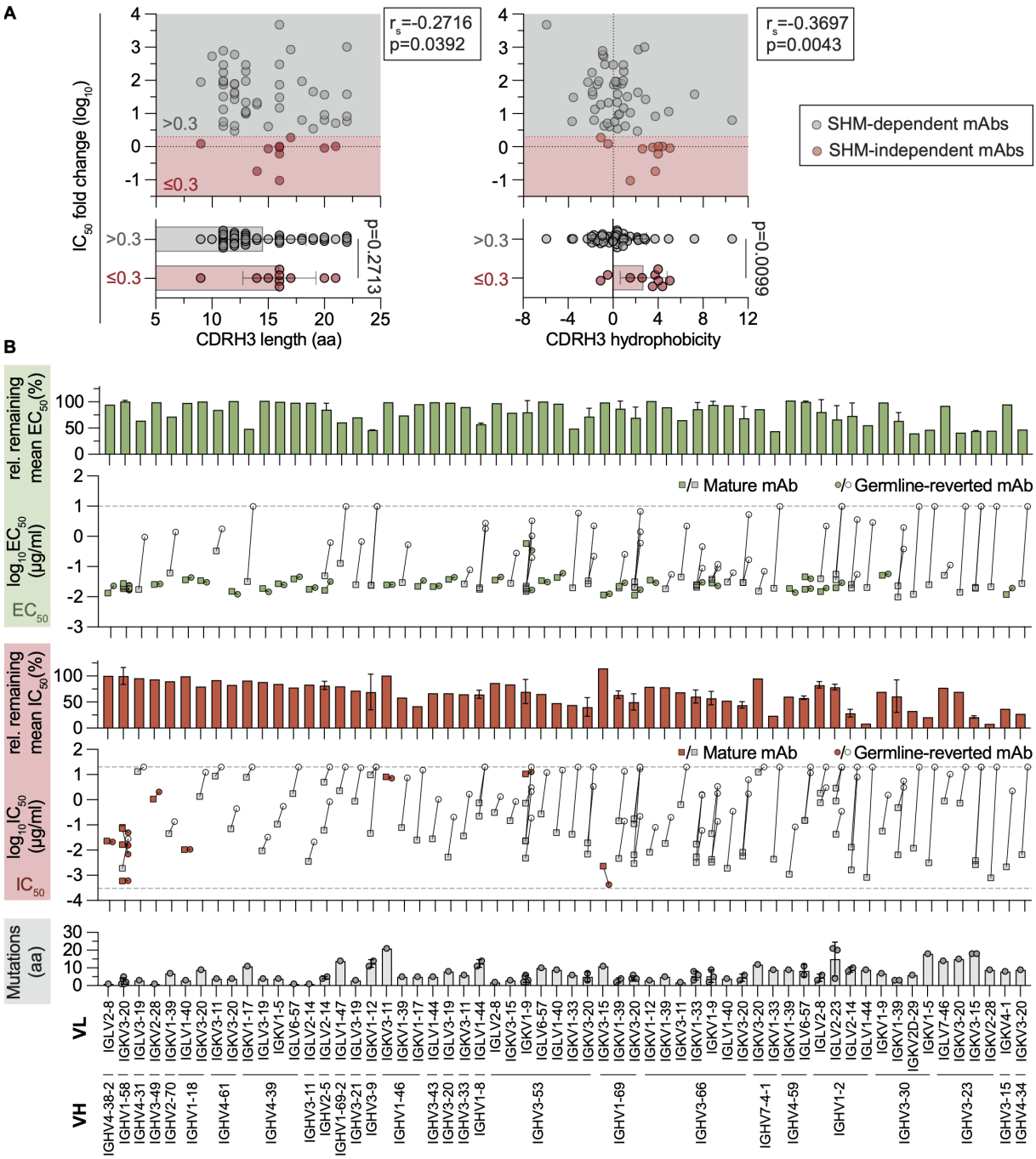

Figure 20. Change in neutralization between MT and GL antibodies correlated with CDRH3 characteristics as well as binding and neutralization characteristics grouped by V gene segments.

(A) For antibodies containing at least 1 mutation and still neutralized after germline reversion (log_{10} fold change after reversion ≤0,3; n=58), CDRH3 length in amino acids and hydrophobicity based in the Eisenberg scale were correlated with log_{10} fold change IC_{50} after germline reversion. P values from two-tailed, unpaired t-tests are depicted in the plots, and a Spearman correlation coefficient rs and corresponding p values. (B) MAbs were grouped by V gene segment and sorted by mean log_{10} fold IC_{50} change in each group as in Figure 13. Bars depict the mean remaining EC_{50} after germline reversion normalized to the maximum detectable difference i.e., LLOQ (0,0001 µg/ml) to ULOQ (10µg/ml) in the upper panel. Log_{10} EC_{50} values for individual MT (squares) and GL (circles) antibodies are shown in scatter plots with corresponding pairs connected by a line. A dashed line depicts the ULOQ. Middle panels show bars depicting the mean remaining IC_{50} after germline reversion normalized to the maximum detectable difference, i.e., LLOQ (0,0003 µg/ml) to ULOQ (20 µg/ml). Log_{10} IC_{50}

values for individual MT (squares) and GL (circles) antibodies are shown in scatter plots with corresponding pairs connected by a line. ULOQ/LLOQ are depicted as dashed lines. For each V gene segment group individual (dots) and mean (bars) number of mutations are shown in the lower panel. Antibodies remaining unaffected by GL reversion (log_{10} fold change ≤0,3) are highlighted in green for binding and red for neutralization. [published in *Korenkov et al., 2023, Immunity; Supplementary Figure 3*][148]

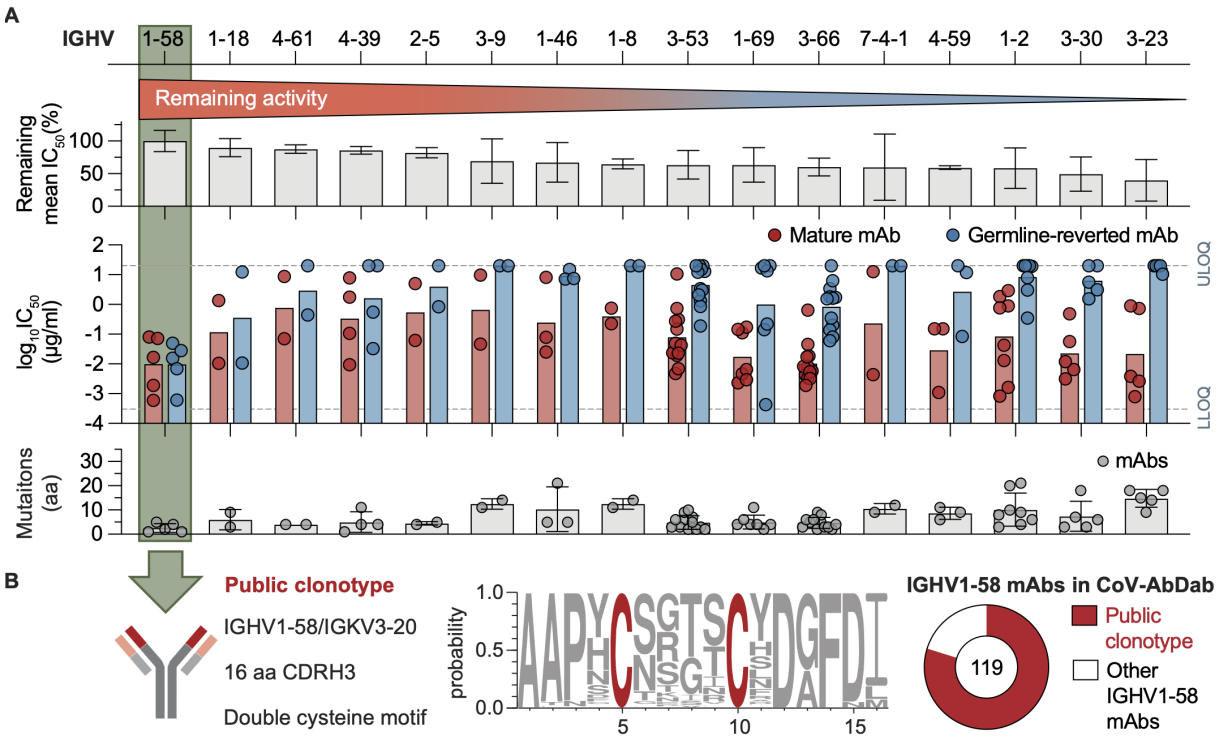

Figure 21. VH1-58/VK3-20 public clonotype members neutralize SARS-CoV-2 Wu01 variant independently of SHM.

(A) Antibodies were categorized based on VH gene segments and arranged by the mean log_{10}-fold change in IC_{50} within each group. The top bars show the mean remaining IC_{50} after germline reversion normalized to the maximum detectable difference spanning from LLOQ (0,0003 µg/ml) to ULOQ (20 µg/ml). Mean log_{10} IC_{50} values of MT (red) and GL (blue) antibodies are shown in the middle bar graph, with individual antibodies depicted as dots. The bottom bar graph shows the mean number of mutations per VH group with individual antibodies depicted as dots. Only VH groups with at least 2 members are displayed here. (B) Sequence characteristics (left panel) and total number of antibodies found in the CoV-AbDab[149] (right panel) are depicted for the VH1-58/VK3-20 public clonotype. [published in *Korenkov et al., 2023, Immunity; Figure 2*][148]

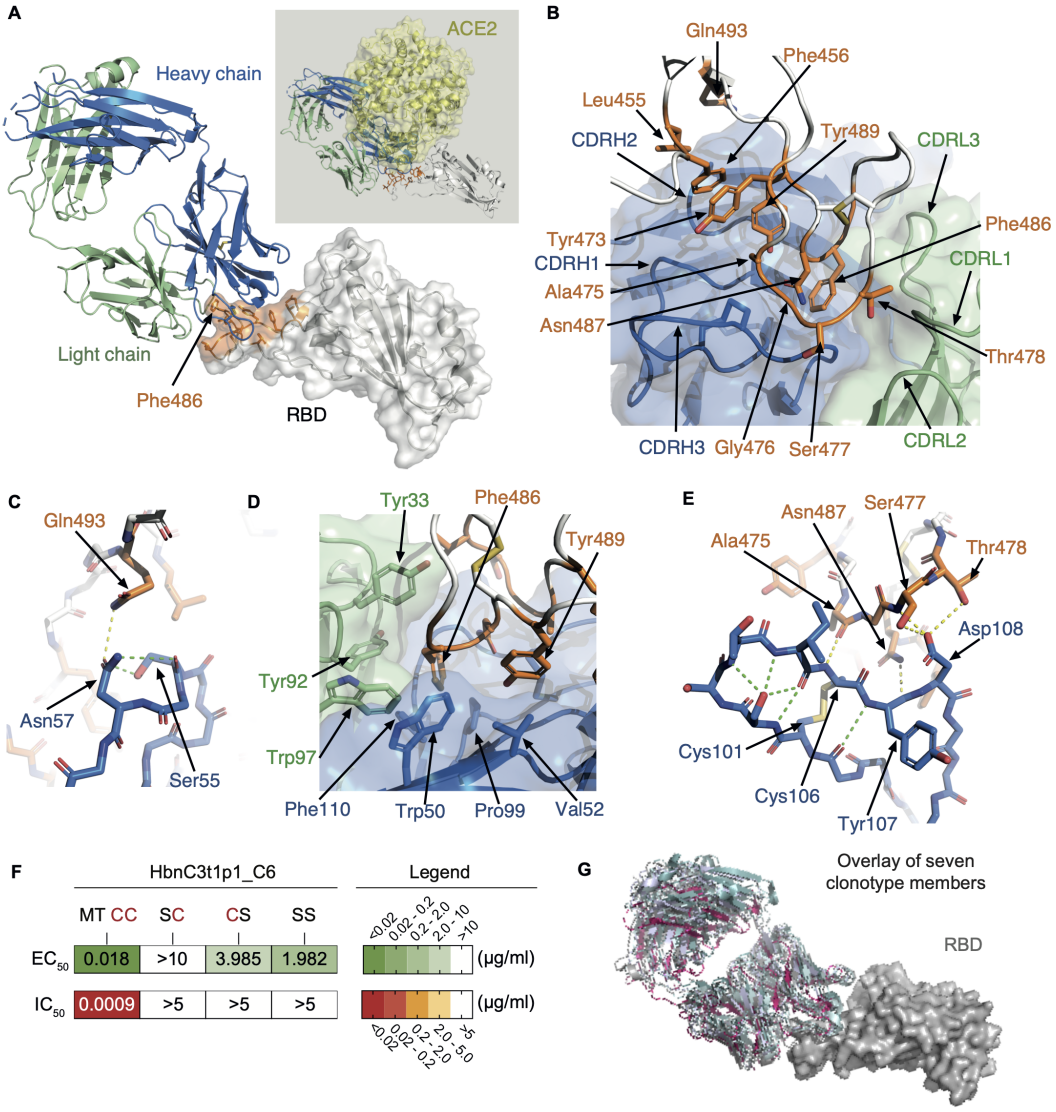

Figure 22. A disulfide bridge formed in the CDRH3 of VH1-58/VK3-20 antibody HbnC3t1p1_C6 is critical for antibody functionality.

(A) HbnC3t1p1_C6 Fab (blue and green for HC and LC, respectively) overall structure in complex with the SARS-CoV-2 Wu01 RBD (grey, semitransparent surface representation). The epitope is highlighted in orange, and a central feature of the complex, Phe486, is marked. In the grey insert, the ACE2/RBD structure (PDB: 6M17) is shown with the HbnC3t1p1_C6/RBD complex superimposed. The antibody substantially overlaps with the ACE2 binding site, indicating that neutralization is achieved through blockage of the ACE2 interaction with the S protein. (B) An overview of HbnC3t1p1_C6 epitopes is shown. Residues comprising the SARS-CoV-2 RBD epitope of HbnC3t1p1_C6 are labeled and presented as orange sticks. Semitransparent surfaces in blue and green show HC and LC of HbnC3t1p1_C6, respectively. (C) HbnC3t1p1_C6 CDRH2 forms a polar interaction with the RBD. Asn57 forms hydrogen bonds (yellow dashed line) with Gln493 of the RBD while also being stabilized by hydrogen bonds (green dashed lines) to the nearby Ser55. (D) A hydrophobic pocket consisting of Tyr33 from CDRL1, Tyr92, and Trp97 from CDRL3, Pro99, and Phe110 from the CDRH3 interacts with Phe486 of the RBD at the interface between HC and LC. Trp50 from the HC framework region contributes to the pockets side. Val52 makes a hydrophobic interaction from the CDRH2 with Tyr489 of the RBD. (E) HbnC3t1p1_C6 CDRH3 region forms polar interactions with the RBD. Cys106 and Cys101 form a disulfide bridge, stabilizing the CDRH3 conformation with a series of hydrogen bonds (green dashed lines) involving the main chain atoms. Hydrogen bonds (yellow dashed lines) are made between Asp108 through its side chain and Cys106 and Tyr107

through their main chain with Thr478, Ser477, Asn487, and Ala475 of the RBD. CDRH3 main chain is depicted as sticks. (F) HbnC3t1p1_C6 binding and neutralization data with single (SC, CS) and double (SS) cysteine substitutions to serine. (G) 7 VH1-58/VK3-20 antibodies in a structural overlay binding the SARS-CoV-2 RBD (PDB: 7B0B, 7E3K, 7E3L, 7BEN, 7P40, 7EZV, and 7LR). [published in Korenkov et al., 2023, Immunity; Figure 3][148]

5.2.3. Acquired mutations are important for Omicron BA.1 and BA.2 subvariants neutralization by VH1-58 class antibodies

To study how VH1-58 public clonotype antibodies that were isolated from the first SARS-CoV-2 convalescent individuals cope with viral evolution and the relevance of SHM within this context, 17 additional clonotype members totaling 22 antibodies were produced from at least 16 different individuals 2 of which were mRNA vaccinated and investigated for their neutralization potency against Wu01, Alpha, Beta, Delta as well as Omicron BA.1 and BA.2 variants (Supplementary Table 8).[148] This public clonotype is especially suited to address this question due to its highly conserved CDRH3 and exclusive VK3-20 light chain pairing, minimizing potential interference by other factors.[148] All VH1-58 antibodies could neutralize Alpha, Beta, and Delta variants.[148] However, only a subset neutralized the more distant Omicron subvariants (Figure 23A).[148] Interestingly, no or only moderate effects in neutralization potency against Wu01, Alpha, Beta, and Delta variants were observed for GL reverted antibodies compared to their MT counterparts but substantially weakened or complete loss of activity against Omicron subvariants for most MT Omicron neutralizing mAbs.[148] This indicates that some VH1-58 public clonotype members acquired mutations that could account for differences in the SARS-CoV-2 S protein interaction of antibodies in prior variants and in Omicron.[148] A similar observation of SHM-dependent separation of Wu01, Delta, and Omicron BA.1 reactivity could also be observed for spike binding determined by ELISA (Figure 24A and B).[148] To further understand the role of SHM in fostering Omicron neutralization, the number and pattern of mutations in all 22 VH1-58 antibodies were analyzed.[148] Generally, SHM tended to be enriched in the heavy chains of Omicron-neutralizing antibodies with some potential mutational hotspot regions and shared mutations (e.g., T30S in CDRH1).[148] In contrast, light chain SHM seemed to focus on CDRL1 and 2 with a prominent S30R mutation in the CDRL1 (Figure 23B).[148] Notably, when heavy chains from Omicron neutralizing antibodies were paired with light chains from Omicron non-neutralizing antibodies, Omicron neutralization capacity was mostly retained but not vice versa (Figure 23C).[148] These findings indicate that heavy chain mutations more strongly influence Omicron neutralization.[148] To find critical amino acid substitutions in the heavy chains of Omicron neutralizing antibodies, CDRs 1-2 or FWR 1-3 were reverted to germline by region or in combination (Figure 25A).[148] Additionally, single and combinations of mutations were reverted to germline for two of the most potent Omicron neutralizing

antibodies, C043 and CQTS004 (Figure 25B).[148] Surprisingly, almost all antibodies tolerated the partial reversion of SHM with only up to one $\log_{10}$-fold change decrease in neutralization capacity, suggesting that heavy chain mutations mostly act additively to enable Omicron neutralization.[148] However, for CQTS004, the N47D mutation in the CDRH2 could be identified as a critical single substitution for Omicron neutralization.[148] Notably, the neutralization activity of CQTS004 against Wu01 was increased by some germline reversions in CQTS004, including N47D.[148] In summary, some specific VH1-58 public clonotype antibodies elicited prior to the SARS-CoV-2 Omicron variant emergence accumulated divergent “bystander” mutations that additively convey Omicron BA.1 and BA.2 neutralization activity.[148]

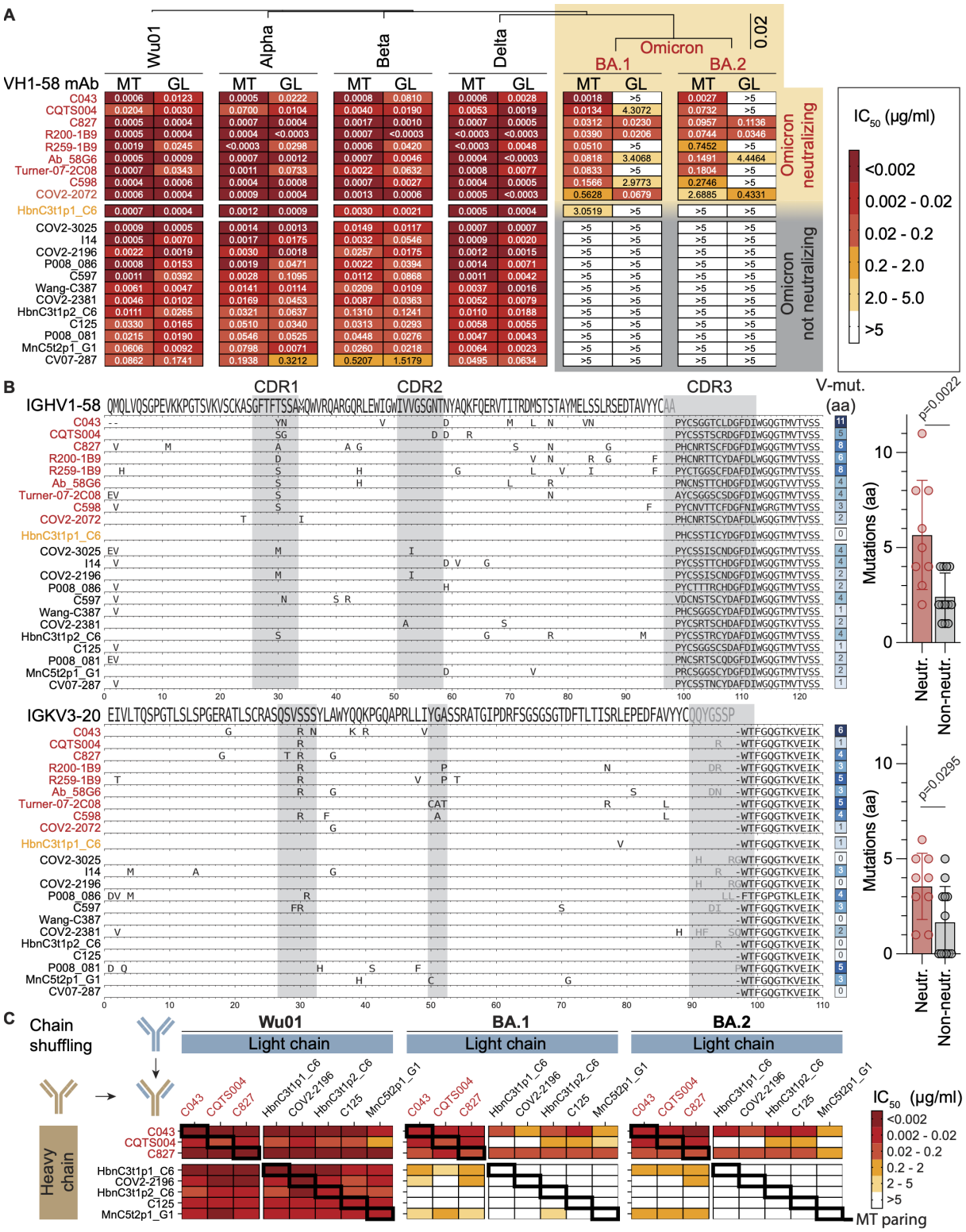

Figure 23. Distinct mutational profiles within VH1-58/VK3-20 public clonotype antibodies can restore neutralization activity against Omicron BA.1 and BA.2 sublineages.

(A) Neutralization potency of 22 MT and GL antibodies against Wu01-, Alpha-, Beta-, Delta-, BA.1-, and BA.2-pseudotyped virus. Mean IC_{50} values of at least two independent experiments are shown in the heatmaps, and IC50 values ranked antibodies against BA.1. The amino acid distance between different SARS-CoV-2 S protein variants is shown using a phylogenetic tree with the scale bar set to 0,02 substitution per site. (B) Multiple sequence alignment with V gene amino acid mutations (FWR1 to FWR3, excluding CDR3) are shown for IGHV1-58 heavy (top panel) and IGKV3-20 light chains (lower panel) for the 22 tested antibodies. (C) Neutralization

potency against Wu01, BA.1, and BA.2 for shuffled HC (rows) and LC (columns) VH1-58 antibodies. The mean IC_{50} values of two technical replicates are shown in the heatmap. [published in *Korenkov et al., 2023, Immunity; Figure 4*][148]

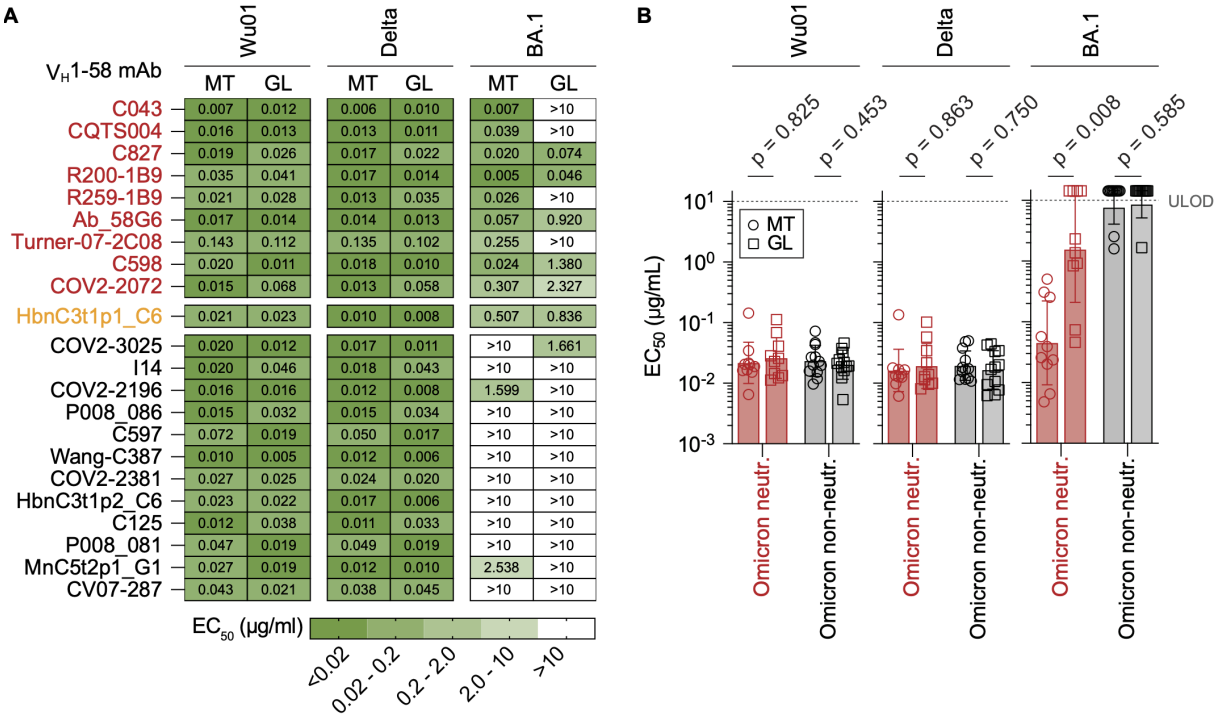

Figure 24. The influence of SHM on binding of VH1-58 class antibodies to Wu01, Delta and Omicron BA.1 S proteins.

(A) EC_{50} values of 22 MT and GL antibodies determined by ELISA against Wu01, Delta, and Omicron BA.1 S proteins are shown. Biological duplicates were tested. Omicron BA.1 and BA.2 neutralizing antibodies are depicted with red labels. (B) EC_{50} values from panel (A) are shown in a scatter plot grouped by Omicron neutralization activity with bar graphs and error bars showing geometric mean and SD. ULOD: upper limit of detection (10 µg/ml). [published in *Korenkov et al., 2023, Immunity; Supplementary Figure 4*][148]

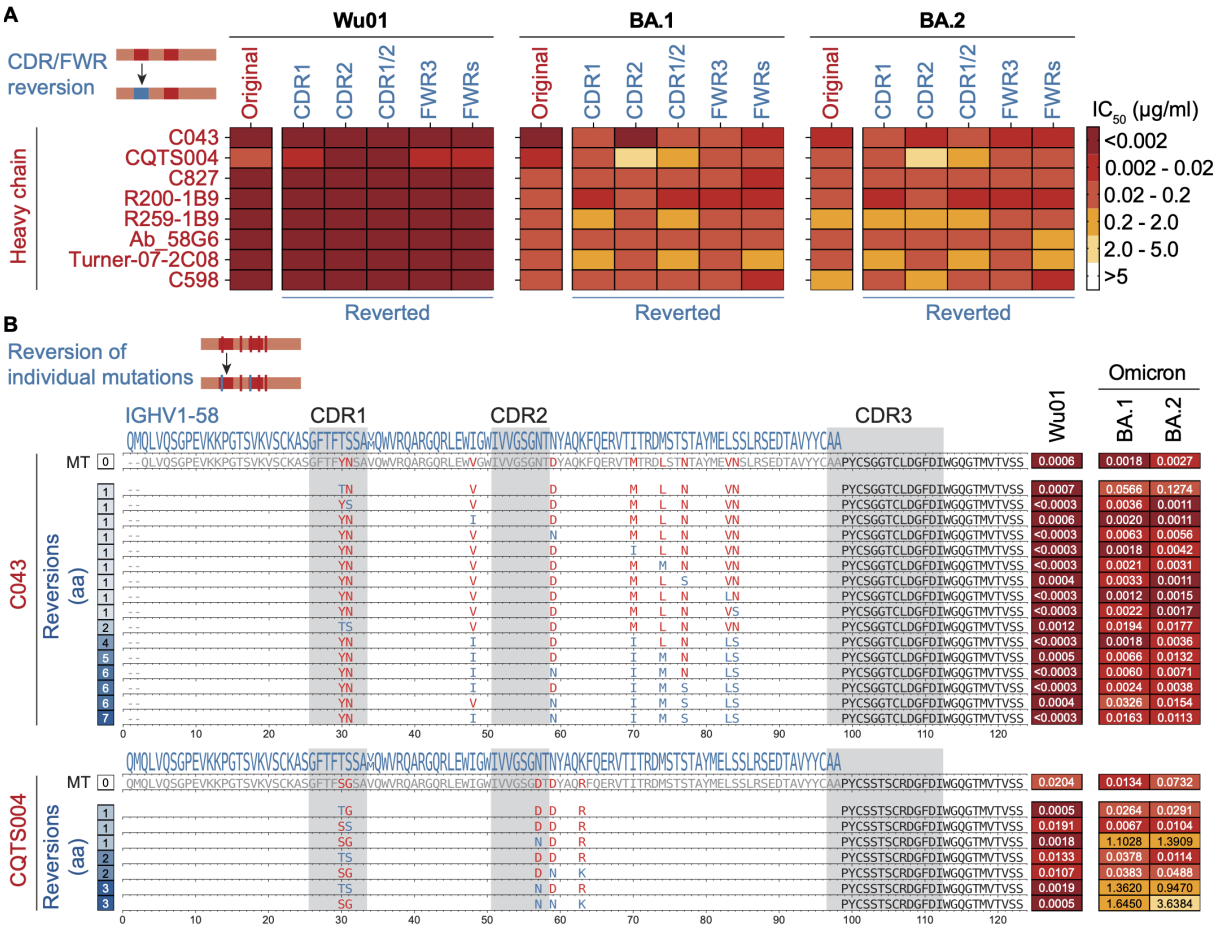

Figure 25. The effect of individual or grouped mutation reversion on Omicron neutralization by VH1-58 antibodies.

(A) HC CDRs and FWRs were reverted to GL for eight Omicron neutralizing antibodies. Partially reverted antibodies (reverted HC paired with original LC) were tested against Wu01, BA.1, and BA.2 in a pseudovirus neutralization assay. Mean IC_{50} values from two independent experiments are shown in the heatmap. (B) For CQTS004 and C043, additional individual or combinations of HC mutations were reverted to GL, as highlighted by blue amino acids in the multiple sequence alignment. IC_{50} values were determined and represent means from two independent experiments. Antibody variants are sorted by the number of reverted mutations. Original MT neutralization values were taken from Figure 15A. [published in *Korenkov et al., 2023, Immunity; Supplementary Figure 5*][148]

5.2.4. Omicron BA.1 and BA.2 neutralization activity in non-neutralizing VH1-58 antibodies can be conferred by a single mutation

Since antibodies belonging to the VH1-58 public clonotype are marked by a highly convergent CDRH3 region, it was speculated that SHM can be transferred from VH1-58 Omicron neutralizing clonotype members onto VH1-58 Omicron non-neutralizing clonotype members to restore Omicron neutralization capacity.[148] For this purpose, eight fully mutated VH genes from BA.1/2 neutralizing antibodies (donor) were transferred onto six non- or weakly neutralizing Omicron antibodies (acceptor) while keeping their original CDRH3 and light chain combination.[148] This included the VH1-58 antibody tixagevimab (COV2-2196),

which has been used in combination with cilgavimab to treat and prevent SARS-CoV-2 infection and that lost neutralization potency against Omicron BA.1 and BA.2.[148] Strikingly, the transfer of at least four different VH gene mutation patterns fully restored neutralization activity against BA.1 and BA.2 subvariants in all non-neutralizing antibodies and markedly improved the neutralization potency of weak neutralizers (Figure 26A).[148] Interestingly, mutation patterns from antibodies R200-1B9 and C827 restored Omicron neutralization in other VH1-58 antibodies but were not essential for their Omicron neutralization activity (Figure 23A).[148] To further pinpoint critical single mutations or patterns that convey Omicron neutralization, ten mutational patterns with single or combinations of up to five amino acid substitutions identified from Omicron neutralizing VH1-58 antibodies were transferred onto HbnC3t1p1_C6 a partially Omicron neutralizing antibody or two non-Omicron neutralizing antibodies C125 and COV2-2196 (Figure 26B).[148] All ten transferred mutational patterns improved BA.1, and seven mutational patterns restored BA.2 neutralization in antibody HbnC3t1p1_C6. For COV2-2196, BA.1 and BA.2 neutralization activity was restored for seven out of ten combinations.[148] For C125, seven out of ten combinations restored Omicron neutralizing activity, but only four restored BA.2 neutralization.[148] A higher initial binding capacity of these tested antibodies towards Omicron S protein could explain the observed improvement in Omicron neutralization.[148] While HbnC3t1p1_C6 MT showed limited neutralization activity against BA.1 and no activity against BA.2 within the range of concentrations tested, it exhibited the lowest EC_{50} with 0,5 µg/ml against BA.1 spike followed by COV2-2196 with 1,6 µg/ml and no detectable binding for C125 (Figure 25).[148] In agreement with this observation, the CDRH3 of HbnC3t1p1_C6 is more closely related to the CDRH3s of antibodies R200-1B9, C827, and COV2-2072 with a histidine at position 100 and an aromatic tyrosine residue at position 107 all of which can neutralize Omicron independent of SHM.[148] Importantly, Omicron BA.1 and BA.2 neutralization activity could be restored in VH1-58 antibodies HbnC3t1p1_C6 and COV2-2196 by only inserting a single aspartic acid at position 57, which is the same substitution critical for Omicron neutralization in antibody CQTS004 (Figure 25B).[148] This is structurally explained by a glutamine to arginine replacement at position 493 in the BA.1/2 spike proteins, annulling a strong double hydrogen bond interaction with Asn57 of HbnC3t1p1_C6.[148] Therefore, introducing aspartic acid in position 57 could enable the formation of a salt bridge between Asp57 and Arg499, restoring the ability to bind BA.1/2 spike proteins.[148] In conclusion, VH1-58 antibodies depend on different SHM patterns in neutralizing Omicron BA.1/2 subvariants.[148] The transfer of distinct V-gene SHM patterns can restore Omicron neutralization activity in non-Omicron neutralizing VH1-58 clonotype members, including the clinical antibody tixagevimab, which could be used to rapidly adapt therapeutic mAbs against novel SARS-CoV-2 variants.[148]

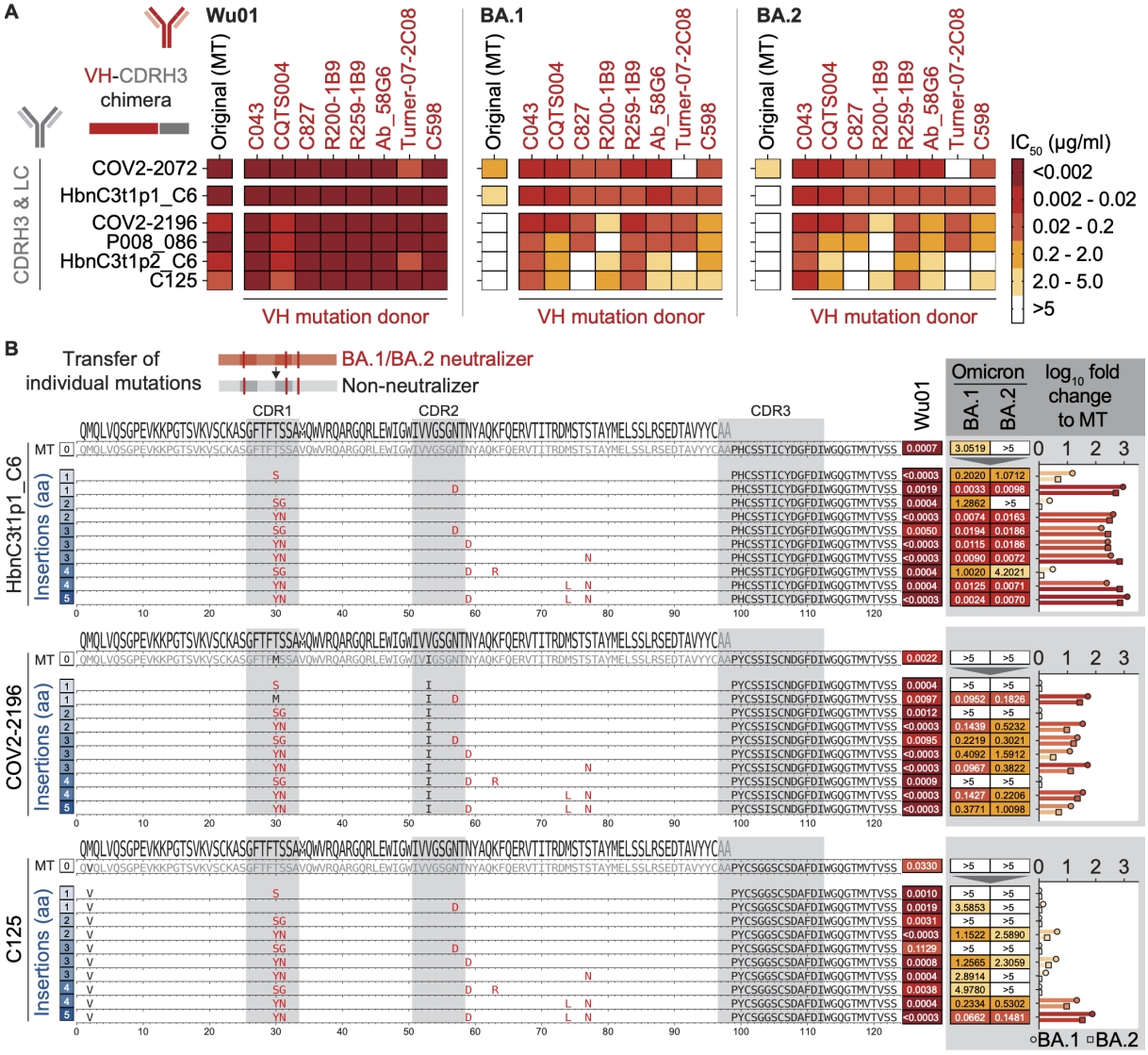

Figure 26. Transfer of somatic mutations enables Omicron neutralization in previously non-neutralizing VH1-58 antibodies.

(A) VH region (FWR1 to FWR3) of BA.1/2 weakly, partially, or non-neutralizing VH1-58 antibodies (n=6) were replaced with the VH region of potently neutralizing BA.1/2 VH1-58 antibodies (n=8) while retaining the original CDRH3 and light chain to generate VH-CDRH3 chimeras. The rows on the left depict CDRH3/LC donors, and VH mutations are shown on the top. Mean IC_{50} values of two independent experiments for VH-CDRH3 chimeras are shown for Wu01, BA.1, and BA.2 pseudovirus neutralization. For comparison, the original MT antibody's IC_{50} values were taken from Figure 15A. (B) Multiple sequence alignment of HbnC3t1p1_C6, COV2-2196, and C125 MT antibodies with individual variants are depicted with the IGHV1-58 gene segment used as a reference. Antibodies were sorted by number of inserted mutations. The heatmaps on the right side show the mean IC_{50} values of two independent Wu01, BA.1, and BA.2 pseudovirus neutralization assays. Log_{10} fold change IC_{50} against BA.1 (circles) and BA.2 (squares) are depicted in the bar graphs with original MT antibodies with values ">5" set to 5 for calculation purposes. [published in *Korenkov et al., 2023, Immunity; Figure 5*][148]

5.3. Different SARS-CoV-2 Omicron sublineages harbor distinct antibody escape profiles

All results, including figures and tables in section 5.3, are adapted from *Gruell et al., 2022, Cell Host & Microbe*.[155]

5.3.1. Omicron sublineages differ from BA.1 in key residues of the S protein and will likely be among the dominant variants

The initial Omicron case surge was mainly dominated by BA.1 and BA.1.1 lineages, with the spike protein of BA.1 differing in 39 amino acid residues from the ancestral Wu01 SARS-CoV-2 strain (Figure 27A).[155] Other Omicron sublineages share several BA.1 residues that diverge at various critical amino acid positions (Figure 27A and B).[155] For example, the BA.1.1 spike protein has the same R346K substitution in the RBD that is associated with escape from neutralizing antibodies and was observed in the SARS-CoV-2 Mu variant (Figure 27A).[155,169] The BA.2 variant, which rapidly outcompeted BA.1 and BA.1.1, shares 21 of 31 amino acid changes in the spike protein with BA.1 but has an entirely different set of residues in both the N-terminal domain and the RBD, both regions that are epitopes for the most potent SARS-CoV-2 neutralizing antibodies (Figure 27A-C).[155] However, new Omicron sublineages are rapidly emerging following a decrease in reported cases from the initial BA.1/BA.2 wave.[155] For example, the BA.2.12.1 lineage outpaced the other BA.2 lineages, increasing the number of SARS-CoV-2 cases observed in the United States.[155] Additionally, the BA.4 and BA.5 sublineages with identical spike proteins became the dominant variants in South Africa and Portugal within weeks of identification, driving a rise in case numbers (Figure 27C).[84,155] BA.2.12.1 and BA.4/5, which share 94% and 90% of their spike mutations with BA.2, contain additional changes at key residues associated with increased antibody escape properties.[155] These include substitutions also recorded for the Lambda and Delta variants at residue 452 with L452Q in BA.2.12.1 and L452R in BA.4/5 (Figure 27A)[170,171] and an F486V substitution in the RBD of BA.4/5 that was not previously described in other variants of interest or concern but is associated with mAb affinity.[155,172] In conclusion, key residues of the spike protein in the newly emerged Omicron sublineages differ from BA.1.[155] It is highly probable, considering their apparent growth advantages compared to BA.1 and the prevalent BA.2, that Omicron sublineages BA.2.12.1 and BA.4/5 will emerge as dominant variants in the future.[155]

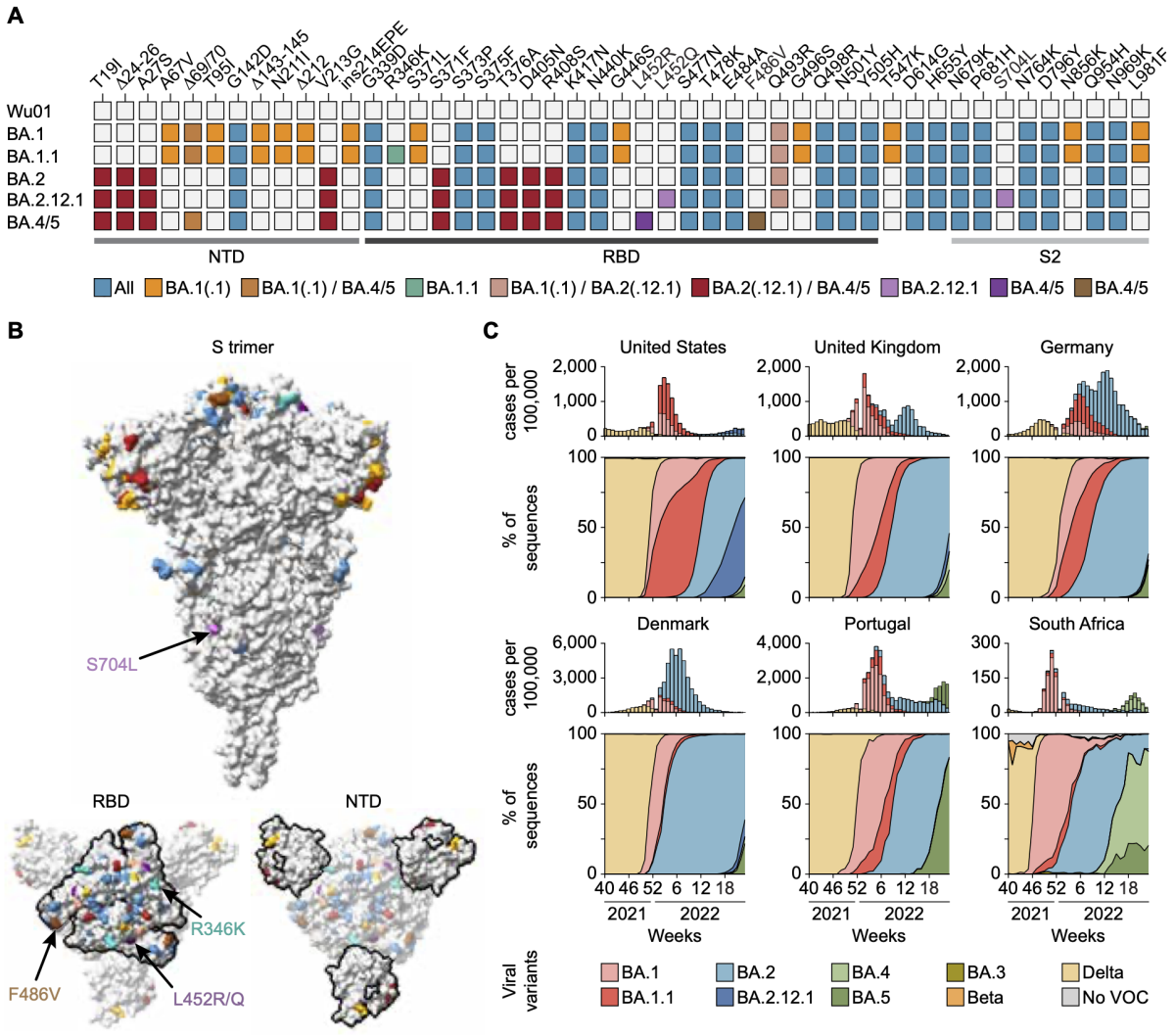

Figure 27. Newly emerged Omicron sublineages differ from BA.1 in key residues of the S protein.
(A) S protein amino acid differences in Omicron sublineages relative to Wu01. (B) Omicron sublineage S protein amino acid differences are located on the SARS-CoV-2 S protein (PDB: 6xR8), and the same colors are used in (A). In the bottom model, RBD and NTD are outlined. Arrows indicate residues with mutations exclusively found in individual sublineages. (C) Weekly reported SARS-CoV-2 infection data (taken from Johns Hopkins University CSSE COVID-19 data repository[165] and Our World in Data[173]) are shown in the top panels. Data on variant proportions extrapolated from weekly GISAID SARS-CoV-2 database variant sequences[85–87] (accessed on 20.06.2022) are shown in the bottom panels. [published in *Gruell et al., 2022, Cell Host & Microbe; Figure 1*][155]

5.3.2. Booster immunizations are important for neutralizing serum activity against all prevalent Omicron sublineages

To investigate the capability of different Omicron sublineages, namely BA.1, BA.1.1, BA.2, BA.2.12.1, and BA.4/5, to evade neutralization by polyclonal serum and mAbs, a lentivirus-based pseudovirus assay, was used to assess neutralization activity against the ancestral Wu01 strain.[155] For this purpose, 30 serum samples from vaccinated healthcare workers and 20 from SARS-CoV-2 convalescent individuals were longitudinally collected (Supplementary Table 9).[100,155,174] After a median of 9- and 14-months following infection or

two-dose vaccination with BNT162b2, individuals in both cohorts received a BNT162b2 booster immunization, respectively.[155] The median age of convalescent individuals was 51 years (IQR: 35-60), and all individuals were infected between February and April 2020 in the initial phase of the pandemic prior to the emergence of SARS-CoV-2 variants of concern with a history of mild or asymptomatic disease.[155] Samples from the early post-infection period (V1) were collected at a median of 48 days (IQR: 34-58) after SARS-CoV-2 disease onset or diagnosis and ID_{50}s determined in the pseudovirus neutralization assay (Figure 28A).[155] Wu01 was neutralized in all samples obtained after infection with ID_{50} values ranging from 16 to 2607 with a geometric mean ID_{50} [GeoMeanID_{50}] of 264 (Figure 28B) while neutralization activity of V1 serum samples against Omicron sublineages was greatly reduced and only detectable in 0%–15% for BA.1 and BA1.1, and 45%–50% for BA.2, BA.2.12.1, and BA.4/5 (Figure 28B).[155] In contrast, neutralization activity of sera collected at a median of 33 days (IQR 27-54) after a single BNT162b2 booster immunization showed GeoMeanID_{50}s ranging from 1456 against BA.4/5 to 2.103 against BA.2 (Figure 28B and Figure 29A and B).[155] Additionally, Omicron neutralization activity was determined in samples taken at a median of 28 days (IQR: 27-32) after solely receiving the initial two-dose course of BNT162b2 (V1; Figure 28C).[155] Similarly, Wu01 neutralizing serum activity could be detected in all 30 individuals with a GeoMeanID_{50} of 561 (Figure 28D).[155] In contrast, serum from vaccinated individuals at V1 showed Omicron sublineage neutralization activity in 43%-73% with GeoMeanID_{50}s ranging from 8 to 17 (Figure 28D).[155] Similar to the convalescent group, a substantial increase in neutralization activity with 27- to 70-fold GeoMeanID_{50} increases against all Omicron sublineages as well as a 8-fold rise in Wu01 neutralization potency could be observed in follow-up samples collected at a median of 29 days (IQR 26-35) after booster immunization (Figure 28D, Figure 29C and D) with the lowest GeoMeanID_{50} of 312 observed against the BA.4/5 variants (Figure 28D).[155] Of note, the neutralization activity was significantly lower against BA.4/5 compared to BA.1, BA.1.1, and BA.2 with GeoMeanID_{50}s of 648, 557, and 582, among vaccinated individuals, respectively (Figure 28E).[155] In conclusion, this data highlights the importance of booster immunizations for eliciting neutralizing serum activity against all prevalent Omicron sublineages in previously vaccinated and convalescent individuals.[155] Interestingly, polyclonal serum exhibits a reduced neutralization activity against the BA.4/5 variant, indicating increased antigenic escape despite the limited number of spike protein differences compared to BA.2.[155]

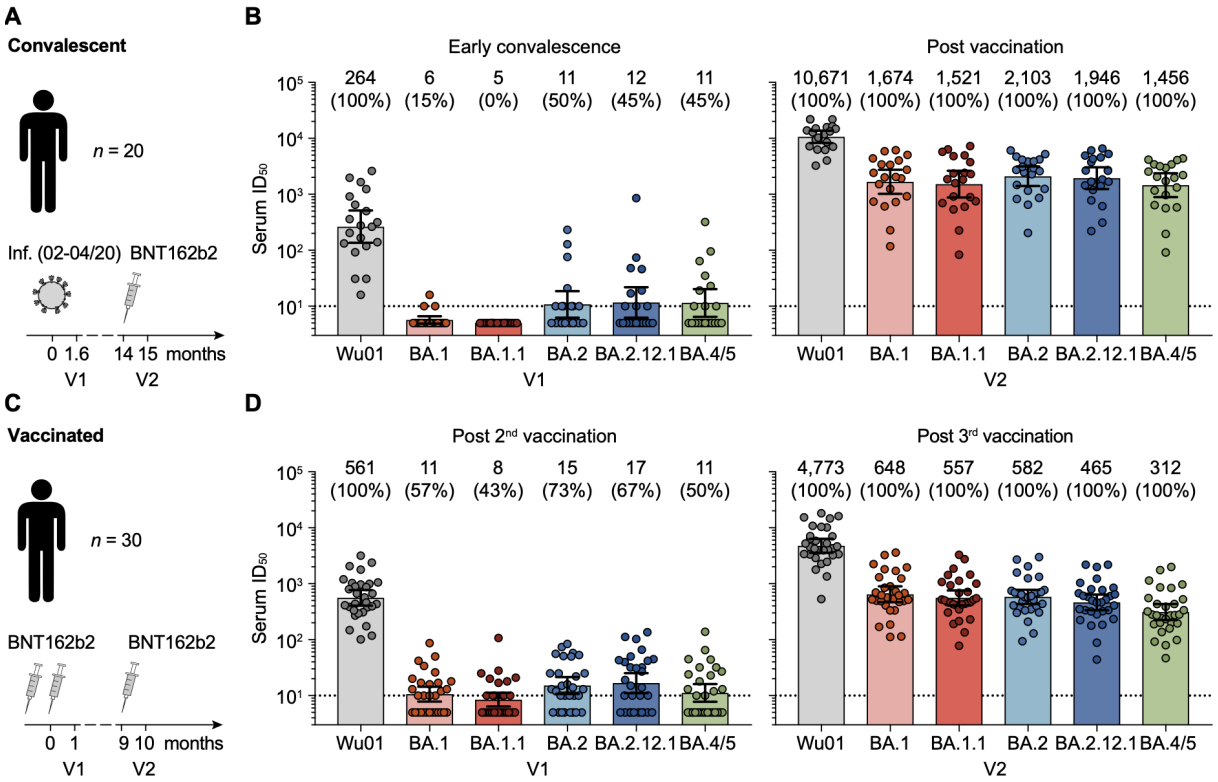

E

Convalescent cohort

V2	Wu01	BA.1	BA.1.1	BA.2	BA.2.12.1	BA.4/5
Wu01		0.8720	0.8404	0.8283	0.8795	0.7319
BA.1	**<0.0001**		0.9594	0.9053	0.9639	0.8030
BA.1.1	**<0.0001**	>0.9999		0.8932	0.9579	0.8030
BA.2	**0.0042**	>0.9999	0.1684		0.9353	0.9008
BA.2.12.1	**0.0021**	>0.9999	0.2694	>0.9999		0.8857
BA.4/5	**<0.0001**	>0.9999	>0.9999	0.0609	0.1026	

Vaccinated cohort

V2	Wu01	BA.1	BA.1.1	BA.2	BA.2.12.1	BA.4/5
Wu01		0.7415	0.7126	0.7335	0.6699	0.6575
BA.1	**0.0065**		0.9235	0.9608	0.8763	0.8045
BA.1.1	**<0.0001**	0.8001		0.8612	0.8861	0.7890
BA.2	**<0.0001**	>0.9999	>0.9999		0.8661	0.7856
BA.2.12.1	**<0.0001**	**0.0038**	>0.9999	0.8001		0.8435
BA.4/5	**<0.0001**	**<0.0001**	**0.0004**	**0.0002**	0.1947	

p value (Dunn's test) Spearman's Rho

Figure 28. Booster immunization is critical for Omicron sublineage serum neutralization activity in vaccinated and convalescent individuals.

(A) Study outline for COVID-19 convalescent individuals. (B) Bar graphs show GeoMeanID_{50}s from convalescent individuals with 95% CIs. Numbers show GeoMeanID50s and the percentage of individuals with detectable neutralizing activity (ID_{50} > 10; in parentheses). (C) Study outline for vaccinated individuals. (D) Bar graphs show GeoMeanID_{50}s from vaccinated individuals with 95% CIs. Numbers show GeoMeanID50s and the percentage of vaccinated individuals with detectable neutralizing activity (ID_{50} > 10; in parentheses). (E) Spearman's rank correlation coefficients (rho) at V2 are shown in black. P values determined after the Friedman test by Dunn's multiple comparison tests at V2 are shown in red (bold numbers indicate statistical significance). For (B) and (D), ID_{50}s below the lower limit of quantification (LLOQ, ID_{50} = 10) indicated by the black dotted lines were imputed to ½ 3 LLOQ (ID_{50} = 5), and ID_{50}s above the upper limit of quantification (ULOQ, ID_{50} = 21,870) were imputed to 21,871. [published in *Gruell et al., 2022, Cell Host & Microbe; Figure 2*][155]

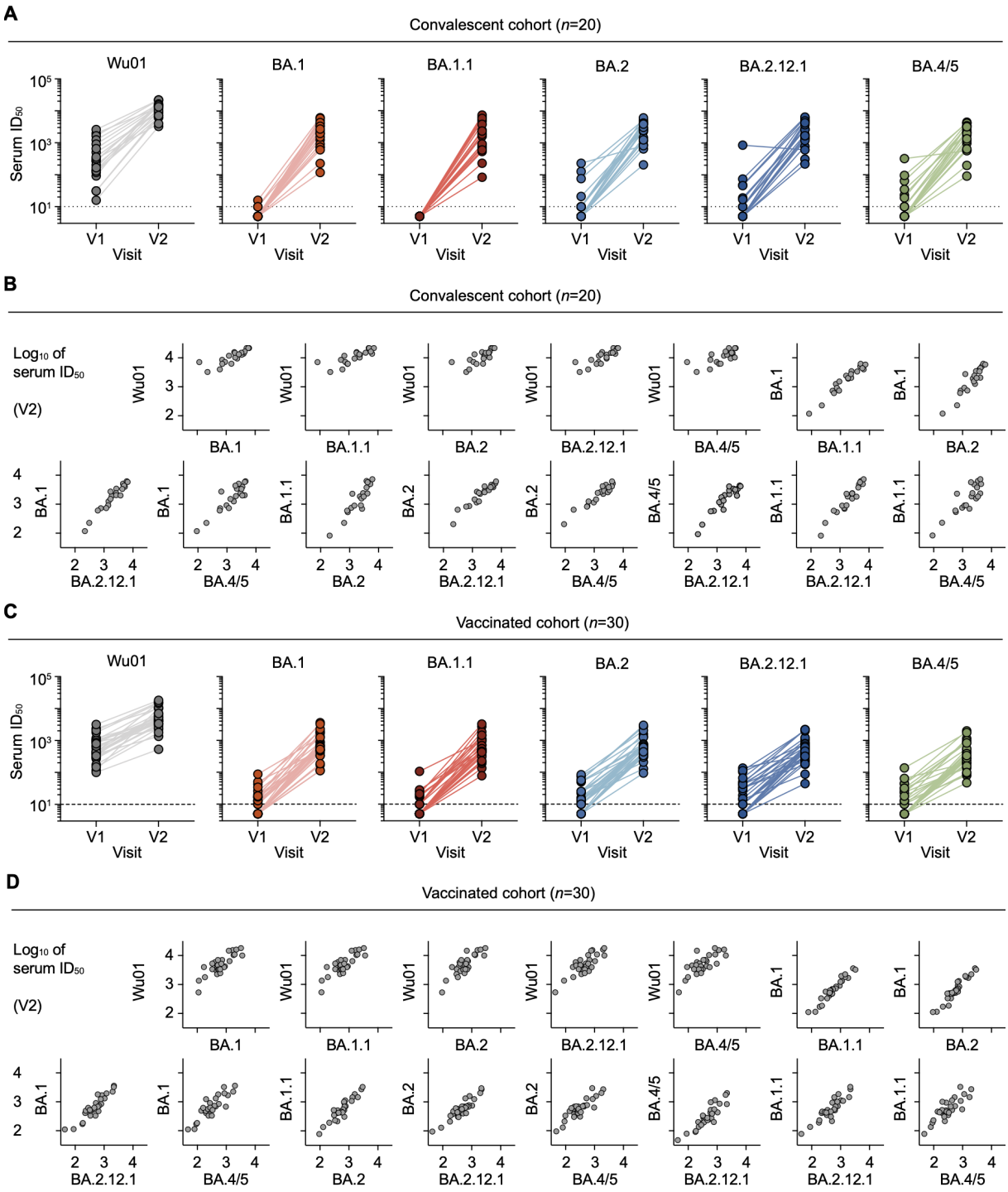

Figure 29. Omicron sublineage neutralization by serum.

(A) Serum ID50s from convalescent individuals after infection (V1) and BNT162b2 booster immunization (V2) are shown in Figure 18. Solid lines connect the ID50s of individual participants. The dashed lines indicate the LLOQ (ID_{50} = 10). (B) Log_{10} serum ID_{50}s are correlated against indicated viruses in convalescent individuals at V2. (C) Serum ID_{50}s of BNT162b2 vaccinated individuals after the second (V1) and third vaccine dose (V2) as in Figure 18. Solid lines connect the ID_{50}s of individual participants. The dashed lines indicate the LLOQ (ID_{50} = 10). (D) Log_{10} serum ID_{50}s are correlated against indicated viruses in vaccinated individuals at V2. Serum ID_{50}s < LLOQ were imputed to 1/2x LLOQ (ID_{50} = 5). [published in *Gruell et al., 2022, Cell Host & Microbe; Figure S1*][155]

5.3.3. Omicron sublineages exhibit different neutralization sensitivities towards mAbs in contrast to subtle differences in serum

To further decode Omicron escape from neutralizing antibodies, 158 mAbs isolated from individuals after SARS-CoV-2 infection were produced and tested against all sublineages.[155] Of these, 79 mAbs were previously isolated in different projects,[100,127] 67 were randomly selected from the CoV-AbDab[149] , and 12 were clinically tested mAbs.[155] In total, this selection included a broad spectrum of SARS-CoV-2 neutralizing antibodies with 92 VH/VL combinations, diverse lengths of CDR3s, and V gene mutations originating from at least 43 different unvaccinated individuals out of 19 independent studies prior to the emergence of the Omicron variant (Figure 30A; Supplementary Table 10).[155] Antibodies included in this panel preferentially targeted the RBD (97%) with previously described public clonotypes such as the VH3-53/3-66 subgroup included (Figure 30A; Supplementary Table 10).[155] Similar to the results observed for polyclonal serum, all 158 antibodies neutralized the ancestral Wu01 strain, but only 18%, 17%, 22%, 23%, and 18% retained neutralization activity against BA.1, BA.1.1, BA.2, BA.2.12.1, and BA.4/5, respectively (Figure 30B and Figure 31).[155] Antibodies that retained neutralization activity exhibited a 6- to 14-fold overall reduction in neutralization potency against Omicron subvariants when compared to Wu01 with GeoMeanIC_{50}s of 0,42 (BA.1), 0,52 (BA.1.1), 0,17 (BA.2), 0,18 (BA.2.12.1), and 0,28 mg/mL (BA.4/5; Figure 30C).[155] The evaluation of neutralization profiles highlighted similarities and differences in antibody sensitivity among the distinct Omicron sublineages (Figure 30D-F, Figure 31B and C).[155] Comparisons of antibody susceptibility revealed a high degree of variation between the main sublineages BA.1, BA.2, and BA.4/5 (Figure 30E and F).[155] For instance, BA.2 showed a higher resistance (>1 $\log_{10}$ IC_{50} difference) than BA.1 to only a single antibody (2%) but was more sensitive to ten antibodies (23%; Figure 30E) while BA.4/5 exhibited over 10-fold higher resistance to a higher antibody fraction than other Omicron variants (Figure 30E).[155] In contrast, only a small difference with rs of 0,81 and 0,86 could be observed between the most closely related sublineages BA.1 and BA.1.1 as well as BA.2 and BA.2.12.1, respectively (Figure 30E and F, Figure 31C).[155] When comparing BA.4/5 to BA.1 and BA.1.1, a heterogeneity in sensitivity to the antibody panel was observed with no discernible correlation.[155] However, a stronger correlation in sensitivity with rs of 0,58 and 0,68 could be observed between BA.4/5 and BA.2 or BA.2.12.1, respectively (Figure 30E and F).[155] Notably, whereas BA.4/5 demonstrated higher sensitivities to only 0%–5% of antibodies compared to BA.2 and BA.2.12.1, BA.4/5 displayed increased resistance to 21% of the antibodies that neutralized Omicron (Figure 30E).[155] Three classes of Omicron-neutralizing antibodies became discernable based on the analysis of neutralization profiles of the different sublineages: (1) 21 out of 43 (49%) antibodies showed broadly similar activity against all Omicron, (2) 7 out of 43 (16%)

antibodies with strongly reduced activity against BA.1 and BA.1.1 compared to BA.2, BA.2.12.1, and BA.4/5 and (3) 6 out of 43 (14%) antibodies with markedly reduced activity against BA.4/5 compared with BA.1, BA.1.1, as well as BA.2 and/or BA.2.12.1.[155] Omicron sublineages display considerably different levels of sensitivities towards mAbs in contrast to the subtle differences observed with polyclonal serum.[155] Importantly, BA.4/5 showed a strong bias to higher resistance compared to the more prevalent BA.2 sublineages.[155]

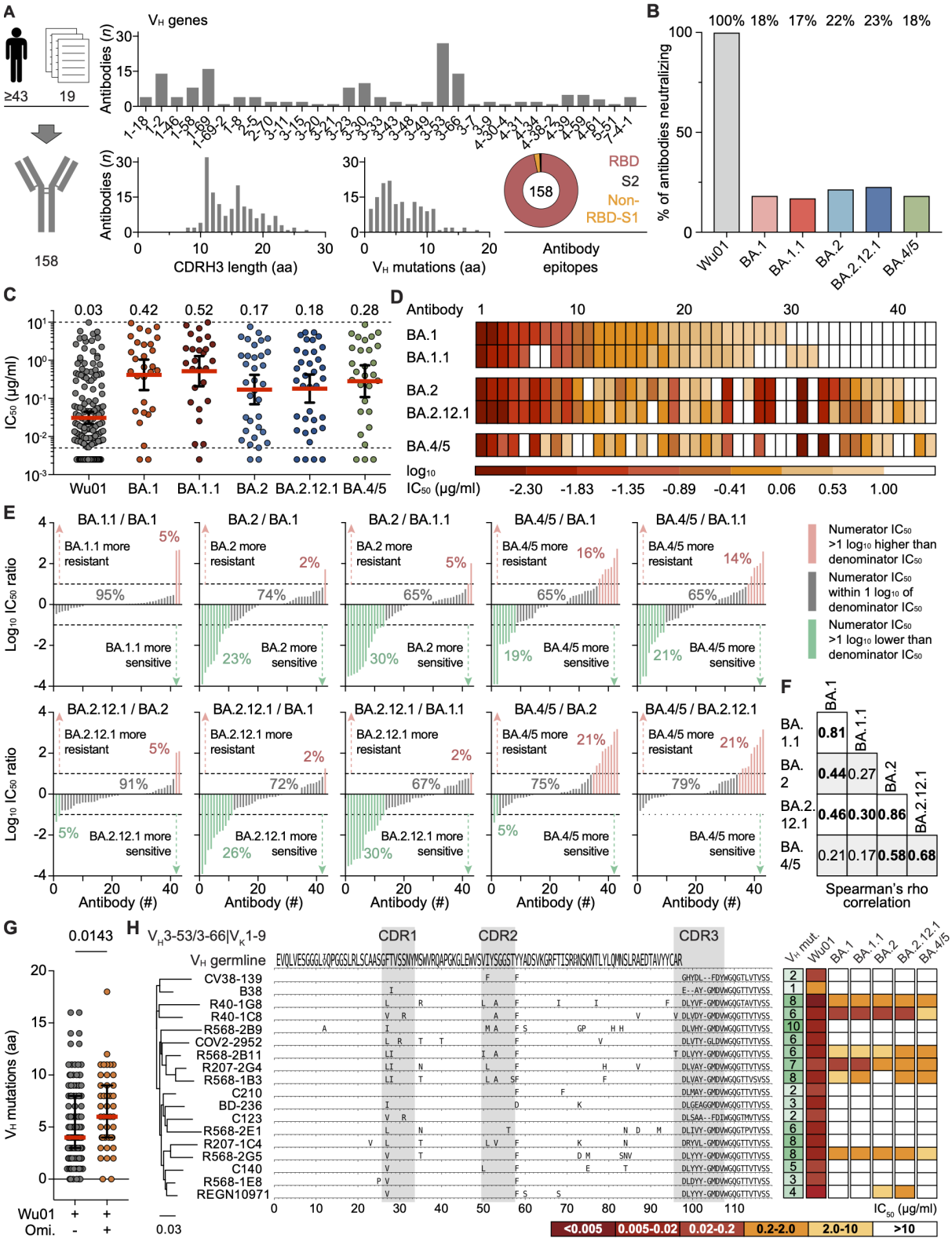

Figure 30. Omicron sublineage immune escape is dependent on minimal variation in antibody sequences.

(A) 158 mAbs were taken from 19 studies and at least 43 convalescent individuals. Bar graphs indicate VH gene segment distribution, CDRH3 length in amino acids, and VH amino acid mutations. Epitope information is shown in a pie chart. (B) The bar graph depicts the antibody fractions neutralizing Wu01 and Omicron sublineages (IC_{50} < 10 μg/ml). (C) Neutralizing antibody IC_{50}s against Wu01 and Omicron sublineages (n = 158 for Wu01, n = 29 for BA.1, n = 27 for BA.1.1, n = 34 for BA.2, n = 36 for BA.2.12.1 and n = 29 for BA.4/5). Solid lines mark

geoMeanIC_{50}s, including 95% CI. LLOQ (0,005 µg/ml) and ULOQ (10 µg/ml) are indicated by dashed lines. IC_{50}s < LLOQ were imputed to ½ 3 LLOQ (IC_{50} = 0,0025). (D) IC_{50} heatmap of 43 antibodies with neutralization activity (IC_{50} < 10 µg/ml) against at least 1 Omicron sublineage sorted by potency against BA.1. (E) Omicron sublineages are compared using log_{10} IC_{50} ratios of Omicron sublineage neutralizing antibodies. Antibodies are sorted by increasing IC_{50} rations within each panel. Numbers indicate fractions of antibodies with higher, similar, or lower sublineage activity. IC_{50}s < LLOQ were imputed to ½ 3 LLOQ (IC_{50} = 0,0025) and IC_{50}s > ULOQ were imputed to 2/3 ULOQ (IC_{50} = 20). (F) Spearman's rank correlation coefficients are shown for 43 Omicron sublineage neutralizing antibodies. Bold numbers indicate significance. (G) Amino acid mutations of antibodies neutralizing either Wu01 only or both Wu01 and at least one Omicron sublineage. Lines indicate medians and interquartile ranges. A two-tailed Mann-Whitney U test was used to compare groups. (H) Multiple sequence alignment of heavy chain sequences from the VH3-53/3-66|VK1-9 (VH3-53*01, VH3-53*04, and VH3-66*01) public clonotype and a corresponding phylogenetic tree are shown. Mutations are relative to the VH germline-encoded residues are indicated by letters. Number of mutations and neutralization activity are provided in a heatmap on the right side. [published in *Gruell et al., 2022, Cell Host & Microbe; Figure 3*][155]

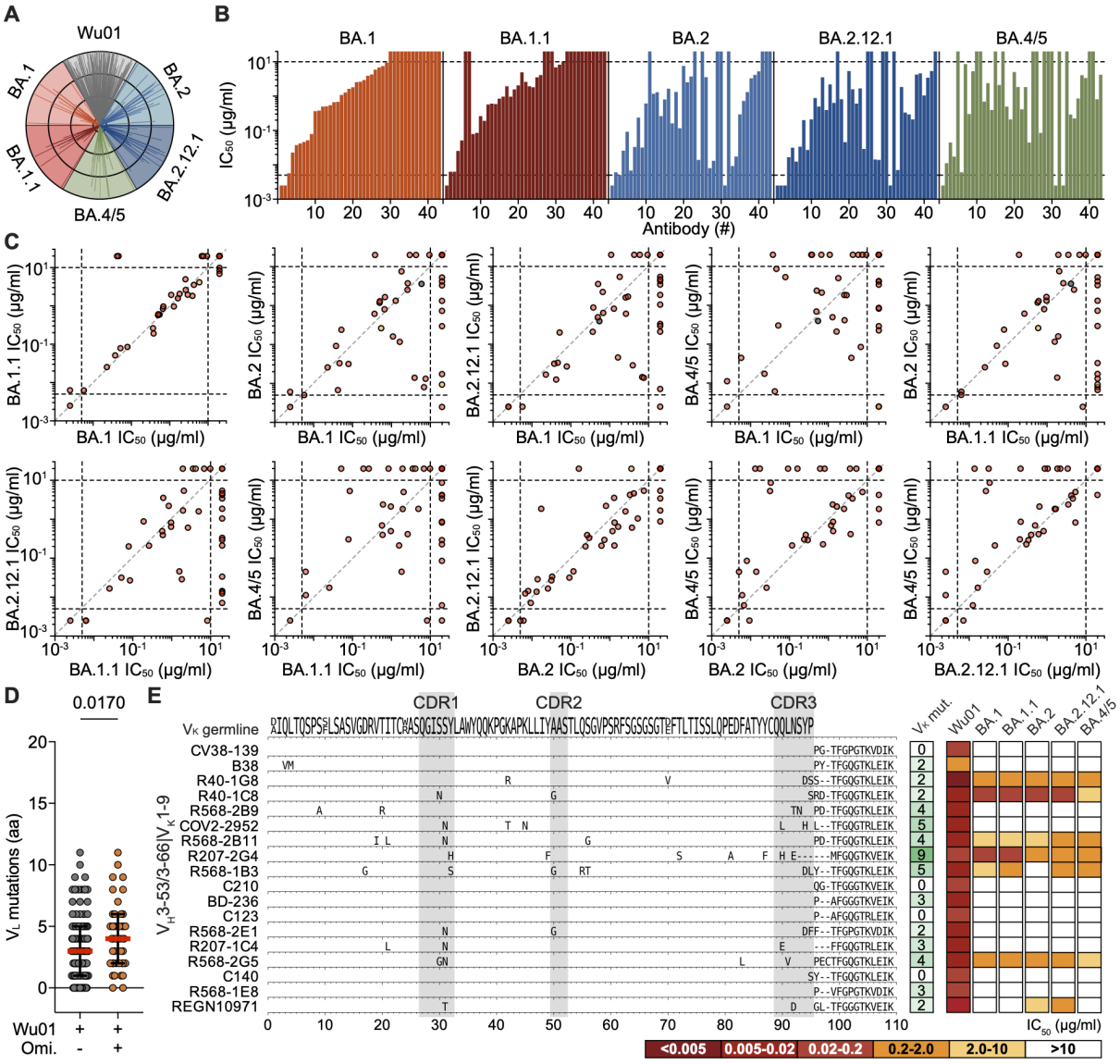

Figure 31. Antibody Omicron neutralization profile.

(A) IC_{50} spider plots for all 158 antibodies were sorted arbitrarily but equally for each virus. IC_{50}s are indicated by circles (from outer to inner circle: 0,005, 0,05, 0,5, and 5 µg/ml). (B) Antibody neutralization activity (IC_{50} < 10 µg/ml) against ≥ 1 Omicron sublineage (n=43) depicted as bar charts with antibodies sorted by BA.1 neutralization. The dotted lines show lower (LLOQ, 0,005 µg/ml) and upper limits of quantification (ULOQ; 10 µg/ml). (C) IC_{50} correlation plots for antibodies neutralizing at least 1 Omicron sublineage (n=43). Epitopes are indicated by color, as in Figure 19A. Identity lines are indicated in grey, and limits of quantification are indicated by dashed black lines. IC_{50}s <LLOQ were imputed to 1/2x LLOQ (IC_{50} = 0,0025), and IC_{50}s > ULOQ were imputed to 2x ULOQ (IC_{50} = 20) in (A) – (C). (D) VL gene amino acid mutations of Wu01 only or both Wu01 and ≥ 1 Omicron sublineage neutralizing antibodies. Lines indicate medians and IQR. A two-tailed Mann-Whitney U test was used to compare groups. (E) Light chain multiple sequence alignments for the public clonotype VH3-53/3-66|VK1-9. Amino acid mutations are indicated by letters relative to the light chain V gene segment GL encoded residues. Neutralization activity and number of amino acid mutations are given. GL VK represents a consensus of identified antibody GL alleles. [published in *Gruell et al., 2022, Cell Host & Microbe; Figure S2*][155]

5.3.4. Antibody activity is highly affected by only minor sequence variations

When investigating sequence features, Omicron-neutralizing antibodies carried a slightly higher number of amino acid mutations, with 6 in the heavy and 4 in the light chain variable genes, compared to Omicron non-neutralizing antibodies with 4 and 3 mutations, respectively (p=0,0143 and p=0,0170; Figure 30G and Figure 31D).[155] This indicates that a higher sequence diversification might be beneficial for Omicron neutralization.[155] As described previously, the high convergence in the mAb response against SARS-CoV-2 can be seen in public clonotypes with conserved sequence characteristics and neutralization mechanisms.[155] From the analyzed panel, 18 sequences from 11 individuals could be matched to the prominent VH3-53/3-66|VK1-9 clonotype.[155] Interestingly, Omicron neutralization capacity differed substantially among the VH3-53/3-66|VK1-9 clonotype members, even though these antibodies were highly conserved at a sequence level (Figure 30H and Figure 31E).[155] For instance, antibodies R207-1C4 and R568-2G5 each harbor eight amino acid mutations in their VH gene, not counting the CDRH3, of which three are identical, and five are at the same residue.[155] While both antibodies had similar Wu01 neutralization potency, R207-1C4 failed to neutralize any Omicron sublineages, while R568-2G5 exhibited neutralizing activity against all sublineages.[155] Notably, antibody C140 failed to neutralize any Omicron variant despite being a member of the same clonotype with an identical CDRH3 as R568-2G5.[155] Therefore, Omicron neutralization or resistance depends on minimal variation in antibody sequences.[155] In conclusion, experimental testing of individual mAb neutralization activity remains critical since antibody sequence- or class-based predictions of Omicron neutralization can be difficult.[155]

5.3.5. Omicron sublineages escape most mAbs in clinical use

SARS-CoV-2 neutralizing mAbs play a crucial role in preventing and treating SARS-CoV-2 infections.[155] Several clinical trials established a significant reduction in morbidity and mortality in infected individuals treated with SARS-CoV-2, neutralizing monoclonal antibodies and a protective effect through passive immunization of most vulnerable individuals.[155,175] To examine how clinically approved antibodies are affected by Omicron sublineages, 9 mAbs that received authorization for clinical use (Figure 32A and B) and a further 9 antibodies in clinical development were tested for Omicron neutralization properties (Figure 32B and Figure 33).[155] All tested antibodies targeted the RBD.[155] Expectedly, most antibodies were highly potent against Wu01 with IC_{50}s below 0,005 µg/ml (Figure 32B).[155] However, sotrovimab showed less potent and incomplete Wu01 neutralization activity consistent with impaired activity against pseudoviruses lacking the dominant D614G spike mutation (Figure 32A).[155,176,177] Interestingly, only five out of 18 (28%) tested antibodies showed neutralization against BA.1 with IC_{50}s<10 µg/ml, out of which three hat strongly reduced potency (Figure 32B).[155] Although the neutralization profiles of BA.1.1 generally resembled that of BA.1, some differences could be observed.[155] For instance, DZIF-10c lost neutralization potency against BA.1.1 but retained activity against BA.1 with an IC_{50} of 0,046 µg/ml (Figure 32B and Figure 33).[155] While the number of antibodies with neutralization activity against the Omicron sublineages was limited, neutralization profiles for BA.2, BA.2.12.1, and BA.4/5 differed with 5 out of 18 (28%) for BA.2, 7 out of 18 (39%) for BA.2.12.1 and 6 out of 18 for BA.4/5 (33%; Figure 32B).[155] For instance, mAb cilgavimab neutralized BA.2 and BA.2.12.1 with IC_{50}s of 0,008 µg/ml and 0,014 µg/ml, respectively, but was >480 fold less potent against BA.1 and BA.1.1 (Figure 32A and B).[155] Compared to antibody DZIF-10c cilgavimab remained potent against BA.4/5 with an IC_{50} of 0,085 µg/mL while neutralization potency of DZIF-10c was strongly reduced against BA.4/5 when compared with BA.2 and BA.2.12.1 with IC_{50}s of 8,64 µg/mL versus 0,03 µg/mL (Figure 32B).[155] In comparison, antibody imdevimab had no neutralization activity against BA.1 and BA.1.1 but had low neutralization levels against BA.2, BA.2.12.1, and BA.4/5 (Figure 32A and B).[155] Among all assessed clinical antibodies, only bebtelovimab showed potent neutralization against all Omicron sublineages with IC_{50}s<0,005 µg/ml (Figure 32A and B).[155] Additionally, to identify further promising antibody candidates that can neutralize all Omicron sublineages, previously isolated antibodies from individuals with exceptionally high IgG neutralization activity.[101,155] Surprisingly, potent neutralization activity against previously circulating variants Wu01, B.1, Alpha, Beta, Delta, Epsilon and Kappa as well as against newly circulating Omicron BA.1, BA.1.1, BA.2, BA.2.12.1, and BA.4/5 with IC_{50}s<0,05 µg/ml could be observed for antibodies R200-1F9, R207-2F11, and R568-1G9 (Figure 32D; Supplementary Table 10).[155] Remarkably, these

antibodies were isolated from three different convalescent individuals during the early phase of the pandemic within weeks of infection.[101,155] These results underscore the immune system's ability to generate potent neutralizing antibodies against highly divergent Omicron sublineages after only being exposed to the ancestral SARS-CoV-2 spike protein.[155] In conclusion, escape from most mAbs in clinical use can be observed for newly emerged Omicron sublineages, including BA.2.12.1 and BA.4/5.[155] However, sensitivities to these antibodies can vary strongly between different sublineages.[155]

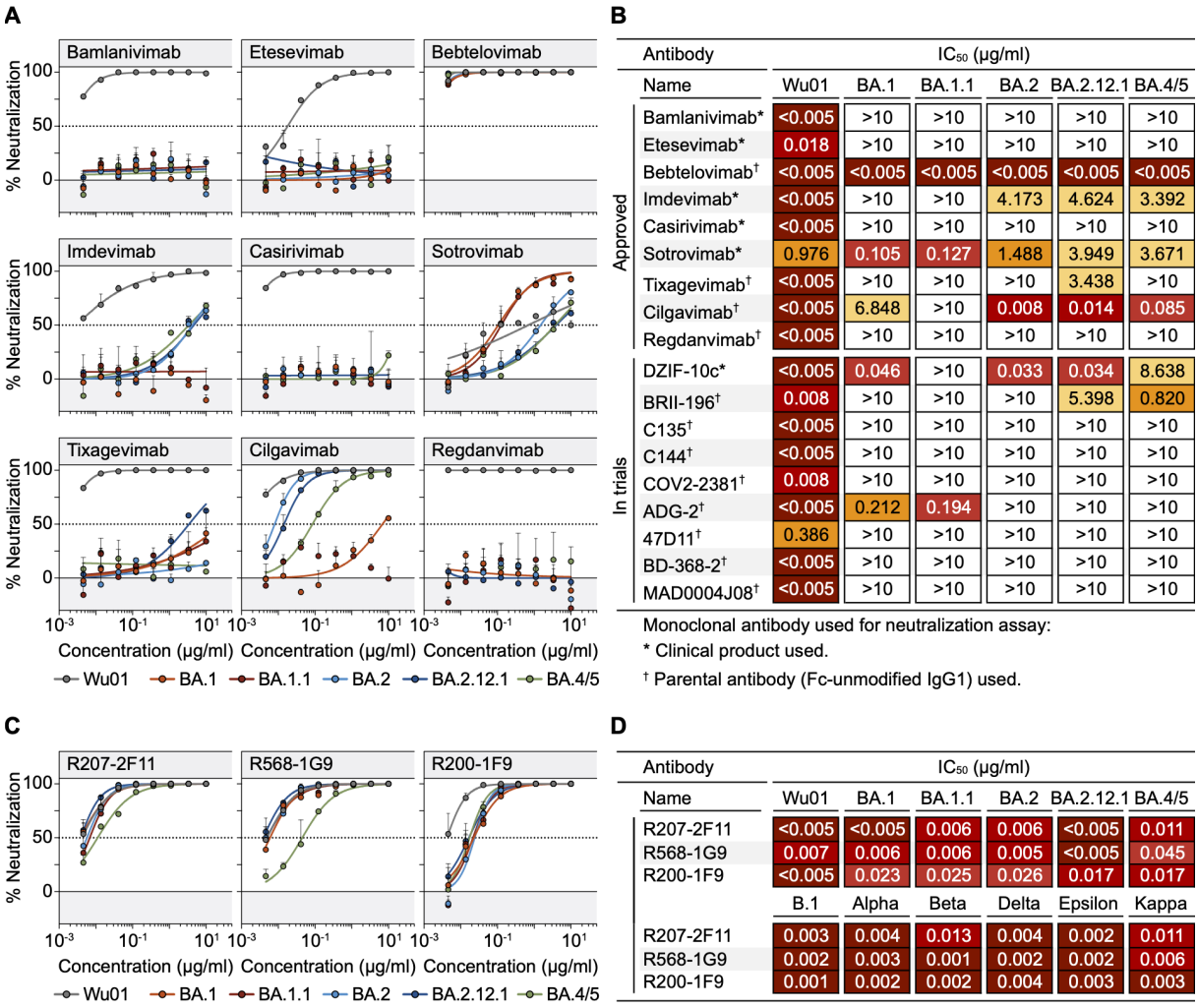

Figure 32. Omicron sublineages escape from most mAbs in clinical use.

(A) Dose response curves for pseudovirus-based neutralization assays for antibodies in clinical use against Wu01 and Omicron sublineages. Error bars show standard deviation, and circles indicate averages. The dotted lines indicate IC_{50}. (B) Table shows IC_{50}s of antibodies in current or previous clinical use or in clinical trials. Symbols mark if the clinical or parental antibody (produced as human IgG1) is used. (C) Dose response curves for pseudovirus-based neutralization assays for highly potent and broad antibodies tested against Wu01 and Omicron sublineages. See (A) for more details. (D) Table of highly potent and broad monoclonal antibodies depicting IC_{50}s against Wu01 and Omicron sublineages (upper rows) and IC_{50}s for previously circulating variants (lower rows) as determined in Vanshylla et al., 2022.[101] [published in *Gruell et al., 2022, Cell Host & Microbe; Figure 4*][155]

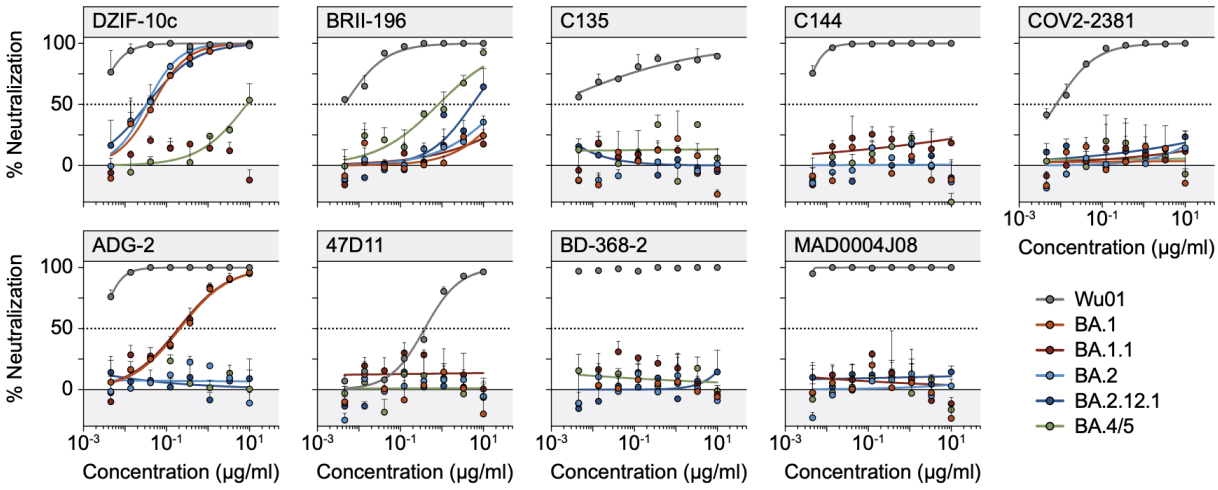

Figure 33. Neutralization activity of mAbs under clinical evaluation against Omicron sublineages. Dose-response curves from a pseudovirus neutralization assay are shown. Circles show averages and standard deviation is indicated by error bars. Dotted lines show IC_{50}. [published in *Gruell et al., 2022, Cell Host & Microbe; Figure S3*][155]

6. Discussion

The following discussion section is in parts based on the discussion sections of the referenced publications *Kreer et al., 2020, Cell*; *Gruell et al., 2022, Cell Host & Microbe* and *Korenkov et al., 2023, Immunity*.[127,148,155]

Neutralizing antibodies induced by infection or vaccination plays a critical role in the adaptive immune response towards infectious agents and is a key indicator for disease protection in infectious diseases.[1,3,92,113] Given the emergence of SARS-CoV-2 in December 2019 and its consequent rapid spreading worldwide, a detailed understanding of the human antibody response towards SARS-CoV-2 was essential for the development of novel therapeutics as well as vaccines.[30,41,42] In the underlying works of this thesis, we have comprehensively investigated the SARS-CoV-2 B cell response using high-throughput single-cell sequencing and identified highly potent SARS-CoV-2 neutralizing antibodies.[127] Using a broad panel of previously isolated mAbs representative of the SARS-CoV-2 antibody response and reverting their acquired mutations to germline form, we were able to investigate the role of SHM in their binding and neutralization capabilities.[148] Through this, we identified “bystander” mutations that were dispensable for antibody functionality but became critical for their ability to neutralize emerging variants.[148] Lastly, we examined the impact of emerging viral variants on established humoral immunity and therapeutic mAbs by analyzing a broad range of sera and mAbs for variant neutralization activity.[155]

By single-cell sorting more than 4.000 SARS-CoV-2 S-protein reactive B cells from 12 infected individuals, we were able to identify 79 (31%) binding and 27 (11%) SARS-CoV-2 neutralizing mAbs that can block authentic virus infections at concentrations at low as 0,04 µg/ml.[127] Like other studies, most isolated SARS-CoV-2 S reactive mAbs could not block viral cell entry, with the epitopes mainly outside the RBD.[60,127,178,179] However, all neutralizing antibodies identified in this work are bound to the RBD of the S protein, which aligns with other studies defining the RBD as the primary target for a potent neutralizing antibody response.[60,127,180] The neutralization ability is additionally influenced by epitope accessibility as the RBD can adapt "up" or "down" conformational states and possesses flexibility.[50,121,179] However, SARS-CoV-2 neutralization is not exclusively directed towards the RBD as mAbs targeting the NTD antigenic supersite and the S2 domain have been identified in multiple donors.[60,181–183] Antibodies targeting the NTD supersite can potently neutralize SARS-CoV-2 by interfering with conformational changes of the S protein required for membrane fusion.[60,182,184] An alternative target for neutralizing antibodies is the conserved S2 domain of the S protein.[181] Antibodies against the S2 domain are usually less potent, but exhibit increased cross-reactivity towards other coronaviruses as a conserved stem-helix region is targeted for membrane fusion.[60,181] In the presented thesis, no neutralizing mAbs targeting the S2 or NTD region of the S protein were isolated.

As mAbs can be used to prevent or treat viral infections, one of our mAbs isolated in this work (HbnC3t1p1_F4) advanced into clinical development and testing as BI 767551 (DZIF-10c) at Boehringer Ingelheim.[127,185–187] DZIF-10c and many other antibodies isolated from spike-reactive B cells from COVID-19 convalescent individuals advancing into clinical trials or approved to treat or prevent COVID-19 infection are primarily targeting the RBD.[127] These antibodies were safe and well tolerated, with trial outcomes dependent on the target population, clinical setting, and circulating variant.[60,188–191] For example, they reduced the risk of disease progression by approximately 70-80% when given early after infection and the incidence of symptomatic disease as pre- or post-exposure prophylaxis during the circulation of early SARS-CoV-2 variants.[60,188–190,192,193] However, the administration of therapeutic mAbs in hospitalized late-stage COVID-19 patients revealed no or only limited benefits.[60,194–196] Similarly, most randomized controlled trials could not show a clinical benefit of convalescent plasma therapy in patients with severe COVID-19.[110–112,197]

To better understand the SARS-CoV-2 antibody response, we investigated mAb characteristics such as V gene segment distribution and SHM levels.[127] In line with the observed polyclonal SARS-CoV-2 antibody response, the isolated neutralizing mAbs were derived from various variable V gene segments.[118,119,122,127,179,198] However, a convergent

SARS-CoV-2 antibody response has been described in previous publications, and antibodies belonging to the public clonotypes IGHV1-58, IGHV3-30, or IGHV3-53/66 were isolated in the present work.[60,122,127,179,199] Surprisingly, SARS-CoV-2 neutralizing mAbs isolated from several individuals showed low SHM levels, with potent neutralizers having germline identities of 94,6% up to 100%.[127] For chronic infections such as HIV1 or HBV, extensive SHM up to 30% of the V gene encoding regions are described.[128,200,201] The low degree of SHM observed in our isolated mAbs also aligns with other studies that isolated mAbs from SARS-CoV-2 convalescent individuals early in the pandemic.[118,122,198] However, these studies only obtained samples from single time points, preventing further conclusions about B cell dynamics in SARS-CoV-2 infection.[127] Here, we were able to longitudinally sample and analyze the memory B cell response of five convalescent individuals for up to 2,5 months.[127] In the observed period, only a little additional SHM or clonal B cell expansion is present in the analyzed B cells.[127] One potential explanation for this could be the limited availability of SARS-CoV-2 antigen due to the rapid clearance of infection to which different cellular responses or additional immune factors might contribute.[127,202,203] Therefore, a limited degree of antigenic B cell stimulation might be responsible for the low levels of SHM observed. This is also supported by findings that SARS-CoV-2 neutralization titers correlate with the severity of infection as a higher antigenic stimulus is available in those individuals with a high disease burden.[90,127,204] Additionally, antibody affinity maturation could be observed 6 months after infection, potentially due to the persistence of SARS-CoV-2 mRNA and proteins found in the intestine's epithelium.[123] However, it is also plausible that high-affinity near-germline antibodies limit the access of SARS-CoV-2 antigen to the germinal center in which affinity maturation occurs.[15,127] A structural rationale for the limited degree of observed SHM is provided by the described interaction of germline-encoded residues with the SARS-CoV-2 S protein RBD from antibodies belonging to the VH3-53/VH3-66 public clonotype.[60,205]

To further investigate SHM dependence on a mAb level we reverted heavy and light chain V gene segment mutations in 92 monoclonal SARS-CoV-2 Wu01-neutralizing antibodies back to germline and tested both mature and germline antibody variants in ELISA and neutralization assay.[148] In our study we show that the mutations present in most SARS-CoV-2 neutralizing antibody are important for binding and neutralization which is in line with results from previous studies on antibodies targeting SARS-CoV-2 or other viruses.[148,206–210] In addition, we observed a slight positive correlation between the total number of reverted mutations and the decline in antibody activity, suggesting that antibodies with a greater number of mutations are more reliant on them.[148] Interestingly, a fraction of mutated SARS-CoV-2 neutralizing antibodies bound and neutralized Wu01 in mature and germline antibody

variant at least within the resolution of our assay meaning that these antibodies can act independently of acquired SHM.[148] In the context of other pathogens such as HIV-1, HCV, or RSV, research has demonstrated that antibodies can carry mutations that have neglectable impact on binding and neutralization properties.[148,211–213] In our study, most of these antibodies were unrelated by sequence, however, a subgroup was comprised of antibodies belonging to the highly convergent VH1-58 public clonotype class.[148] There are several potential explanations for why mutations with no measured impact for Wu01 reactivity could be observed.[148] These mutations might have been selected against subliminal viral mutants circulating in the infected individual, they might contribute to the elimination of autoreactivity caused by other affinity enhancing mutations or because of surface expression effects impacting clonal selection.[9,148,214] However, we propose that these "bystander" mutations only exhibit a limited or no impact on antibody affinity and are therefore not specifically selected in a classical fashion during the process of affinity maturation.[148] These "bystander" mutations could be the result of random "clonal bursts" which were described recently in the germinal center reaction that partially uncouples SHM from affinity maturation.[21,148,215] There are limitations to our study design reverting back mature antibody to their respective germline versions.[148] First, we used the amino acid sequence to determine the V gene variant because of limited nucleotide sequence availability.[148] Some mutations might therefore be occasionally wrongly reverted if they originated from a different allelic variant.[148] However, for the three IGHV1-58 alleles deposited in the IMGT database only one amino acid difference is described, meaning that the error of reversion for this clonotype should be minimal.[148] Second, we only reverted the V-gene segments excluding the CDRH3 region of the antibody, as we lacked additional repertoire data which would have enabled us to track a common ancestor through clonal lineages.[148] Lastly, our analyzes on "bystander" mutations are based on one public clonotype only.[148] Nevertheless, the VH1-58 public clonotype is abundant in vaccinated and convalescent individuals.[119,148,199,216–219]

The low rate of SHM in most binding and neutralizing antibodies emphasized the necessity for unique germline recombination in the naïve human B cell repertoire.[60,148,220] To investigate potential precursor B cells an unbiased HC and LC next-generation sequencing of samples from 48 healthy donors collected prior to the SARS-CoV-2 outbreak was performed.[127,221] We identified potential HC and/or LC precursor sequences of potent SARS-CoV-2 neutralizing antibodies in every single individual.[127] In other publications SARS-CoV-2 S protein reactive antibodies were identified from different SARS-CoV-2 naïve individuals.[222,223] We investigated if prior exposure to other human coronaviruses, as described for SARS-CoV-2 reactive T cells, could explain the observation of such antibodies in SARS-CoV-2 naïve individuals.[203,224] By extensively studying the humoral immunity in 150

adults sampled before the SARS-CoV-2 pandemic analyzing 8.174 S protein reactive B cells on a single cell level and testing 158 mAbs, none of those antibodies exhibited relevant binding or neutralization capacity (*Ercanoglu et al., iScience, 2022*; data not described in this thesis).[225] This suggests that prior background immunity, if present, has only a limited impact on SARS-CoV-2 immunity.[225] Additionally, we also investigated if the SARS-CoV-2 neutralizing mAbs included in our panel might have developed from cross-reactive HCoV induced memory B cells as described previously.[148,222,226] In our ELISAs none of the mature or germline variant antibodies showed any reactivity against the OC43, NL63, 229E and HKU1 S proteins which supports the previous finding that found only little to no recall from memory HCoV responses upon SARS-CoV-2 infection.[148,225,227] Limitations of our approach include that for NL63 and 229E only the S1 subunit of the full trimeric S protein was tested in ELISA and that we could have missed key mutations enabling HCoV binding since we only tested the germline version.[148] However, since all tested antibodies bound the SARS-CoV-2 S1 subunit it is unlikely that cross-reactivity would be directed against a different epitope on the HCoV S protein.[148]

Throughout the COVID-19 pandemic a periodic emergence of viral variants such as Alpha, Beta, Delta, and Omicron variants has confronted the antibody mediated immunity in the context of increased population immunity.[79,155,228] Especially the Omicron sublineages emerging in November 2021 with its diverse spike protein mutations exhibited an increased immune escape and/or transmissibility.[84,155,217,229] Thus, at the time of emergence, understanding the impact of Omicron sublineages BA.2.12.1 and BA.4/5 on the polyclonal and mAb response was critical to guide antibody therapeutics as well as strategies for prevention such as vaccine design.[155] Therefore, we conducted pseudovirus neutralization assays using Omicron sublineage pseudoviruses with samples from convalescent as well as vaccinated individuals to determine the effect of antibody escape on a serum and on a mAb level.[155] Additionally, we studied the impact of an “booster” immunization with ancestral Wu01 mRNA vaccine on Omicron reactivity.[155] We show that Wu01 mRNA vaccination boosters elicit serum neutralization activity against diverse Omicron sublineages in all study participants.[155] However, the observed increase in neutralization activity is limited when compared with Wu01 neutralization.[155] Additionally, the lower BA.4/5 neutralization titers are indicative for a more pronounced immune evasion relative to other Omicron sublineages studied, which other publications have also demonstrated.[155,217,230] Of note, convalescent individuals had a higher activity against BA.4/5 after booster immunization than infection naïve two times mRNA vaccinated individuals.[155] This could indicate a potential benefit of “hybrid immunity” in terms of breadth and potency of the neutralizing antibody response as also demonstrated in subsequent publications.[155,231–233] Our results therefore underline the

importance of booster immunization for the establishment of a sufficient Omicron neutralization response in Wu01 convalescent and vaccinated individuals.[155] We then analyzed neutralization potency of our extended 158 mAb panel against the different Omicron sublineages.[155] Interestingly, while there was only a modest difference in the polyclonal response there were distinct patterns in sublineage neutralization sensitivity on a mAb level.[155] Additionally, our results indicate a large antigenic distance between BA.1/1.1 and BA.4/5 whereas BA.2/2.12.1 and BA.4/5 showed a more similar antibody susceptibility with the most difference observed as a higher resistance to BA.4/5.[155] Notably, only small differences in antibody sequence were enough to strongly influence the ability to potently neutralize Omicron sublineages, highlighting the difficulty of inducing optimal Omicron neutralization after a single Wu01 S protein contact.[155] With analyzing Omicron sublineage neutralization sensitivity we hypothesized that the rapid emergence of the BA.4/5 sublineage might be due to its higher antigenic distance and therefore higher resistance to neutralization.[155] An increased transmissibility as well as a heightened immune evasion for BA.4/5 could be demonstrated in subsequent works.[83,84,170,217,229,230]

Consistent with other studies conducted on the impact of Omicron sublineages on mAbs used in clinical settings we showed that almost all antibodies exhibited no or substantially reduced neutralization potency against Omicron.[155] Only the approved Bebtelovimab demonstrated potent neutralization against all Omicron sublineages.[155,234] However, we and others also identified novel antibodies with remarkable potency against all tested variants.[155,235–238] Additionally, we tested Alpha, Beta, Delta and Omicron BA.1/2 neutralization potency on the previously described public clonotype VH1-58 with its conserved CDRH3 and binding mode to examine the role of pre-existing mutations on viral escape.[148] In the pseudovirus assays all VH1-58 public clonotype members neutralized Wu01, Alpha, Beta, and Delta SARS-CoV-2 variants independently of SHM.[148] Interestingly, only a subset of VH1-58 antibodies showed neutralizing activity against Omicron BA.1/2 subvariants despite being isolated prior to the emergence of Omicron.[148] However, upon germline reversion Omicron neutralizing activity was lost or substantially impaired, showing that previously acquired mutations are required for potent Omicron neutralization.[148] From a biological perspective this finding is in line with the observation that antibodies from late B cell lineage members can neutralize viral escape variants emerging in the presence of early predecessor antibodies from the same antibody lineage in vitro.[148,239] Interestingly, Omicron BA.1/2 neutralization was restored by different mutational patterns in VH1-58 public clonotype members.[148] This suggests that a divergent antibody evolution of the otherwise convergent VH1-58 public clonotype occurred in varied hosts.[148] Especially, while some mutations played a critical role in retaining repertoire diversity and flexibility attenuating the

effects of antigenic imprinting on a clonal level, they had no substantial impact on effectively targeting the initial pathogen.[148] Therefore, to cope with antigenically drifted pathogens in the future diversification through ongoing SHM can be of benefit for the immune response, an idea initially proposed by *Longo and Lipsky*.[148,240] Using this knowledge on SHM patterns we transferred “bystander” mutations from VH1-58 public clonotype members that potently neutralized BA.1/2 to non-neutralizing clonotype members.[148] Surprisingly, we successfully induced BA.1/2 neutralization in previously non-neutralizing VH1-58 clonotype members.[148] While different patterns restored BA.1/2 neutralization activity, a single substitution was sufficient to restore the neutralization potency of COV2-2196, the parental version of the clinically approved tixagevimab antibody providing a proof of concept to alter therapeutically applied antibodies to overcome escape mechanisms posed by viral variants.[148]

In conclusion, in this thesis, we isolated highly potent SARS-CoV-2 neutralizing mAbs from convalescent individuals at the beginning of the COVID-19 pandemic. We also demonstrated that Omicron sublineages show distinct antibody escape profiles and that booster immunization elicits neutralization activity against them. Additionally, we identified broad and potent SARS-CoV-2 antibodies with pan-omicron activity even though most clinical antibodies were inactive against the Omicron sublineages. Furthermore, we highlight that most SARS-CoV-2 Wu01 neutralizing antibodies depend on SHM, but a small subset can act independently. Finally, we present evidence that some SARS-CoV-2 neutralizing mAbs contain “bystander” mutations that are beneficial for the neutralization of upcoming variants by increasing the diversity of the imprinted memory B cell pool but with only a limited contribution to the selection against the ancestral Wu01 strain.

7. References

1 Murphy KM, Weaver C, Janeway C, Travers P, Walport M. Janeway Immunologie, 9. Auflage. Berlin [Heidelberg]: Springer Spektrum, 2018 DOI:10.1007/978-3-662-56004-4.

2 Marshall JS, Warrington R, Watson W, Kim HL. An introduction to immunology and immunopathology. *Allergy Asthma Clin Immunol* 2018; **14**: 49.

3 Chaplin DD. Overview of the immune response. *Journal of Allergy and Clinical Immunology* 2010; **125**: S3–23.

4 Alberts B. Molecular biology of the cell, Sixth edition. New York, NY: Garland Science, Taylor and Francis Group, 2015.

5 Schatz DG, Ji Y. Recombination centres and the orchestration of V(D)J recombination. *Nat Rev Immunol* 2011; **11**: 251–63.

6 Bassing CH, Swat W, Alt FW. The Mechanism and Regulation of Chromosomal V(D)J Recombination. *Cell* 2002; **109**: S45–55.

7 Cyster JG, Allen CDC. B Cell Responses: Cell Interaction Dynamics and Decisions. *Cell* 2019; **177**: 524–40.

8 Busch DH, Pamer EG. T Cell Affinity Maturation by Selective Expansion during Infection. *The Journal of Experimental Medicine* 1999; **189**: 701–10.

9 Mesin L, Ersching J, Victora GD. Germinal Center B Cell Dynamics. *Immunity* 2016; **45**: 471–82.

10 Vitetta ES, Berton MT, Burger C, Kepron M, Lee WT, Yin XM. Memory B and T Cells. *Annu Rev Immunol* 1991; **9**: 193–217.

11 Gray D. Immunological Memory. *Annu Rev Immunol* 1993; **11**: 49–77.

12 Hardy RR, Hayakawa K. B Cell Development Pathways. *Annu Rev Immunol* 2001; **19**: 595–621.

13 Schroeder HW, Cavacini L. Structure and function of immunoglobulins. *Journal of Allergy and Clinical Immunology* 2010; **125**: S41–52.

14 Stavnezer J, Guikema JEJ, Schrader CE. Mechanism and Regulation of Class Switch Recombination. *Annu Rev Immunol* 2008; **26**: 261–92.

15 Di Noia JM, Neuberger MS. Molecular Mechanisms of Antibody Somatic Hypermutation. *Annu Rev Biochem* 2007; **76**: 1–22.

16 Briney BS, Jr. JEC. Secondary mechanisms of diversification in the human antibody repertoire. *Front Immunol* 2013; **4**. DOI:10.3389/fimmu.2013.00042.

17 Klein U, Dalla-Favera R. Germinal centres: role in B-cell physiology and malignancy. *Nat Rev Immunol* 2008; **8**: 22–33.

18 Shlomchik MJ, Weisel F. Germinal center selection and the development of memory B and plasma cells. *Immunological Reviews* 2012; **247**: 52–63.

19 Wagner SD, Neuberger MS. SOMATIC HYPERMUTATION OF IMMUNOGLOBULIN GENES. *Annu Rev Immunol* 1996; **14**: 441–57.

20 Yoshikawa K, Okazaki I, Eto T, *et al.* AID Enzyme-Induced Hypermutation in an Actively Transcribed Gene in Fibroblasts. *Science* 2002; **296**: 2033–6.

21 Victora GD, Nussenzweig MC. Germinal Centers. *Annu Rev Immunol* 2022; **40**: 413–42.

22 Shinnakasu R, Inoue T, Kometani K, *et al.* Regulated selection of germinal-center cells into the memory B cell compartment. *Nat Immunol* 2016; **17**: 861–9.

23 Paus D, Phan TG, Chan TD, Gardam S, Basten A, Brink R. Antigen recognition strength regulates the choice between extrafollicular plasma cell and germinal center B cell differentiation. *The Journal of Experimental Medicine* 2006; **203**: 1081–91.

24 Phan TG, Paus D, Chan TD, *et al.* High affinity germinal center B cells are actively selected into the plasma cell compartment. *The Journal of Experimental Medicine* 2006; **203**: 2419–24.

25 Chiu ML, Goulet DR, Teplyakov A, Gilliland GL. Antibody Structure and Function: The Basis for Engineering Therapeutics. *Antibodies* 2019; **8**: 55.

26 Bournazos S, Gupta A, Ravetch JV. The role of IgG Fc receptors in antibody-dependent enhancement. *Nat Rev Immunol* 2020; **20**: 633–43.

27 Salfeld JG. Isotype selection in antibody engineering. *Nat Biotechnol* 2007; **25**: 1369–72.

28 Geisberger R, Lamers M, Achatz G. The riddle of the dual expression of IgM and IgD. *Immunology* 2006; **118**: 429–37.

29 Coronaviridae Study Group of the International Committee on Taxonomy of Viruses, Gorbalenya AE, Baker SC, *et al.* The species Severe acute respiratory syndrome-related coronavirus: classifying 2019-nCoV and naming it SARS-CoV-2. *Nat Microbiol* 2020; **5**: 536–44.

30 Zhu N, Zhang D, Wang W, *et al.* A Novel Coronavirus from Patients with Pneumonia in China, 2019. *N Engl J Med* 2020; **382**: 727–33.

31 Fung TS, Liu DX. Human Coronavirus: Host-Pathogen Interaction. *Annu Rev Microbiol* 2019; **73**: 529–57.

32 Corman VM, Muth D, Niemeyer D, Drosten C. Hosts and Sources of Endemic Human Coronaviruses. In: Advances in Virus Research. Elsevier, 2018: 163–88.

33 Su S, Wong G, Shi W, *et al.* Epidemiology, Genetic Recombination, and Pathogenesis of Coronaviruses. *Trends in Microbiology* 2016; **24**: 490–502.

34 Li P, Ikram A, Peppelenbosch MP, Ma Z, Pan Q. Systematically Mapping Clinical Features of Infections With Classical Endemic Human Coronaviruses. *Clinical Infectious Diseases* 2021; **73**: 554–5.

35 Ruiz-Aravena M, McKee C, Gamble A, *et al.* Ecology, evolution and spillover of coronaviruses from bats. *Nat Rev Microbiol* 2022; **20**: 299–314.

36 Drosten C, Günther S, Preiser W, *et al.* Identification of a Novel Coronavirus in Patients with Severe Acute Respiratory Syndrome. *N Engl J Med* 2003; **348**: 1967–76.

37 Zaki AM, Van Boheemen S, Bestebroer TM, Osterhaus ADME, Fouchier RAM. Isolation of a Novel Coronavirus from a Man with Pneumonia in Saudi Arabia. *N Engl J Med* 2012; **367**: 1814–20.

38 ECDC. Geographical distribution of confirmed MERS-CoV cases, by reporting country, April 2012 – October 2023. https://www.ecdc.europa.eu/en/publications-data/geographical-distribution-confirmed-mers-cov-cases-reporting-country-april-2012-8 (accessed Dec 8, 2023).

39 WHO. Summary of probable SARS cases with onset of illness from 1 November 2002 to 31 July 2003. https://www.who.int/publications/m/item/summary-of-probable-sars-cases-with-onset-of-illness-from-1-november-2002-to-31-july-2003 (accessed Dec 8, 2023).

40 Worobey M, Levy JI, Malpica Serrano L, *et al.* The Huanan Seafood Wholesale Market in Wuhan was the early epicenter of the COVID-19 pandemic. *Science* 2022; **377**: 951–9.

41 Wu F, Zhao S, Yu B, *et al.* A new coronavirus associated with human respiratory disease in China. *Nature* 2020; **579**: 265–9.

42 Zhou P, Yang X-L, Wang X-G, *et al.* A pneumonia outbreak associated with a new coronavirus of probable bat origin. *Nature* 2020; **579**: 270–3.

43 WHO. WHO Director-General's opening remarks at the media briefing on COVID-19 - 11 March 2020. 2020; published online March 11. https://www.who.int/director-general/speeches/detail/who-director-general-s-opening-remarks-at-the-media-briefing-on-covid-19---11-march-2020 (accessed Dec 8, 2023).

44 WHO. WHO Coronavirus (COVID-19) Dashboard. https://covid19.who.int (accessed Dec 8, 2023).

45 Lu R, Zhao X, Li J, *et al.* Genomic characterisation and epidemiology of 2019 novel coronavirus: implications for virus origins and receptor binding. *The Lancet* 2020; **395**: 565–74.

46 Hu B, Guo H, Zhou P, Shi Z-L. Characteristics of SARS-CoV-2 and COVID-19. *Nat Rev Microbiol* 2021; **19**: 141–54.

47 Temmam S, Vongphayloth K, Baquero E, *et al.* Bat coronaviruses related to SARS-CoV-2 and infectious for human cells. *Nature* 2022; **604**: 330–6.

48 Chan JF-W, Kok K-H, Zhu Z, *et al.* Genomic characterization of the 2019 novel human-pathogenic coronavirus isolated from a patient with atypical pneumonia after visiting Wuhan. *Emerging Microbes & Infections* 2020; **9**: 221–36.

49 Arya R, Kumari S, Pandey B, *et al.* Structural insights into SARS-CoV-2 proteins. *Journal of Molecular Biology* 2021; **433**: 166725.

50 Ke Z, Oton J, Qu K, *et al.* Structures and distributions of SARS-CoV-2 spike proteins on intact virions. *Nature* 2020; **588**: 498–502.

51 Wrapp D, Wang N, Corbett KS, *et al.* Cryo-EM structure of the 2019-nCoV spike in the prefusion conformation. *Science* 2020; : eabb2507.

52 Jackson CB, Farzan M, Chen B, Choe H. Mechanisms of SARS-CoV-2 entry into cells. *Nat Rev Mol Cell Biol* 2022; **23**: 3–20.

53 Hoffmann M, Kleine-Weber H, Schroeder S, *et al.* SARS-CoV-2 Cell Entry Depends on ACE2 and TMPRSS2 and Is Blocked by a Clinically Proven Protease Inhibitor. *Cell* 2020; **181**: 271-280.e8.

54 Hoffmann M, Kleine-Weber H, Pöhlmann S. A Multibasic Cleavage Site in the Spike Protein of SARS-CoV-2 Is Essential for Infection of Human Lung Cells. *Molecular Cell* 2020; **78**: 779-784.e5.

55 Damas J, Hughes GM, Keough KC, *et al.* Broad host range of SARS-CoV-2 predicted by comparative and structural analysis of ACE2 in vertebrates. *Proc Natl Acad Sci USA* 2020; **117**: 22311–22.

56 V'kovski P, Kratzel A, Steiner S, Stalder H, Thiel V. Coronavirus biology and replication: implications for SARS-CoV-2. *Nat Rev Microbiol* 2021; **19**: 155–70.

57 Thoms M, Buschauer R, Ameismeier M, *et al.* Structural basis for translational shutdown and immune evasion by the Nsp1 protein of SARS-CoV-2. *Science* 2020; **369**: 1249–55.

58 Sawicki SG, Sawicki DL. Coronaviruses use Discontinuous Extension for Synthesis of Subgenome-Length Negative Strands. In: Talbot PJ, Levy GA, eds. Corona- and Related Viruses. Boston, MA: Springer US, 1995: 499–506.

59 Gordon DE, Jang GM, Bouhaddou M, *et al.* A SARS-CoV-2 protein interaction map reveals targets for drug repurposing. *Nature* 2020; **583**: 459–68.

60 Gruell H, Vanshylla K, Weber T, Barnes CO, Kreer C, Klein F. Antibody-mediated neutralization of SARS-CoV-2. *Immunity* 2022; **55**: 925–44.

61 Meselson M. Droplets and Aerosols in the Transmission of SARS-CoV-2. *N Engl J Med* 2020; **382**: 2063–2063.

62 Stadnytskyi V, Bax CE, Bax A, Anfinrud P. The airborne lifetime of small speech droplets and their potential importance in SARS-CoV-2 transmission. *Proc Natl Acad Sci USA* 2020; **117**: 11875–7.

63 Wölfel R, Corman VM, Guggemos W, *et al.* Virological assessment of hospitalized patients with COVID-2019. *Nature* 2020; **581**: 465–9.

64 Jones TC, Biele G, Mühlemann B, *et al.* Estimating infectiousness throughout SARS-CoV-2 infection course. *Science* 2021; **373**: eabi5273.

65 Hakki S, Zhou J, Jonnerby J, *et al.* Onset and window of SARS-CoV-2 infectiousness and temporal correlation with symptom onset: a prospective, longitudinal, community cohort study. *The Lancet Respiratory Medicine* 2022; **10**: 1061–73.

66 Byrne AW, McEvoy D, Collins AB, *et al.* Inferred duration of infectious period of SARS-CoV-2: rapid scoping review and analysis of available evidence for asymptomatic and symptomatic COVID-19 cases. *BMJ Open* 2020; **10**: e039856.

67 Endo A, Centre for the Mathematical Modelling of Infectious Diseases COVID-19 Working Group, Abbott S, Kucharski AJ, Funk S. Estimating the overdispersion in COVID-19 transmission using outbreak sizes outside China. *Wellcome Open Res* 2020; **5**: 67.

68 Kevadiya BD, Machhi J, Herskovitz J, *et al.* Diagnostics for SARS-CoV-2 infections. *Nat Mater* 2021; **20**: 593–605.

69 Guan W, Ni Z, Hu Y, *et al.* Clinical Characteristics of Coronavirus Disease 2019 in China. *N Engl J Med* 2020; **382**: 1708–20.

70 Wiersinga WJ, Rhodes A, Cheng AC, Peacock SJ, Prescott HC. Pathophysiology, Transmission, Diagnosis, and Treatment of Coronavirus Disease 2019 (COVID-19): A Review. *JAMA* 2020; **324**: 782.

71 Qiu X, Nergiz AI, Maraolo AE, Bogoch II, Low N, Cevik M. The role of asymptomatic and pre-symptomatic infection in SARS-CoV-2 transmission—a living systematic review. *Clinical Microbiology and Infection* 2021; **27**: 511–9.

72 Huang C, Wang Y, Li X, *et al.* Clinical features of patients infected with 2019 novel coronavirus in Wuhan, China. *The Lancet* 2020; **395**: 497–506.

73 Johns Hopkins University & Medicine. MORTALITY ANALYSES. 2023; published online March 16. https://coronavirus.jhu.edu/data/mortality.

74 European Medicines Agency. COVID-19 medicines. https://www.ema.europa.eu/en/human-regulatory-overview/public-health-threats/coronavirus-disease-covid-19/covid-19-medicines#ema-inpage-item-14490 (accessed Dec 12, 2023).

75 Murakami N, Hayden R, Hills T, *et al.* Therapeutic advances in COVID-19. *Nat Rev Nephrol* 2023; **19**: 38–52.

76 Forni D, Cagliani R, Clerici M, Sironi M. Molecular Evolution of Human Coronavirus Genomes. *Trends in Microbiology* 2017; **25**: 35–48.

77 Dolan PT, Whitfield ZJ, Andino R. Mechanisms and Concepts in RNA Virus Population Dynamics and Evolution. *Annu Rev Virol* 2018; **5**: 69–92.

78 Markov PV, Ghafari M, Beer M, *et al.* The evolution of SARS-CoV-2. *Nat Rev Microbiol* 2023; **21**: 361–79.

79 Carabelli AM, Peacock TP, Thorne LG, *et al.* SARS-CoV-2 variant biology: immune escape, transmission and fitness. *Nat Rev Microbiol* 2023; published online Jan 18. DOI:10.1038/s41579-022-00841-7.

80 O'Toole Á, Pybus OG, Abram ME, Kelly EJ, Rambaut A. Pango lineage designation and assignment using SARS-CoV-2 spike gene nucleotide sequences. *BMC Genomics* 2022; **23**: 121.

81 Plante JA, Liu Y, Liu J, *et al.* Spike mutation D614G alters SARS-CoV-2 fitness. *Nature* 2021; **592**: 116–21.

82 McCrone JT, Hill V, Bajaj S, *et al.* Context-specific emergence and growth of the SARS-CoV-2 Delta variant. *Nature* 2022; **610**: 154–60.

83 Viana R, Moyo S, Amoako DG, *et al.* Rapid epidemic expansion of the SARS-CoV-2 Omicron variant in southern Africa. *Nature* 2022; **603**: 679–86.

84 Tegally H, Moir M, Everatt J, *et al.* Emergence of SARS-CoV-2 Omicron lineages BA.4 and BA.5 in South Africa. *Nat Med* 2022; **28**: 1785–90.

85 Elbe S, Buckland Merrett G. Data, disease and diplomacy: GISAID's innovative contribution to global health. *Global Challenges* 2017; **1**: 33–46.

86 Shu Y, McCauley J. GISAID: Global initiative on sharing all influenza data – from vision to reality. *Eurosurveillance* 2017; **22**. DOI:10.2807/1560-7917.ES.2017.22.13.30494.

87 Khare S, Gurry C, Freitas L, *et al.* GISAID's Role in Pandemic Response. *China CDC Weekly* 2021; **3**: 1049–51.

88 Tsueng G, Mullen JL, Alkuzweny M, *et al.* Outbreak.info Research Library: a standardized, searchable platform to discover and explore COVID-19 resources. *Nat Methods* 2023; **20**: 536–40.

89 Qi H, Liu B, Wang X, Zhang L. The humoral response and antibodies against SARS-CoV-2 infection. *Nat Immunol* 2022; **23**: 1008–20.

90 Long Q-X, Liu B-Z, Deng H-J, *et al.* Antibody responses to SARS-CoV-2 in patients with COVID-19. *Nat Med* 2020; **26**: 845–8.

91 Yaugel-Novoa M, Bourlet T, Paul S. Role of the humoral immune response during COVID-19: guilty or not guilty? *Mucosal Immunology* 2022; **15**: 1170–80.

92 Khoury DS, Cromer D, Reynaldi A, *et al.* Neutralizing antibody levels are highly predictive of immune protection from symptomatic SARS-CoV-2 infection. *Nat Med* 2021; **27**: 1205–11.

93 Barouch DH. Covid-19 Vaccines — Immunity, Variants, Boosters. *N Engl J Med* 2022; **387**: 1011–20.

94 Seow J, Graham C, Merrick B, *et al.* Longitudinal observation and decline of neutralizing antibody responses in the three months following SARS-CoV-2 infection in humans. *Nat Microbiol* 2020; **5**: 1598–607.

95 Lapuente D, Winkler TH, Tenbusch M. B-cell and antibody responses to SARS-CoV-2: infection, vaccination, and hybrid immunity. *Cell Mol Immunol* 2023; published online Nov 10. DOI:10.1038/s41423-023-01095-w.

96 Iyer AS, Jones FK, Nodoushani A, *et al.* Persistence and decay of human antibody responses to the receptor binding domain of SARS-CoV-2 spike protein in COVID-19 patients. *Sci Immunol* 2020; **5**: eabe0367.

97 Röltgen K, Powell AE, Wirz OF, *et al.* Defining the features and duration of antibody responses to SARS-CoV-2 infection associated with disease severity and outcome. *Sci Immunol* 2020; **5**: eabe0240.

98 Garcia-Beltran WF, Lam EC, Astudillo MG, *et al.* COVID-19-neutralizing antibodies predict disease severity and survival. *Cell* 2021; **184**: 476-488.e11.

99 Lucas C, Klein J, Sundaram ME, *et al.* Delayed production of neutralizing antibodies correlates with fatal COVID-19. *Nat Med* 2021; **27**: 1178–86.

100 Vanshylla K, Di Cristanziano V, Kleipass F, *et al.* Kinetics and correlates of the neutralizing antibody response to SARS-CoV-2 infection in humans. *Cell Host & Microbe* 2021; **29**: 917-929.e4.

101 Vanshylla K, Fan C, Wunsch M, *et al.* Discovery of ultrapotent broadly neutralizing antibodies from SARS-CoV-2 elite neutralizers. *Cell Host & Microbe* 2022; **30**: 69-82.e10.

102 Walsh EE, Frenck RW, Falsey AR, *et al.* Safety and Immunogenicity of Two RNA-Based Covid-19 Vaccine Candidates. *N Engl J Med* 2020; **383**: 2439–50.

103 Jackson LA, Anderson EJ, Rouphael NG, *et al.* An mRNA Vaccine against SARS-CoV-2 — Preliminary Report. *N Engl J Med* 2020; **383**: 1920–31.

104 Tober-Lau P, Schwarz T, Vanshylla K, *et al.* Long-term immunogenicity of BNT162b2 vaccination in older people and younger health-care workers. *The Lancet Respiratory Medicine* 2021; **9**: e104–5.

105 Stephenson KE, Le Gars M, Sadoff J, *et al.* Immunogenicity of the Ad26.COV2.S Vaccine for COVID-19. *JAMA* 2021; **325**: 1535.

106 Stuart ASV, Shaw RH, Liu X, *et al.* Immunogenicity, safety, and reactogenicity of heterologous COVID-19 primary vaccination incorporating mRNA, viral-vector, and protein-adjuvant vaccines in the UK (Com-COV2): a single-blind, randomised, phase 2, non-inferiority trial. *The Lancet* 2022; **399**: 36–49.

107 Barros-Martins J, Hammerschmidt SI, Cossmann A, *et al.* Immune responses against SARS-CoV-2 variants after heterologous and homologous ChAdOx1 nCoV-19/BNT162b2 vaccination. *Nat Med* 2021; **27**: 1525–9.

108 Lipsitch M, Krammer F, Regev-Yochay G, Lustig Y, Balicer RD. SARS-CoV-2 breakthrough infections in vaccinated individuals: measurement, causes and impact. *Nat Rev Immunol* 2022; **22**: 57–65.

109 Krammer F, Ellebedy AH. Variant-adapted COVID-19 booster vaccines. *Science* 2023; **382**: 157–9.

110 Korley FK, Durkalski-Mauldin V, Yeatts SD, *et al.* Early Convalescent Plasma for High-Risk Outpatients with Covid-19. *N Engl J Med* 2021; **385**: 1951–60.

111 Abani O, Abbas A, Abbas F, *et al.* Convalescent plasma in patients admitted to hospital with COVID-19 (RECOVERY): a randomised controlled, open-label, platform trial. *The Lancet* 2021; **397**: 2049–59.

112 Simonovich VA, Burgos Pratx LD, Scibona P, *et al.* A Randomized Trial of Convalescent Plasma in Covid-19 Severe Pneumonia. *N Engl J Med* 2021; **384**: 619–29.

113 Pantaleo G, Correia B, Fenwick C, Joo VS, Perez L. Antibodies to combat viral infections: development strategies and progress. *Nat Rev Drug Discov* 2022; **21**: 676–96.

114 Zhang A, Stacey HD, D'Agostino MR, Tugg Y, Marzok A, Miller MS. Beyond neutralization: Fc-dependent antibody effector functions in SARS-CoV-2 infection. *Nat Rev Immunol* 2023; **23**: 381–96.

115 Hansen J, Baum A, Pascal KE, *et al.* Studies in humanized mice and convalescent humans yield a SARS-CoV-2 antibody cocktail. *Science* 2020; **369**: 1010–4.

116 Liu L, Wang P, Nair MS, *et al.* Potent neutralizing antibodies against multiple epitopes on SARS-CoV-2 spike. *Nature* 2020; **584**: 450–6.

117 Ju B, Zhang Q, Ge J, *et al.* Human neutralizing antibodies elicited by SARS-CoV-2 infection. *Nature* 2020; **584**: 115–9.

118 Rogers TF, Zhao F, Huang D, *et al.* Isolation of potent SARS-CoV-2 neutralizing antibodies and protection from disease in a small animal model. *Science* 2020; **369**: 956–63.

119 Zost SJ, Gilchuk P, Chen RE, *et al.* Rapid isolation and profiling of a diverse panel of human monoclonal antibodies targeting the SARS-CoV-2 spike protein. *Nat Med* 2020; **26**: 1422–7.

120 Chen Y, Zhao X, Zhou H, Zhu H, Jiang S, Wang P. Broadly neutralizing antibodies to SARS-CoV-2 and other human coronaviruses. *Nat Rev Immunol* 2023; **23**: 189–99.

121 Barnes CO, Jette CA, Abernathy ME, *et al.* SARS-CoV-2 neutralizing antibody structures inform therapeutic strategies. *Nature* 2020; **588**: 682–7.

122 Robbiani DF, Gaebler C, Muecksch F, *et al.* Convergent antibody responses to SARS-CoV-2 in convalescent individuals. *Nature* 2020; **584**: 437–42.

123 Gaebler C, Wang Z, Lorenzi JCC, *et al.* Evolution of antibody immunity to SARS-CoV-2. *Nature* 2021; **591**: 639–44.

124 Wang Z, Muecksch F, Schaefer-Babajew D, *et al.* Naturally enhanced neutralizing breadth against SARS-CoV-2 one year after infection. *Nature* 2021; **595**: 426–31.

125 Sakharkar M, Rappazzo CG, Wieland-Alter WF, *et al.* Prolonged evolution of the human B cell response to SARS-CoV-2 infection. *Sci Immunol* 2021; **6**: eabg6916.

126 Dan JM, Mateus J, Kato Y, *et al.* Immunological memory to SARS-CoV-2 assessed for up to 8 months after infection. *Science* 2021; **371**: eabf4063.

127 Kreer C, Zehner M, Weber T, *et al.* Longitudinal Isolation of Potent Near-Germline SARS-CoV-2-Neutralizing Antibodies from COVID-19 Patients. *Cell* 2020; **182**: 843-854.e12.

128 Schommers P, Gruell H, Abernathy ME, *et al.* Restriction of HIV-1 Escape by a Highly Broad and Potent Neutralizing Antibody. *Cell* 2020; **180**: 471-489.e22.

129 Corti D, Voss J, Gamblin SJ, *et al.* A Neutralizing Antibody Selected from Plasma Cells That Binds to Group 1 and Group 2 Influenza A Hemagglutinins. *Science* 2011; **333**: 850–6.

130 Ehrhardt SA, Zehner M, Krähling V, *et al.* Polyclonal and convergent antibody response to Ebola virus vaccine rVSV-ZEBOV. *Nat Med* 2019; **25**: 1589–600.

131 Stadlbauer D, Amanat F, Chromikova V, *et al.* SARS CoV 2 Seroconversion in Humans: A Detailed Protocol for a Serological Assay, Antigen Production, and Test Setup. *CP Microbiology* 2020; **57**: e100.

132 Kowarz E, Löscher D, Marschalek R. Optimized Sleeping Beauty transposons rapidly generate stable transgenic cell lines. *Biotechnology Journal* 2015; **10**: 647–53.

133 Kreer C, Döring M, Lehnen N, *et al.* openPrimeR for multiplex amplification of highly diverse templates. *Journal of Immunological Methods* 2020; **480**: 112752.

134 Gieselmann L, Kreer C, Ercanoglu MS, *et al.* Effective high-throughput isolation of fully human antibodies targeting infectious pathogens. *Nat Protoc* 2021; **16**: 3639–71.

135 Ye J, Ma N, Madden TL, Ostell JM. IgBLAST: an immunoglobulin variable domain sequence analysis tool. *Nucleic Acids Research* 2013; **41**: W34–40.

136 Ye J, Ma N, Madden TL, Ostell JM. IgBLAST: an immunoglobulin variable domain sequence analysis tool. *Nucleic Acids Research* 2013; **41**: W34–40.

137 Sievers F, Wilm A, Dineen D, *et al.* Fast, scalable generation of high quality protein multiple sequence alignments using Clustal Omega. *Molecular Systems Biology* 2011; **7**: 539.

138 Vander Heiden JA, Yaari G, Uduman M, *et al.* pRESTO: a toolkit for processing high-throughput sequencing raw reads of lymphocyte receptor repertoires. *Bioinformatics* 2014; **30**: 1930–2.

139 Tiller T, Meffre E, Yurasov S, Tsuiji M, Nussenzweig MC, Wardemann H. Efficient generation of monoclonal antibodies from single human B cells by single cell RT-PCR and expression vector cloning. *Journal of Immunological Methods* 2008; **329**: 112–24.

140 Li MZ, Elledge SJ. SLIC: A Method for Sequence- and Ligation-Independent Cloning. In: Peccoud J, ed. Gene Synthesis. Totowa, NJ: Humana Press, 2012: 51–9.

141 Koch T, Dahlke C, Fathi A, *et al.* Safety and immunogenicity of a modified vaccinia virus Ankara vector vaccine candidate for Middle East respiratory syndrome: an open-label, phase 1 trial. *The Lancet Infectious Diseases* 2020; **20**: 827–38.

142 Van Rossum G, Drake Jr FL. Python reference manual. Centrum voor Wiskunde en Informatica Amsterdam, 1995.

143 R Core Team. R: A language and environment for statistical computing. Vienna, Austria: R Foundation for Statistical Computing, 2022 https://www.R-project.org/.

144 Pinheiro J, Bates D, R Core Team. nlme: Linear and nonlinear mixed effects models. 2023 https://CRAN.R-project.org/package=nlme.

145 Eisenberg D, Schwarz E, Komaromy M, Wall R. Analysis of membrane and surface protein sequences with the hydrophobic moment plot. *Journal of Molecular Biology* 1984; **179**: 125–42.

146 Edler D, Klein J, Antonelli A, Silvestro D. raxmlGUI 2.0: A graphical interface and toolkit for phylogenetic analyses using RAxML. *Methods Ecol Evol* 2021; **12**: 373–7.

147 Stamatakis A. RAxML version 8: a tool for phylogenetic analysis and post-analysis of large phylogenies. *Bioinformatics* 2014; **30**: 1312–3.

148 Korenkov M, Zehner M, Cohen-Dvashi H, *et al.* Somatic hypermutation introduces bystander mutations that prepare SARS-CoV-2 antibodies for emerging variants. *Immunity* 2023; : S1074761323004855.

149 Raybould MIJ, Kovaltsuk A, Marks C, Deane CM. CoV-AbDab: the coronavirus antibody database. *Bioinformatics* 2021; **37**: 734–5.

150 Stothard P. The Sequence Manipulation Suite: JavaScript Programs for Analyzing and Formatting Protein and DNA Sequences. *BioTechniques* 2000; **28**: 1102–4.

151 Cock PJA, Antao T, Chang JT, *et al.* Biopython: freely available Python tools for computational molecular biology and bioinformatics. *Bioinformatics* 2009; **25**: 1422–3.

152 Hunter JD. Matplotlib: A 2D Graphics Environment. *Comput Sci Eng* 2007; **9**: 90–5.

153 Vanshylla K, Fan C, Wunsch M, *et al.* Discovery of ultrapotent broadly neutralizing antibodies from SARS-CoV-2 elite neutralizers. *Cell Host & Microbe* 2022; **30**: 69-82.e10.

154 Crawford KHD, Eguia R, Dingens AS, *et al.* Protocol and Reagents for Pseudotyping Lentiviral Particles with SARS-CoV-2 Spike Protein for Neutralization Assays. *Viruses* 2020; **12**: 513.

155 Gruell H, Vanshylla K, Korenkov M, *et al.* SARS-CoV-2 Omicron sublineages exhibit distinct antibody escape patterns. *Cell Host & Microbe* 2022; **30**: 1231-1241.e6.

156 Otwinowski Z, Minor W. [20] Processing of X-ray diffraction data collected in oscillation mode. In: Methods in Enzymology. Elsevier, 1997: 307–26.

157 Emsley P, Cowtan K. *Coot*: model-building tools for molecular graphics. *Acta Crystallogr D Biol Crystallogr* 2004; **60**: 2126–32.

158 Liebschner D, Afonine PV, Baker ML, *et al.* Macromolecular structure determination using X-rays, neutrons and electrons: recent developments in *Phenix*. *Acta Crystallogr D Struct Biol* 2019; **75**: 861–77.

159 Lefranc M-P, Giudicelli V, Ginestoux C, *et al.* IMGT, the international ImMunoGeneTics database. *Nucleic Acids Research* 1999; **27**: 209–12.

160 Katoh K. MAFFT: a novel method for rapid multiple sequence alignment based on fast Fourier transform. *Nucleic Acids Research* 2002; **30**: 3059–66.

161 Madeira F, Park YM, Lee J, *et al.* The EMBL-EBI search and sequence analysis tools APIs in 2019. *Nucleic Acids Research* 2019; **47**: W636–41.

162 team T pandas development. pandas-dev/pandas: Pandas. 2020; published online Feb. DOI:10.5281/zenodo.3509134.

163 Harris CR, Millman KJ, Van Der Walt SJ, *et al.* Array programming with NumPy. *Nature* 2020; **585**: 357–62.

164 Virtanen P, Gommers R, Oliphant TE, *et al.* SciPy 1.0: fundamental algorithms for scientific computing in Python. *Nat Methods* 2020; **17**: 261–72.

165 Dong E, Du H, Gardner L. An interactive web-based dashboard to track COVID-19 in real time. *The Lancet Infectious Diseases* 2020; **20**: 533–4.

166 Goddard TD, Huang CC, Meng EC, *et al.* UCSF ChimeraX: Meeting modern challenges in visualization and analysis. *Protein Science* 2018; **27**: 14–25.

167 Pettersen EF, Goddard TD, Huang CC, *et al.* UCSF CHIMERAX: Structure visualization for researchers, educators, and developers. *Protein Science* 2021; **30**: 70–82.

168 Cai Y, Zhang J, Xiao T, *et al.* Distinct conformational states of SARS-CoV-2 spike protein. *Science* 2020; **369**: 1586–92.

169 Greaney AJ, Loes AN, Crawford KHD, *et al.* Comprehensive mapping of mutations in the SARS-CoV-2 receptor-binding domain that affect recognition by polyclonal human plasma antibodies. *Cell Host & Microbe* 2021; **29**: 463-476.e6.

170 Kimura I, Yamasoba D, Tamura T, *et al.* Virological characteristics of the SARS-CoV-2 Omicron BA.2 subvariants, including BA.4 and BA.5. *Cell* 2022; **185**: 3992-4007.e16.

171 Planas D, Veyer D, Baidaliuk A, *et al.* Reduced sensitivity of SARS-CoV-2 variant Delta to antibody neutralization. *Nature* 2021; **596**: 276–80.

172 Baum A, Fulton BO, Wloga E, *et al.* Antibody cocktail to SARS-CoV-2 spike protein prevents rapid mutational escape seen with individual antibodies. *Science* 2020; **369**: 1014–8.

173 Mathieu E, Ritchie H, Rodés-Guirao L, *et al.* Coronavirus pandemic (COVID-19). *Our World in Data* 2020.

174 Hillus D, Schwarz T, Tober-Lau P, *et al.* Safety, reactogenicity, and immunogenicity of homologous and heterologous prime-boost immunisation with ChAdOx1 nCoV-19 and BNT162b2: a prospective cohort study. *The Lancet Respiratory Medicine* 2021; **9**: 1255–65.

175 Focosi D, McConnell S, Casadevall A, Cappello E, Valdiserra G, Tuccori M. Monoclonal antibody therapies against SARS-CoV-2. *The Lancet Infectious Diseases* 2022; **22**: e311–26.

176 Liu C, Ginn HM, Dejnirattisai W, *et al.* Reduced neutralization of SARS-CoV-2 B.1.617 by vaccine and convalescent serum. *Cell* 2021; **184**: 4220-4236.e13.

177 Weissman D, Alameh M-G, De Silva T, *et al.* D614G Spike Mutation Increases SARS CoV-2 Susceptibility to Neutralization. *Cell Host & Microbe* 2021; **29**: 23-31.e4.

178 Amanat F, Thapa M, Lei T, *et al.* SARS-CoV-2 mRNA vaccination induces functionally diverse antibodies to NTD, RBD, and S2. *Cell* 2021; **184**: 3936-3948.e10.

179 Barnes CO, West AP, Huey-Tubman KE, *et al.* Structures of Human Antibodies Bound to SARS-CoV-2 Spike Reveal Common Epitopes and Recurrent Features of Antibodies. *Cell* 2020; **182**: 828-842.e16.

180 Dejnirattisai W, Zhou D, Ginn HM, *et al.* The antigenic anatomy of SARS-CoV-2 receptor binding domain. *Cell* 2021; **184**: 2183-2200.e22.

181 Pinto D, Sauer MM, Czudnochowski N, *et al.* Broad betacoronavirus neutralization by a stem helix–specific human antibody. *Science* 2021; **373**: 1109–16.

182 Chi X, Yan R, Zhang J, *et al.* A neutralizing human antibody binds to the N-terminal domain of the Spike protein of SARS-CoV-2. *Science* 2020; **369**: 650–5.

183 Wang Z, Muecksch F, Cho A, *et al.* Analysis of memory B cells identifies conserved neutralizing epitopes on the N-terminal domain of variant SARS-Cov-2 spike proteins. *Immunity* 2022; **55**: 998-1012.e8.

184 Suryadevara N, Shrihari S, Gilchuk P, *et al.* Neutralizing and protective human monoclonal antibodies recognizing the N-terminal domain of the SARS-CoV-2 spike protein. *Cell* 2021; **184**: 2316-2331.e15.

185 Klein F. A Phase 1/2a Trial of the Inhaled Administration of the SARS-CoV-2-Neutralizing Monoclonal Antibody DZIF-10c in SARS-CoV-2-Infected and -Uninfected Individuals. clinicaltrials.gov, 2021 https://clinicaltrials.gov/study/NCT04631705 (accessed Jan 1, 2024).

186 Klein F. A Phase 1/2a Trial of the Intravenous Administration of the SARS-CoV-2-Neutralizing Monoclonal Antibody DZIF-10c in SARS-CoV-2-Infected and -Uninfected Individuals. clinicaltrials.gov, 2021 https://clinicaltrials.gov/study/NCT04631666 (accessed Jan 1, 2024).

187 Boehringer Ingelheim. A Phase II/III Seamless, Randomized, Double-blind, Placebo-controlled, Parallel-group, Group-sequential Study to Evaluate Efficacy, Safety and Tolerability of BI 767551 for the Treatment of Symptomatic, Non-hospitalized Adults With Mild to Moderate COVID-19. clinicaltrials.gov, 2022 https://clinicaltrials.gov/study/NCT04822701 (accessed Jan 1, 2024).

188 Weinreich DM, Sivapalasingam S, Norton T, *et al.* REGN-COV2, a Neutralizing Antibody Cocktail, in Outpatients with Covid-19. *N Engl J Med* 2021; **384**: 238–51.

189 Gupta A, Gonzalez-Rojas Y, Juarez E, *et al.* Early Treatment for Covid-19 with SARS-CoV-2 Neutralizing Antibody Sotrovimab. *N Engl J Med* 2021; **385**: 1941–50.

190 Levin MJ, Ustianowski A, De Wit S, *et al.* Intramuscular AZD7442 (Tixagevimab–Cilgavimab) for Prevention of Covid-19. *N Engl J Med* 2022; **386**: 2188–200.

191 Montgomery H, Hobbs FDR, Padilla F, *et al.* Efficacy and safety of intramuscular administration of tixagevimab–cilgavimab for early outpatient treatment of COVID-19 (TACKLE): a phase 3, randomised, double-blind, placebo-controlled trial. *The Lancet Respiratory Medicine* 2022; **10**: 985–96.

192 Dougan M, Nirula A, Azizad M, *et al.* Bamlanivimab plus Etesevimab in Mild or Moderate Covid-19. *N Engl J Med* 2021; **385**: 1382–92.

193 O'Brien MP, Forleo-Neto E, Sarkar N, *et al.* Effect of Subcutaneous Casirivimab and Imdevimab Antibody Combination vs Placebo on Development of Symptomatic COVID-19 in Early Asymptomatic SARS-CoV-2 Infection: A Randomized Clinical Trial. *JAMA* 2022; **327**: 432.

194 ACTIV-3/TICO LY-CoV555 Study Group. A Neutralizing Monoclonal Antibody for Hospitalized Patients with Covid-19. *N Engl J Med* 2021; **384**: 905–14.

195 Abani O, Abbas A, Abbas F, *et al.* Casirivimab and imdevimab in patients admitted to hospital with COVID-19 (RECOVERY): a randomised, controlled, open-label, platform trial. *The Lancet* 2022; **399**: 665–76.

196 Self WH, Sandkovsky U, Reilly CS, *et al.* Efficacy and safety of two neutralising monoclonal antibody therapies, sotrovimab and BRII-196 plus BRII-198, for adults hospitalised with COVID-19 (TICO): a randomised controlled trial. *The Lancet Infectious Diseases* 2022; **22**: 622–35.

197 Iannizzi C, Chai KL, Piechotta V, *et al.* Convalescent plasma for people with COVID-19: a living systematic review. *Cochrane Database of Systematic Reviews* 2023; **2023**. DOI:10.1002/14651858.CD013600.pub6.

198 Brouwer PJM, Caniels TG, van der Straten K, *et al.* Potent neutralizing antibodies from COVID-19 patients define multiple targets of vulnerability. *Science* 2020; **369**: 643–50.

199 Wang Y, Yuan M, Lv H, Peng J, Wilson IA, Wu NC. A large-scale systematic survey reveals recurring molecular features of public antibody responses to SARS-CoV-2. *Immunity* 2022; **55**: 1105-1117.e4.

200 Klein F, Mouquet H, Dosenovic P, Scheid JF, Scharf L, Nussenzweig MC. Antibodies in HIV-1 Vaccine Development and Therapy. *Science* 2013; **341**: 1199–204.

201 Wu X, Yang Z-Y, Li Y, *et al.* Rational Design of Envelope Identifies Broadly Neutralizing Human Monoclonal Antibodies to HIV-1. *Science* 2010; **329**: 856–61.

202 Ni L, Ye F, Cheng M-L, *et al.* Detection of SARS-CoV-2-Specific Humoral and Cellular Immunity in COVID-19 Convalescent Individuals. *Immunity* 2020; **52**: 971-977.e3.

203 Grifoni A, Weiskopf D, Ramirez SI, *et al.* Targets of T Cell Responses to SARS-CoV-2 Coronavirus in Humans with COVID-19 Disease and Unexposed Individuals. *Cell* 2020; **181**: 1489-1501.e15.

204 Wang P, Liu L, Nair MS, *et al.* SARS-CoV-2 neutralizing antibody responses are more robust in patients with severe disease. *Emerging Microbes & Infections* 2020; **9**: 2091–3.

205 Yuan M, Liu H, Wu NC, *et al.* Structural basis of a shared antibody response to SARS-CoV-2. *Science* 2020; **369**: 1119–23.

206 Klein F, Diskin R, Scheid JF, *et al.* Somatic Mutations of the Immunoglobulin Framework Are Generally Required for Broad and Potent HIV-1 Neutralization. *Cell* 2013; **153**: 126–38.

207 Tan TJC, Yuan M, Kuzelka K, *et al.* Sequence signatures of two public antibody clonotypes that bind SARS-CoV-2 receptor binding domain. *Nat Commun* 2021; **12**: 3815.

208 Pappas L, Foglierini M, Piccoli L, *et al.* Rapid development of broadly influenza neutralizing antibodies through redundant mutations. *Nature* 2014; **516**: 418–22.

209 Sok D, Laserson U, Laserson J, *et al.* The Effects of Somatic Hypermutation on Neutralization and Binding in the PGT121 Family of Broadly Neutralizing HIV Antibodies. *PLoS Pathog* 2013; **9**: e1003754.

210 Aleman F, Tzarum N, Kong L, *et al.* Immunogenetic and structural analysis of a class of HCV broadly neutralizing antibodies and their precursors. *Proc Natl Acad Sci USA* 2018; **115**: 7569–74.

211 Bates JT, Keefer CJ, Utley TJ, Correia BE, Schief WR, Crowe JE. Reversion of Somatic Mutations of the Respiratory Syncytial Virus–Specific Human Monoclonal Antibody Fab19 Reveal a Direct Relationship between Association Rate and Neutralizing Potency. *The Journal of Immunology* 2013; **190**: 3732–9.

212 Wiehe K, Bradley T, Meyerhoff RR, *et al.* Functional Relevance of Improbable Antibody Mutations for HIV Broadly Neutralizing Antibody Development. *Cell Host & Microbe* 2018; **23**: 759-765.e6.

213 Jardine JG, Sok D, Julien J-P, *et al.* Minimally Mutated HIV-1 Broadly Neutralizing Antibodies to Guide Reductionist Vaccine Design. *PLoS Pathog* 2016; **12**: e1005815.

214 Sabouri Z, Schofield P, Horikawa K, *et al.* Redemption of autoantibodies on anergic B cells by variable-region glycosylation and mutation away from self-reactivity. *Proc Natl Acad Sci USA* 2014; **111**. DOI:10.1073/pnas.1406974111.

215 Tas JMJ, Mesin L, Pasqual G, *et al.* Visualizing antibody affinity maturation in germinal centers. *Science* 2016; **351**: 1048–54.

216 Cao Y, Jian F, Wang J, *et al.* Imprinted SARS-CoV-2 humoral immunity induces convergent Omicron RBD evolution. *Nature* 2022; published online Dec 19. DOI:10.1038/s41586-022-05644-7.

217 Cao Y, Yisimayi A, Jian F, *et al.* BA.2.12.1, BA.4 and BA.5 escape antibodies elicited by Omicron infection. *Nature* 2022; **608**: 593–602.

218 Kim W, Zhou JQ, Horvath SC, *et al.* Germinal centre-driven maturation of B cell response to mRNA vaccination. *Nature* 2022; **604**: 141–5.

219 Schmitz AJ, Turner JS, Liu Z, *et al.* A vaccine-induced public antibody protects against SARS-CoV-2 and emerging variants. *Immunity* 2021; **54**: 2159-2166.e6.

220 Chen EC, Gilchuk P, Zost SJ, *et al.* Convergent antibody responses to the SARS-CoV-2 spike protein in convalescent and vaccinated individuals. *Cell Reports* 2021; **36**: 109604.

221 Kreer C, Gruell H, Mora T, Walczak AM, Klein F. Exploiting B Cell Receptor Analyses to Inform on HIV-1 Vaccination Strategies. *Vaccines* 2020; **8**: 13.

222 Ng KW, Faulkner N, Cornish GH, *et al.* Preexisting and de novo humoral immunity to SARS-CoV-2 in humans. *Science* 2020; **370**: 1339–43.

223 Wec AZ, Wrapp D, Herbert AS, *et al.* Broad neutralization of SARS-related viruses by human monoclonal antibodies. *Science* 2020; **369**: 731–6.

224 Braun J, Loyal L, Frentsch M, *et al.* SARS-CoV-2-reactive T cells in healthy donors and patients with COVID-19. *Nature* 2020; **587**: 270–4.

225 Ercanoglu MS, Gieselmann L, Dähling S, *et al.* No substantial preexisting B cell immunity against SARS-CoV-2 in healthy adults. *iScience* 2022; **25**: 103951.

226 Song G, He W, Callaghan S, *et al.* Cross-reactive serum and memory B-cell responses to spike protein in SARS-CoV-2 and endemic coronavirus infection. *Nat Commun* 2021; **12**: 2938.

227 Aguilar-Bretones M, Westerhuis BM, Raadsen MP, *et al.* Seasonal coronavirus–specific B cells with limited SARS-CoV-2 cross-reactivity dominate the IgG response in severe COVID-19. *Journal of Clinical Investigation* 2021; **131**: e150613.

228 Harvey WT, Carabelli AM, Jackson B, *et al.* SARS-CoV-2 variants, spike mutations and immune escape. *Nat Rev Microbiol* 2021; **19**: 409–24.

229 Yamasoba D, Kimura I, Nasser H, *et al.* Virological characteristics of the SARS-CoV-2 Omicron BA.2 spike. *Cell* 2022; **185**: 2103-2115.e19.

230 Tuekprakhon A, Nutalai R, Dijokaite-Guraliuc A, *et al.* Antibody escape of SARS-CoV-2 Omicron BA.4 and BA.5 from vaccine and BA.1 serum. *Cell* 2022; **185**: 2422-2433.e13.

231 Hornsby H, Nicols AR, Longet S, *et al.* Omicron infection following vaccination enhances a broad spectrum of immune responses dependent on infection history. *Nat Commun* 2023; **14**: 5065.

232 Gruell H, Vanshylla K, Tober-Lau P, *et al.* mRNA booster immunization elicits potent neutralizing serum activity against the SARS-CoV-2 Omicron variant. *Nat Med* 2022; **28**: 477–80.

233 Bobrovitz N, Ware H, Ma X, *et al.* Protective effectiveness of previous SARS-CoV-2 infection and hybrid immunity against the omicron variant and severe disease: a systematic review and meta-regression. *The Lancet Infectious Diseases* 2023; **23**: 556–67.

234 Cox M, Peacock TP, Harvey WT, *et al.* SARS-CoV-2 variant evasion of monoclonal antibodies based on in vitro studies. *Nat Rev Microbiol* 2023; **21**: 112–24.

235 Ueno M, Iwata-Yoshikawa N, Matsunaga A, *et al.* Isolation of human monoclonal antibodies with neutralizing activity to a broad spectrum of SARS-CoV-2 viruses including the Omicron variants. *Antiviral Research* 2022; **201**: 105297.

236 Cameroni E, Bowen JE, Rosen LE, *et al.* Broadly neutralizing antibodies overcome SARS-CoV-2 Omicron antigenic shift. *Nature* 2022; **602**: 664–70.

237 Luo M, Zhou B, Reddem ER, *et al.* Structural insights into broadly neutralizing antibodies elicited by hybrid immunity against SARS-CoV-2. *Emerging Microbes & Infections* 2023; **12**: 2146538.

238 Zhou P, Song G, Liu H, *et al.* Broadly neutralizing anti-S2 antibodies protect against all three human betacoronaviruses that cause deadly disease. *Immunity* 2023; **56**: 669-686.e7.

239 Muecksch F, Weisblum Y, Barnes CO, *et al.* Affinity maturation of SARS-CoV-2 neutralizing antibodies confers potency, breadth, and resilience to viral escape mutations. *Immunity* 2021; **54**: 1853-1868.e7.

240 Longo NS, Lipsky PE. Why do B cells mutate their immunoglobulin receptors? *Trends in Immunology* 2006; **27**: 374–80.

8. Appendix

8.1. List of Main Figures

8.2. Tables

8.3. Publication of Results

8.3.1. Publications used in the submitted thesis

Korenkov, M.*, Zehner, M.*, Cohen-Dvashi, H., Borenstein-Katz, A., Kottege, L., Janicki, H., Vanshylla, K., Weber, T., Gruell, H., Koch, M., Diskin, R., Kreer, C.†, Klein, F.†, 2023. Somatic hypermutation introduces bystander mutations that prepare SARS-CoV-2 antibodies for emerging variants. *Immunity* S1074761323004855. https://doi.org/10.1016/j.immuni.2023.11.004 *contributed equally †contributed equally

Kreer, C.*, Zehner, M.*, Weber, T., Ercanoglu, M.S., Gieselmann, L., Rohde, C., Halwe, S., **Korenkov, M.**, Schommers, P., Vanshylla, K., Di Cristanziano, V., Janicki, H., Brinker, R., Ashurov, A., Krähling, V., Kupke, A., Cohen-Dvashi, H., Koch, M., Eckert, J.M., Lederer, S., Pfeifer, N., Wolf, T., Vehreschild, M.J.G.T., Wendtner, C., Diskin, R., Gruell, H., Becker, S., Klein, F., 2020. Longitudinal Isolation of Potent Near-Germline SARS-CoV-2-Neutralizing Antibodies from COVID-19 Patients. Cell 182, 843-854.e12. https://doi.org/10.1016/j.cell.2020.06.044 *contributed equally

Gruell, H., Vanshylla, K., **Korenkov, M.**, Tober-Lau, P., Zehner, M., Münn, F., Janicki, H., Augustin, M., Schommers, P., Sander, L. E., Kurth, F., Kreer, C., & Klein, F. (2022). SARS-CoV-2 Omicron sublineages exhibit distinct antibody escape patterns. *Cell Host & Microbe*, *30*(9), 1231-1241.e6. https://doi.org/10.1016/j.chom.2022.07.002

8.3.2. Additional publication list

Ercanoglu, M. S., Gieselmann, L., Dähling, S., Poopalasingam, N., Detmer, S., Koch, M., **Korenkov, M.**, Halwe, S., Klüver, M., Di Cristanziano, V., Janicki, H., Schlotz, M., Worczinski, J., Gathof, B., Gruell, H., Zehner, M., Becker, S., Vanshylla, K., Kreer, C., & Klein, F. (2022). No substantial preexisting B cell immunity against SARS-CoV-2 in healthy adults. *IScience*, *25*(3), 103951. https://doi.org/10.1016/j.isci.2022.103951

Korenkov, M.*, Poopalasingam, N.*, Madler, M., Vanshylla, K., Eggeling, R., Wirtz, M., Fish, I., Dewald, F., Gieselmann, L., Lehmann, C., Fätkenheuer, G., Gruell, H., Pfeifer, N., Heger, E., & Klein, F. (2021). Evaluation of a Rapid Antigen Test To Detect SARS-CoV-2 Infection and Identify Potentially Infectious Individuals. *Journal of Clinical Microbiology*, *59*(9), e00896-21. https://doi.org/10.1128/JCM.00896-21 *contributed equally

Poopalasingam, N.*, **Korenkov, M.***, Ashurov, A., Strobel, J., Fish, I., Hellmich, M., Gruell, H., Lehmann, C., Heger, E., & Klein, F. (2022). Determining the reliability of rapid SARS-

CoV-2 antigen detection in fully vaccinated individuals. *Journal of Clinical Virology*, *148*, 105119. https://doi.org/10.1016/j.jcv.2022.105119 *contributed equally

Rehkaemper*, J., **Korenkov, M.***, Quaas, A., Rueschoff, J., Pamuk, A., Zander, T., Hillmer, A. M., Buettner, R., Hoelscher, A. H., Bruns, C. J., Loeser, H., Alakus, H., & Schoemig-Markiefka, B. (2020). Amplification of KRAS and its heterogeneity in non-Asian gastric adenocarcinomas. *BMC Cancer*, *20*(1), 587. https://doi.org/10.1186/s12885-020-06996-x *contributed equally

Dratsch, T., **Korenkov, M.**, Zopfs, D., Brodehl, S., Baessler, B., Giese, D., Brinkmann, S., Maintz, D., & Pinto Dos Santos, D. (2021). Practical applications of deep learning: Classifying the most common categories of plain radiographs in a PACS using a neural network. *European Radiology*, *31*(4), 1812–1818. https://doi.org/10.1007/s00330-020-07241-6

Hescheler, D. A., Plum, P. S., Zander, T., Quaas, A., **Korenkov, M.**, Gassa, A., Michel, M., Bruns, C. J., & Alakus, H. (2020). Identification of targeted therapy options for gastric adenocarcinoma by comprehensive analysis of genomic data. *Gastric Cancer*, *23*(4), 627–638. https://doi.org/10.1007/s10120-020-01045-9

Beste, N. C., Davis, X., Kloeckner, R., Celik, E., **Korenkov, M.**, Maintz, D., Dratsch, T., & Pinto Dos Santos, D. (2022). Comprehensive analysis of Twitter usage during a major medical conference held virtually versus in-person. *Insights into Imaging*, *13*(1), 8. https://doi.org/10.1186/s13244-021-01140-0